ANALYSIS AND DESIGN OF COLD-FORMED C-SECTION MEMBERS AND STRUCTURES

PhD Dissertation

Gábor JAKAB

Budapest University of Technology and Economics

Supervisor:

László DUNAI, PhD

Professor

Budapest University of Technology and Economics

Budapest, 2009

ACKNOWLEDGEMENT

Contents

1. Introduction

1.1. Background

Cold-formed thin-walled members are used in building industry in many fields. The probably largest area of use is in conventional – mainly industrial – steel structures as secondary and tertiary load-bearing elements – purlins, sheeting – on a steel or reinforced concrete primary structure. Cold-formed members are extensively used in North-America and Australia/New Zealand in residential housing as primary load-bearing structures; light-gauge building systems are gaining on popularity and compete with the traditional building material, wood. There are several examples of multi-storey office buildings with a primary load-bearing system consisting entirely of cold-formed members as well. Another large area of use is composite slabs, where trapezoidal sheeting and cold-formed sections are used as tension and a thin concrete slab as compression parts resulting in light floor systems applicable in buildings made of cold-formed members or in refurbishment. Cold-formed members are also extensively used in warehouse racks.

The main reason behind the extensive use of cold-formed members is that these are easy and cheap to fabricate, need minimal maintenance due to the zinc coating, no heavy cranes nor special tools are needed for the erection of the structures, in many cases even the lack of experience with the erection of steel structures may not be a problem.

However, the design of cold-formed members differs from that of conventional steel structures and therefore need special considerations. In most cases cold-formed members exhibit complex behaviour governed by interacting local and global stability phenomena. Conventional design approaches lead in these cases usually to a conservative design since the complex behaviour can only be approximated from the safe side. Also, the calculations easily become very time-consuming, while the gain – i.e. savings on mass – is not always proportional with the efforts. Therefore, cold-formed structures are usually developed as building systems and designed using formulae or tables derived from laboratory tests or models utilizing advanced design methods. With the rise of computers more and more special software are published aiming push-the-button style design requiring limited special knowledge from the user.

In the recent decade the field of cold-formed thin-walled steel structures have been among the busiest research areas at the Department of Structural Engineering, Budapest University of Technology and Economics. Research projects have been carried out on almost all types of structures mentioned previously. The research projects dealt with various types of structures, but they had the very common purpose to develop a design method that is based on the principles of Eurocode 3 (EC3, [1]) and ensures the safety of the structure. In every case the aim was to optimize the structural arrangement and detailing, and to provide structural engineers with tools for design.

One part of the research activity is fundamental research, aiming the better understanding of the complex stability behaviour of thin-walled members: Z- and C-sections, trapezoidal sheeting etc. Within the confines of this work the members are analyzed independently from building systems or structural arrangements, concentrating only on the possible behaviour modes under different loading and support conditions. These results can be used primarily in design method and design standard development. Another part of the research activity is research and development (R&D) work, aiming mainly the development of novel structural arrangements and their design method. The two main areas of the research are strongly bonded, as in many cases the needs of R&D influences the direction of fundamental research

and vice versa, the results of analyses carried out on simple structures may answer basic questions during system development.

The research work is carried out by a team with members from the staff and students of the Department, among them under- and postgraduate students, PhD Students and professors under the lead of László Dunai. The topics of the major finished research projects are:
- Design method development of the semi-rigid joints of a frame system made of cold-formed C-section members [2],
- Design method of a composite slab system using semi-rigid shear connector elements [3],
- Research methodology and design methods of non-conventional steel and composite structures [4],
- Advanced design method for purlin systems [5],
- Laboratory tests on purlin systems [6].

The presented theses summarize the author's research activities and main results as a member of the research team. The subject of the investigation is the stability behaviour of cold-formed thin-walled lipped channel (C-section) structural members to be used in frame systems with a span of 6...12 meters and in a truss system spanning 12...24 meters. In both structures the C-section members are used as primary load-bearing structural elements subjected to dominantly axial actions.

1.2. Main characteristics of cold-formed thin-walled members

The unique properties of thin-walled cold-formed C-section members originate from three factors: the fabrication process, the small thickness and high slenderness of the elements of the cross-section.

In a pure mechanical sense all cross-sections with elements of a width-to-thickness (b/t) ratio over 10 can be considered thin-walled [7]. According to this classification most steel cross-sections, including almost all hot-rolled steel sections may be classified as thin-walled. The reason of pointing out this property in case of steel structures is that it refers to the stability behaviour of these members: from the structural behaviour point-of-view structural members those global behaviour is primarily influenced by local effects and local stability phenomena are called thin-walled.

Cold-formed members are fabricated at room temperature, by introducing big plastic deformations to the base material. The most widely used fabrication technique used is cold roll forming. This technique uses rolled-up steel stripes fed to 6-15 pairs of rolls – depending on the complexity of the cross-section to be made – that progressively form the stripe in the desired shape. Sections produced this way may be almost of arbitrary shape, but there are some common properties that helps identify them:
- cold-formed sections have the same thickness in all their plates and usually the same radii in all edge regions,
- plate thickness is usually not bigger than 3.50 mm,
- width-to-thickness ratios of stiffened plates are usually between 80 and 250.

Due to the plastic deformations during fabrication the material properties cannot be considered isotropic along the cross-section: a certain degree of hardening and build-up of residual stresses in the edge regions is the consequence of the cold forming [8]. The big plastic deformations introduced in the edge areas never result perfect cross-sections, as part of the deformations is elastic wherefore a certain amount of spring-back is always present. Nevertheless the magnitude of spring-back and residual stress is not uniform along the length of the member but they follow a sinusoidal pattern [9]. As a result of this, initial imperfections

of cold-formed thin-walled members are usually caused by the variations in the angle of the edges along the length, whereas global imperfections like initial bow are not typical, [10].

A consequence of the high slenderness elements of the cross-sections of these types of structural members is that if subjected to compression their behaviour is primarily governed by local phenomena that couple to the global stability behaviour of the member reducing its overall strength. It is well known, that local stability behaviour may be strongly influenced by imperfections. In the case of these members even an imperfection usually considered small – the size of 1-2 mm – may have a considerable effect on the load-bearing capacity, since imperfections of this size are comparable with the thickness of the plates of the cross-section. The initial geometrical imperfections of the members so to say built-in due to the fabrication process are usually in this order of magnitude, and they are rather local imperfections involving changes in the shape of the cross-section. The imperfect shape and the typical deformations of the cross-section due to loading are of similar shape, which makes cold-formed thin-walled structural members imperfection sensitive. A common solution to enhance load bearing capacity is to use stiffeners – intermediate or edge stiffeners – in the cross-sections that give full or partial restraint to the stiffened plates. These enhance the critical stress of the elements of the cross-section and thus the overall strength of the member.

Still, the slender, thin plates of the sections have relatively low stiffness, wherefore the cross-section of cold-formed members is deformable. To utilize the potential load-bearing capacity of the members provided by the usually high steel grade the structures made of cold-formed members are extensively stiffened and/or supported by other structural members (stiffening system, built-up sections, sheeting, etc.). Structural members may be considered initially straight, but due to the relatively low stiffness they may become deformed and have global imperfections as well (usually bow and/or twist) during being built in a structure.

1.3. Applicable standards, design methods

The special properties of cold-formed members require special considerations when it comes to design. Hence, major standard codes usually devote separate chapters to the design of thin-walled cold-formed members and their joints, etc.

When speaking of the design of structures made of cold-formed thin-walled members one must not forget that this field of steel structures is much more diverse than that of traditional steel structures. The reason behind this is the much lower machinery demand of producing cold-formed members and the possibility to design and fabricate optimized cross-sections for a given purpose, make up cross-sections that are easier to connect thus enable faster erection or even use special fastening elements – in contrary to the mostly standardized and more generally used hot-rolled or welded sections. This affects especially structural joints where in the case of conventional structures almost standardized solutions and their design methods exist, but in the case of cold-formed members the number of possible joint configurations makes standardization almost impossible. Therefore in most standards rather the principles of design are laid down giving the designer – or in this case better said, the researcher – only principles to be applied to solve the problem, formulae are provided only for basic cases, simple structural details.

There are three major branches of design standards applicable to cold-formed members:
- the standard of the American Iron and Steel Institute (AISI) [11],
- the codes of Australia and New Zealand (AS/NZS) [12],
- the Eurocode 3 Part 1-3 (EC3-1-3:2006) [13], the valid standard for cold-formed structures in Hungary to date.

The history of the last two decades of available standards on cold-formed members in Hungary is adventurous. After cancelling the operational status of the "old" standard MSZ 15026/86 in the beginning of the '90-s only the pre-norm version of Eurocode 3 (EC3-1-3:1996, [14]) was available – but not operational – until 2006 when the final version of this standard was published without the National Annex. However, there have been major changes between the pre-norm and final versions. The changes do not affect the basic principles and possible approaches of design but many application rules have been changed or completely removed from the text.

1.4. EC3 design methods: application rules, test-based design

EC3-1-3 allows two approaches to directly determine design resistances of members: application rules and test-based design method.

Application rules are design methods provided by EC3 to calculate the design resistances for different failure modes by using closed formulae enabling fast and relatively easy calculation. Application rules control every detail of the calculation, and describe when alternative – advanced – methods may be used to enhance the accuracy of the result. However, they may be used directly only to cases that are principally the same as the one handled by the given rule, in any other case approximations from the safe side are to be used.

Test-based design allows deriving design resistances or methods from load-bearing capacities measured in laboratory tests. The developed design method may consist of new formulae, but as possible failure modes are covered by EC3 on application rule level, developing new ones instead of the existing ones may be unnecessary. Existing formulae of the application rules for the pertinent failure modes may be modified – calibrated, simplified or extended – to give a better match of calculated and measured load-bearing capacities but still provide the safety of the design method.

Using test-based design the resistance can be derived already from one laboratory test, but this leads to a very conservative design; by carrying out more experiments and evaluating the results statistically the test-based design resistance can be increased. When looking for results of laboratory tests the researcher is faced with an abundance of results, but the diversity of C-sections – or cold-formed sections in general – makes direct comparisons often difficult. An example of this is one of the most recent papers on C-section compression members, [15], where the results of more test series are summarized. Among the five different lipped channel sections only one is similar to the ones subject to studies in this thesis but has completely different proportions. When carrying out laboratory tests researchers usually try to design these aiming a single phenomenon, and design the test in a way that makes comparison between test and theory easy, enabling the fine-tuning of existing calculation methods, [16], [17], [18]. These tests, however, do not take into account end effects that may reduce the load-bearing capacity, i.e. the effect of load introduction, [19].

These approaches provide design resistances that may be used directly in design. However, the exclusive use of application rules often leads to conservative design, and tests have the major disadvantage of being expensive and time-consuming. The two methods of obtaining design resistances can be mixed: laboratory tests may be used to investigate the behaviour of the test specimen and analyze the processes leading to failure for the given structural arrangement, and based on the observations design methods based on the principles of calculation laid down by EC3 may be developed. This method is particularly advantageous in the case of building systems, where the cost of a unit may be greatly reduced if a non-conservative design method based on laboratory tests is available. These derived design

methods are not application rules – i.e. they are not included in the standard – but are modified versions of them and they are validated by the laboratory tests.

Intensive research of structures made of cold-formed members is carried out in Central-Europe in two centres: at The "Politechnica" University of Timisoara, Department of Steel Structures and Structural Mechanics – with the lead of Dan Dubina – and at the Budapest University of Technology and Economics, Department of Structural Engineering – the team of László Dunai. It is to be emphasized that the two centres work separately, although they have overlapping industrial partners. Hence, mostly the same selection of section is used, which leads to the convergence of solutions for similar problems. Both teams use cold-formed C-sections in their structures as members subject primarily to axial actions as i) columns and beam-columns in frame systems, ii) chord and brace members of trusses.

Publications of the team of Timisoara dealing with C-sections or structures made of C-sections include general design questions regarding single and built-up members, bolted connections of these members, trusses made of C-section members, shear walls, etc. In many cases the structures are tested for monotonic and cyclic loads as well, [20], [21], [22], [23].

1.5. Calculation methods – state of the art

Fundamental contribution to calculate and design thin-walled members using analytical approach was done by Kármán, Vlasov and Winter. Kármán extended Kirchhoff's plate theory to large displacements and introduced the idea of the effective width, [24]. His results were used by Winter to simplify and calibrate the difficult equations by laboratory tests, [25]; the derived formula is included in most modern design codes to calculate the effective cross-section. Vlasov extended the torsion theory Saint Venant to include restrained torsion of thin-walled members, [26], to complement the beam theory first formulated by Bernoulli and Navier. Vlasov's results were spread in Hungary primarily by the works of Csellár, Halász and Réti, [27]. The analytical approach has one major limitation, namely, the distortion of the cross-section, a typical characteristic of thin-walled cold-formed members with high web b/t ratios is not included in this model; to study this effect a numerical model is necessary.

EC3 generally allows the use of advanced numerical methods to obtain the critical stress of the member to be designed from a bifurcation analysis. On a member level, these methods usually lead to a design less conservative than those obtained from the application rules or analytical solutions. Especially the rapid development of two competing theoretical approaches resulted in a significant boom in the practically applicable design tools. These calculation methods are well suited for thin-walled members as they both take cross-sectional distortion into account and can be used to decompose the coupled stability phenomena, but are far less computation-extensive than finite element modelling (FEM).

Researchers of the Technical University of Lisbon (D. Camotim, N. Silvestre, P.B. Dinis) pursued to approach the behaviour of these members [28] on the basics of the generalized beam theory (GBT, [29]). A recently published software (GBTUL, [30]) utilizing the results of the group is available for use in design. The other approach is based on the finite strip method (FSM) first developed for cold-formed members by G.J. Hancock using spline functions (Thin-Wall, [31]), and by B.W. Schafer using sinusoidal functions (CUFSM, [32]). The latter was improved by S. Ádány to the constrained finite strip method (cFSM) enabling the classification of buckling modes [33], [34]. The finite strip method makes an easy-to-understand approach but has many limitations, especially when it comes to modelling supports. Both GBT and FSM/cFSM can be used to calculate the critical stress of a member for a given failure mode, which can be incorporated in the design formulae of either Eurocode 3 or AISI.

Advanced numerical modelling (FE simulation or virtual experiment using a surface model) may be a powerful yet inexpensive tool to analyse the global or local behaviour of structures or parts of structures made of cold-formed members, [35].

Shell numerical models of cold-formed members are often used to reproduce results of laboratory tests and allow a detailed investigation of the processes underlying different failure modes. The models often seem very simple as the geometry is prismatic with same overall plate thickness, and uniform stress distribution at the ends, [36]. However, the use of FE models even instead of laboratory tests is limited for two reasons: there is no standardized methodology of modelling, neither are general guidelines to incorporate mechanical and geometrical imperfections in the models similar to the rules given for plated structures in EC3 Part 1-5 [37], and there is no generally accepted model to simulate the behaviour of the connector elements. Therefore almost only members or parts of structures are investigated using shell FE models, whole structures are usually not modelled, [38], [39].

1.6. The content of the dissertation

The presented dissertation summarizes the author's research activities and main results on C-section structural members and structures made of these.

One part of the work is fundamental research, where compression C-section members with different cross-sections and different end- and lateral supporting conditions are investigated. The other part is R&D work carried out during the development of a truss system made of cold-formed C-section members. These two major parts of the dissertation are strongly bonded, as the majority of the members investigated in confines of the fundamental research programme have supporting and loading conditions similar to that of the members of the truss system but are not fully covered by the standard. A third part of the research work deals with the numerical modelling the members and structures tested in the laboratory. The research was carried out using the product line of the Lindab company wherefore a part of the results (i.e. load-bearing capacities) can be applied directly only to cross-sections with the same dimensions.

In the second Chapter the laboratory tests carried out by the author on C-section compression members and the results derived from these are summarized. The test specimens and the test setup are introduced. The behaviour modes obtained are characterised and classified based on measured load-displacement diagrams and observations. The measured load-bearing capacities are compared to design resistances derived from the test results (test-based design) and calculated design resistances according to the application rules of EC3. The design resistances obtained from the different approaches are discussed and modified. Based on these design rules are proposed for members of the investigated structural arrangements.

In the third Chapter the development of a truss system made of cold-formed C-section members and its results are summarized. The structural arrangement and the most important design considerations resulting from these are presented. Laboratory tests carried out on the prototype of the truss are introduced: test specimens, setup, and measurement system. Behaviour and failure modes are described and characterized based primarily on observations and incorporating measurement data. An EC3-based design method of the truss system is proposed. The proposed design method consists partially of modified or calibrated design application rules but contains also methods previously not applied to cold-formed structures. The safety of the developed truss system and its design method is validated by comparing test results and calculated design resistances.

The fourth Chapter deals with the numerical modelling of cold-formed structures discussed in the previous sections. A unified modelling approach including modelling of contacts, connector elements and members is introduced. The approach is applied to model the specimens investigated in the laboratory with the primary aim to reproduce the test results (behaviour, failure modes, load-bearing capacity, and ductility), thus to verify the models. The results of virtual experiments on compression C-section members are presented; the validity of the design formulae proposed based purely on laboratory tests is verified over a wide range of parameters.

Finally in the fifth Chapter the new scientific results of the research work are summarized.

2. Cold-formed C-section members

2.1. Introduction

The topic of the presented research is the stability behaviour and load-bearing capacity of cold-formed C-section members with different cross-sectional arrangements and load introduction. The studied arrangements are single or double sections where two C-sections or one C-section and one U-section are connected to each other and subjected to axial compression. Due to the arrangement of the load introduction the internal actions of the members are compression or compression and bending about the minor axis. The studied arrangements are potential solutions for structural problems in cold-formed structures (frame, truss, wall panel, etc.), but the majority of them is directly not covered by EC3, thus a non-conservative design of members with these arrangements is not possible. The primary aim of the research is to study the stability behaviour of such arrangements, identify and characterise the possible failure modes and to derive and validate EC3-based design methods.

In order to achieve this goal, two sets of tests were carried out in the Structural Laboratory of the Department of Structural Engineering, BME. The first set of 37 tests was designed and carried out in 2002, with two main goals in head: to check the application rules of EC3-1-3:1996, to study two structural arrangements directly not covered by the standard and derive design methods for them.

The second set of 61 tests was designed and carried out in 2008. This series of tests was designed to enable direct comparisons with the previous set, hence partially same cross-sections, and the same test and measurement setup was used. This latter series aimed primarily the investigation of arrangements and its possible alternatives used in a truss system made of cold-formed C-section members, code checking was of lesser importance.

During the execution of the tests, besides the primary aim to observe and study the stability phenomena and failure modes, a secondary aim was to collect data regarding the deformations of the specimens during loading to enable a detailed quantitative analysis of the test results and provide basis data for numerical modelling. To achieve this, detailed test documentation, photographs and an on-line measurement system was used during the tests enabling the monitoring and recording test results.

In this Chapter, on the basis of the laboratory test results, the observed behaviour of the specimens is described and characterised in order to classify them according to the failure modes. The in-depth evaluation of the results is done by analysing and comparing the measurement results of specimens with similar behaviour. Using the measured load-bearing capacities design resistances are calculated according to the procedure for test-based design as described by EC3 enabling a direct quantitative comparison of results. The measured test resistances are compared to design resistances calculated using the application rules of two versions of EC3, where applicable. Based on the comparison of test and design resistances conclusions are drawn regarding the safety and applicability of the application rules; new and modified design formulae are proposed to provide non-conservative yet safe design for the arrangements directly not covered by the standard.

2.2. Laboratory tests

2.2.1. Test setup

The laboratory tests were carried out in the testing frame setup in the Structural Laboratory of BME (Figure 2.). The specimens were assembled on the floor: gusset plates used to introduce the load were connected to the members, finished specimens were placed vertically in the rig. To position the gusset plates in the rig two bolts were used (Figure 1.) thus the rotation of the members about their axis at both ends was restrained in all tests. The load was applied at the lower end of the loading frame using a 400 kN hydraulic jack; the upper end connection was fixed. The load was applied incrementally by means of a hand pump. The measurement system consisted of displacement transducers and a load cell attached to the hydraulic system to measure the applied load. In the first set eight, in the second set four displacement transducers were used to measure the distortion of the cross-section (Figure 3.) at the half of the specimen length. One transducer was used to measure the shortening of the column. Strain gauges were used in only one test to measure the stress distribution in a cross-section of the specimen. The signals of the sensors were recorded at 2 Hz sampling frequency using a HBM Spider8 amplifier and laptop PC running HBM CatmanExpress measurement software. The test setup and the measurement system were unchanged for all the tests (including both sets of tests) except for the position of the upper beam and the elements supporting the displacement transducers at the half-length, which were relocated according to the length of the specimen.

Figure 1.: Positioning the specimen.
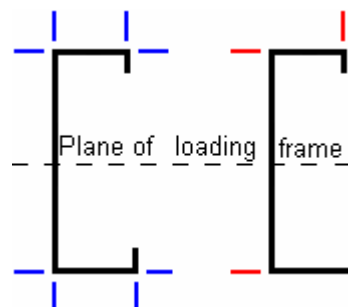

Figure 2.: The loading frame.

Figure 3.: Measurement of cross-sectional displacements (left: in the first set; right: in the second set).

2.2.2. Specimen arrangements

The characteristics of the test specimen configurations are introduced by the following figures, schematic drawings and short descriptions. In the figures the bolts and self-drilling and tapping screws (in the following: self-drilling screws) are shown with red colour to indicate connector elements used to apply load to the members at the ends. Blue lines show screws used to connect the sections to each-other at discrete points along the length. The specimen configurations were labelled during the laboratory tests to make easier referring to them; the same names are used here as well.

Some common characteristics of the specimen and the testing method are as follows:

- four specimen types, consisting of a single C-section, can be considered as primitives of the complex arrangements;

- the number of the bolts and/or screws used at load introduction was calculated based on the estimated load-bearing capacity of the member, but to avoid a local failure at load introduction in many cases more screws are used than necessary;

- in case of built-up sections the specimens are generally made of two sections with the same size and thickness;

- the quality of the assembly of the specimens is comparable to that of the members assembled in a building site, but no initial measurements (e.g.: imperfect shape) were carried out;

- due to the arrangement of the load introduction eccentricity is always present, hence the members are subject to axial compression and bending.

The geometry and dimensions of the sections used are shown in Figure 4 and Table 1. Note that the C-sections are slightly asymmetric, as the flange sizes are not equal.

Section	Total height	Plate thickness	Flange (small)	Flange (large)	Lip	Set where used
C150/1.0	150	1.0	41	47	18.1	1st
C200/1.0	200	1.0	66	74	22.2	1st
C200/1.5		1.5			22.3	2nd
C200/2.0		2.0			22.4	1st, 2nd
C200/2.5		2.5			22.5	2nd
U200	200	1.5	60	60	-	2nd
U200		2.0				
U200		2.5				
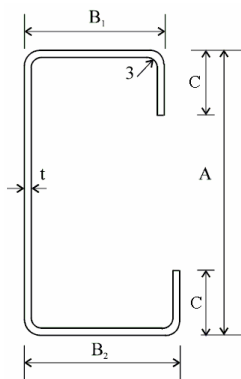
Figure 4: Geometry of the cross-sections.

Table 1: Nominal dimensions of cross-sections [mm].

CompressionC arrangement

This is the simplest arrangement: a single C-section with the load introduced through the end cross-section using an end plate (Figure 5.). Due to the fabrication process the end cut of the member is not perfect, hence the load is introduced primarily through the flanges, the web is not in contact with the end plate. In this only case the endplate was placed on a hinged support that allowed the rotation of the end cross-section in the plane of the testing frame (Figure 6.). Note that the rotation allowed by this arrangement is limited.

Figure 5.: CompressionC arrangement.

Figure 6.: Hinged support.

SimpleC arrangement

This specimen consists of a single C-section with the load introduced at the web using self-drilling screws and a gusset plate (Figure 7., Figure 8.). The internal actions in these kinds of specimens are compression and bending about the minor axis.

Figure 7.: SimpleC arrangement.

Figure 8.: Schematics of the arrangement.

HatC arrangement

This arrangement is based on the SimpleC configuration; the same end support is used, and hat sections are connected to one of the flanges using two self-drilling screws to provide lateral support to the flange (Figure 9., Figure 10.).

Figure 9.: Hole allowing longitudinal motion of the hat section

Figure 10.: Connection of the hat section to the C-section

DoubleC arrangement

This arrangement consists of two C-sections stuck in each-other and connected at their flanges at discrete points; the distances used are 500 mm, 1000 mm, or no screws are used. The load is introduced at both webs using self-drilling screws (Figure 11., Figure 12.). The internal action in these specimens is pure compression.

Figure 11.: DoubleC arrangement.
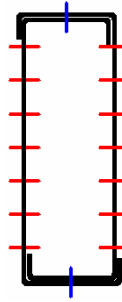
Figure 12.: Schematics of the arrangement.

C arrangement

This arrangement is a modified version of the SimpleC arrangement. In the case of the C arrangement self-drilling screws are used in the flanges and the web as well to introduce the load in the specimen. To achieve this, the gusset plate used with the SimpleC specimens was modified to enable the use of additional screws; the position of the screws in the flanges is variable (Figure 13., Figure 14.). The internal actions in these kinds of specimens are compression and bending about the minor axis.

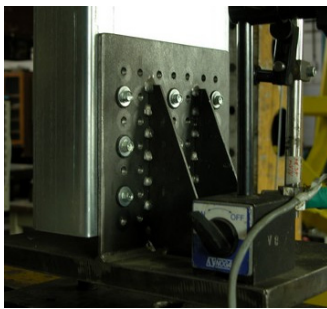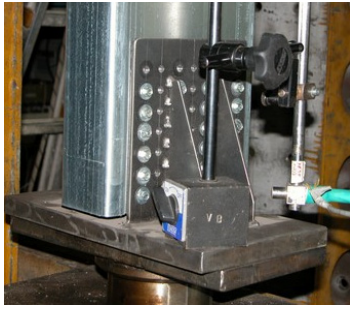Figure 13.: C arrangement.

Figure 14.: Schematics of the arrangement.

CC arrangement

This arrangement is a modified version of the DoubleC arrangement. The specimen is fabricated exactly as in the case of the DoubleC arrangement, and the load is introduced like in the case of the C arrangement: through the web of one of the C-sections and through the flanges (Figure 15., Figure 16.); the gusset plate used with these specimens is the same. The distance of the screws in the flanges are in all cases 500 mm. The internal actions in these kinds of specimens are compression and bending about the minor axis.
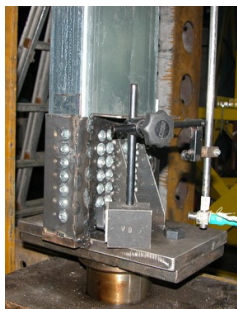
Figure 15.: CC arrangement.

Figure 16.: Schematics of the arrangement.

CU arrangement

This arrangement consists of a C- and a U-section stuck in each-other and connected at their flanges using self-drilling screws each 500 mm. The load is introduced either in the C- or in the U-section through the web and the flanges using the same gusset plate as in the case of the

CC arrangement (Figure 17., Figure 18.). The internal actions in these kinds of specimens are compression and bending about the minor axis.

Figure 17.: CU arrangement.
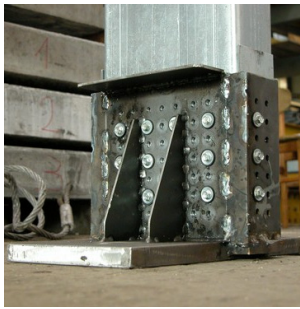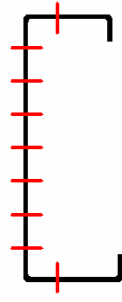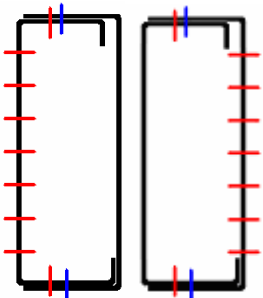

Figure 18.: Schematics of the arrangement.

Brace arrangement

This arrangement consists of a single C-section with the load introduced only in the flanges by means of M12 8.8 grade bolts (Figure 19., Figure 20.) at the half-width of the flanges. The internal actions in these kinds of specimens are compression and bending about the minor axis.

Figure 19.: Brace arrangement.

Figure 20.: Schematics of the arrangement.

IC Column arrangement

This arrangement consists of two C-sections in a back-to-back arrangement (forming an I-shape section) and connected to each-other using self-drilling screws at either three or four cross-sections along the length (distances of 400 mm or 600 mm). The load is introduced in the webs using M12 8.8 grade bolts (Figure 21., Figure 22.). The arrangement may be considered built-up cross-section; the internal actions in these kinds of specimens is pure compression (globally), but compression and bending about the minor axis (with the webs in compression) for the individual members.

Figure 21.: IC Column arrangement.
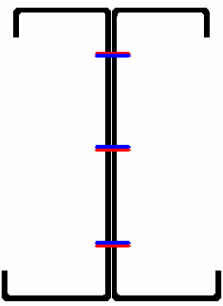
Figure 22.: Schematics of the arrangement.

IC Brace arrangement

This arrangement consists of two C-sections in a back-to-back arrangement and connected to each-other using self-drilling screws at three or four cross-sections along the length, similarly to the IC Column arrangement. In this case the load is introduced in the flanges using M12 8.8

grade bolts (Figure 23., Figure 24.). The arrangement may be considered as built-up cross-section; the internal actions in these kinds of specimens are pure compression (globally), but compression and bending about the minor axis for the individual members.

Figure 23.: IC Brace arrangement.   Figure 24.: Schematics of the arrangement.
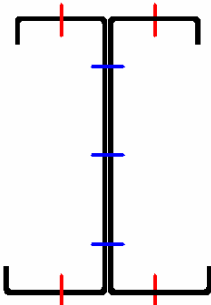
2.2.3. Test programme

To achieve the aims of the first set of tests – code checking and development of design methods for arrangements directly not covered by the standard – a preliminary parametric study using CUFSM [32] was carried out to find the sections and specimen lengths suiting these goals best. The sections chosen were C150/1.0, C200/1.0 and C200/2.0 to represent C-sections with web b/t ratios of 150, 200 and 100, respectively. Figure 25. shows the result of the parametric study for these sections in pure compression: elastic critical force against buckling length, each curve plots the critical force for the given section for buckling lengths ranging 100 mm to 10000 mm obtained as first eigenvalues of the relevant elastic buckling – bifurcation – problem. The local minima of the curves indicate the critical force for a given buckling mode (local, distortional, global), the shape of the buckled cross-sections are obtained as the eigenvectors belonging to the eigenvalues.

Note that the boundary conditions applied to the model are different from the real supporting conditions, as due to the limitations of FSM an accurate modelling of these is not possible; the results provided only insight which lengths are to be used.
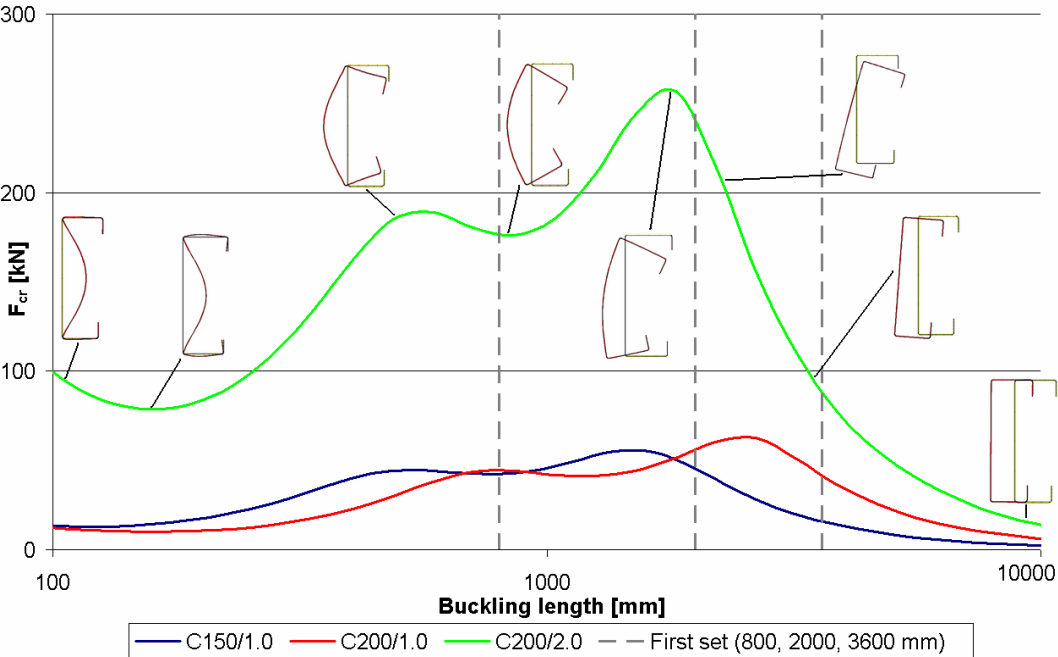
Figure 25: Critical axial force for the sections and buckled shapes.

14

Based on the results of the finite strip analysis in the first set of tests three lengths were chosen to study distortional (l = 800 mm), global (l = 3600 mm) and interacting (l = 2000 mm) stability phenomena. In the second set of tests the lengths used were 1500 and 2500 mm, to provide test results for member lengths usually coming up in practice and provide results for the intermediate member lengths.

The programme of the two test series is summarized in Table 2. In many cases for a given arrangement, section and length more tests are listed; in these cases multiple tests were carried out to double-check a given arrangement, or examine the effect of certain aspects of the specimen (i.e. number of screws used).

Table 2: Test programme.

| First set					Second set			
Length [mm]	Section	Arrange-ment	Test		Length [mm]	Section	Arrange-ment	Test
800	C150/1.0	SimpleC	C03		1500	C200/1.5	SimpleC	C65, C68
		HatC	C07				C	C70
		DoubleC	C10				CC	C75, C78
	C200/1.0	CompC	C05				CU	C76
		SimpleC	C04				Brace	C63
		HatC	C08				IC Column	C85
		DoubleC	C11				IC Brace	C91
	C200/2.0	CompC	C02			C200/2.0	SimpleC	C66, C81, C82
		SimpleC	C01				C	C77
		HatC	C06				CC	C74
		DoubleC	C09				CU	C73
2000	C150/1.0	SimpleC	C14				Brace	C62, C64
		HatC	C18				IC Column	C83, C84, C86, C87
		DoubleC	C21				IC Brace	C90
	C200/1.0	CompC	C16			C200/2.5	SimpleC	C67, C80
		SimpleC	C15				C	C72
		HatC	C19				CC	C71
		DoubleC	C22				CU	C69, C79
	C200/2.0	CompC	C13				Brace	C61
		SimpleC	C12				IC Column	C88
		HatC	C17				IC Brace	C89
		DoubleC	C20		2500	C200/1.5	SimpleC	C40
3600	C150/1.0	SimpleC	C25				DoubleC	C44
		HatC	C29				C	C45, C55, C56
		DoubleC	C32				CC	C43, C47
	C200/1.0	CompC	C27				CU	C46, C54
		SimpleC	C26				Brace	C59
		HatC	C30				IC Column	C94
		DoubleC	C33, C35				IC Brace	C95
	C200/2.0	CompC	C24			C200/2.0	SimpleC	C41
		SimpleC	C23, C34				C	C48
		HatC	C28				CC	C50
		DoubleC	C31, C36, C37				CU	C49
							Brace	C58
							IC Column	C93
							IC Brace	C97, C98
						C200/2.5	SimpleC	C42
							C	C51
							CC	C53
							CU	C52
							Brace	C57, C60***
							IC Column	C92
							IC Brace	C96
							CU	C99*, C100**

C38-C39: no such tests

* different thicknesses:
      C200/2.5 + U200/2.0
** different thicknesses:
      C200/1.5 + U200/2.5
*** test with strain measurement

2.2.4. Definition of behaviour modes

The primary results of the laboratory tests are the observed failure modes and measured load-bearing capacities enabling the development of standard-based design methods. Typical failure modes are presented in Chapter 2.2.5; detailed results – load-bearing capacities, specialities of the tests, failure modes – as well as the results of the material coupon tests are summarized in the Annex, Table A1 – Table A11 for each specimen arrangement.

In Chapter 2.2.5 the test results of specimens with different arrangements are presented in groups based on the similarities in the observed behaviour and failure mode of the specimen. The similarities and differences as well as tendencies are described and discussed in this Chapter group-by-group by means of description of the observed behaviour, figures and typical force-displacement diagrams.

The basis of determining the failure mode of a given specimen is the phenomena observed in the linear and non-linear range of the specimen behaviour. Typically in the tests these were not pure global, distortional (stability), or local (yield or stability) failure modes but in most cases these are coupled. As in the tests the same sections were used and – despite the differences in the arrangement – similar internal forces acted on the specimens, in many cases similar phenomena were observed during the tests. In Chapter 2.2.5 the typical failure modes are presented group-by-group by describing the observed phenomena and illustrating them with figures and force-shortening diagrams. The basis of the grouping is either the arrangement leading to a characteristic behaviour not typical for other arrangements or a governing phenomenon similar for more specimen types. The groups and the specimen arrangements belonging to them and the observed behaviour modes are summarized in Table 3. Specimens in groups A to F exhibit either a global failure mode or a mode typical for a specific arrangement. All specimens with a local failure mode are collected in group G. Note that this grouping aims merely to present the observed failure modes and their characteristics summarized, hence not all specimens with a given configuration are necessarily in the same group (i. e.: SimpleC specimens are in group A and G as well).

Table 3: Behaviour modes and grouping.

Group	Specimen types	Typical behaviour mode
A	SimpleC, CompressionC, C	Interaction of flexural buckling and bending
B	CC, DoubleC, CU	Interaction of distortional buckling, flexural buckling and bending
C	Brace	Interaction of distortional buckling and flexural buckling
D	IC Brace	Distortional buckling
E	IC Column	Interaction of local buckling and flexural buckling of chord member
F	HatC	Interaction of distortional buckling and yielding failure
G	Local failure modes	Local failure at load introduction; joint failure and/or web crippling, plate buckling

2.2.5. Characteristics of behaviour modes

Group A

The test specimens in this group are all subject to axial compression and bending – resulting from the eccentricity of the load – about the minor axis, with the web in compression. From the behaviour point-of-view the difference between the arrangements is the magnitude of the eccentricity: in the case of CompressionC specimens the load is centric, SimpleC sections have clearly the greatest eccentricity as the load is introduced in the web, whilst specimens with a C arrangement – screws in the web and the flanges as well – have an eccentricity between these two extreme values.

The typical behaviour of the specimens of group A is following: first, local buckling of the web (Figure 26.) occurs, which is followed by the flexural buckling of the member about its minor axis (Figure 27.). The final failure is plastic plate buckling at the member half-length (Figure 28.). Figure 29. shows the force-shortening diagram of test specimens of the same section, with arrangements CompressionC, C, SimpleC (C13, C48 and C41, respectively). In case of the CompressionC specimens in some cases plastic plate buckling was observed at the end of the member, as a result of the non-uniform load introduction. The diagram shows the effect of the differences in the load introduction: the more centric the load is introduced the higher the load-bearing capacity is. Note, that in case of test C13 the specimen length is 2000 mm, in the other two cases it is 2500 mm.

Figure 26.:Local buckling in the web.

Figure 27.: Bending/flexural buckling.
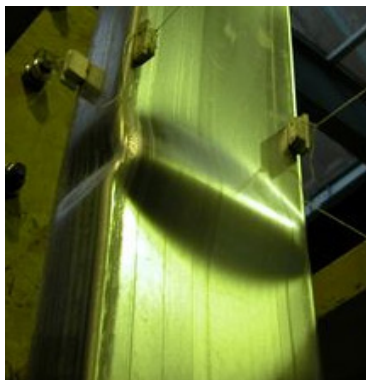
Figure 28.: Plastic mechanism in the web and flange.
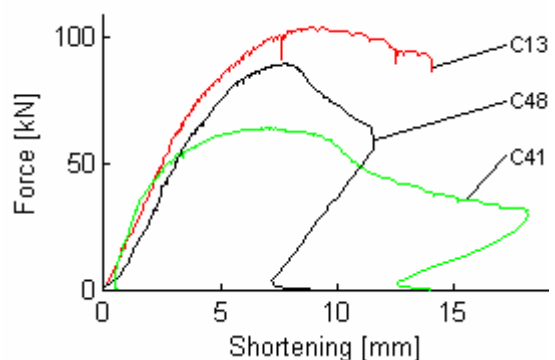
Figure 29.: Force-shortening diagrams.

Group B

The test specimens in this group are all built-up cross-sections made by sticking two sections in each-other to form a box section and – except for tests C35 and C36 – fastening them together at their flanges using self-drilling screws. The load introduction however is not the same: centric in the case of DoubleC test specimens, eccentric in the other two cases.

The main characteristics of the stability behaviour of these specimens are the same. First, local buckling of one of the webs occurred (in case of CC and CU specimens it is the loaded web) followed by flexural buckling. Due to the buckled shape one side of the specimens is in compression, the other one in tension (Figure 30., tension and compression side of C32). In the case of CU specimens local buckling of the part of the flange on the compression side of the member was observed as well (Figure 31.). Note that not the members of the specimen are in compression and tension but the sides of the specimen as it works as a box section.
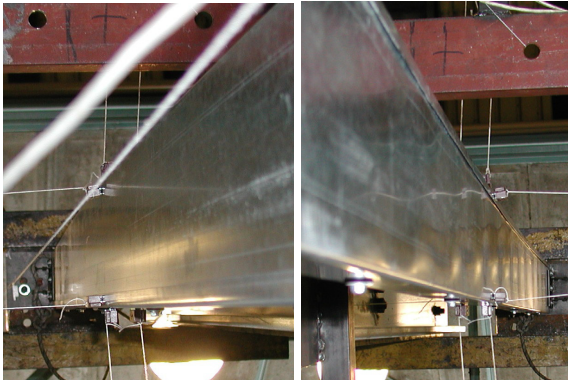
Figure 30.: Tension and compression sides (DoubleC).

Figure 31.: Local buckling (CU).

The first sign of the imminent failure was in all cases the slowly evolving distortional buckling preceded in case of DoubleC and CC specimens by the pop-out of the lip of the flange on the compression side of the column (Figure 32.). In the case of the CU specimens the distortional buckling was immediately followed by the plastic local buckling of both members of the specimen at the half member length (Figure 33.); the final failure of CC and DoubleC specimen was of the same type, but happened less abruptly. In the case of DoubleC specimens plastic yield mechanism was also observed at the specimen ends, as a result of the restrained rotations.

Figure 32.: Local and distortional buckling (CC, DoubleC).

Figure 33.: Plastic mechanism (CU).

Group C

Specimens of type Brace are single specimens with load introduction at the middle of the flanges using metric bolts providing significant restraint against rotation. The resulting internal actions are axial compression and bending about the minor axis, with the web in tension. In all tests flexural buckling occurred but no local buckling of the web was observed. The first sign of failure was the distortional buckling of the smaller flange followed of the section by the pop-out of the lip of this flange near the middle of the column (Figure 34.) and the lateral buckling of the whole flange (Figure 35.) causing loss in the load-bearing capacity but no collapse due to the restrained rotations at the end and the still working larger flange. After this the same phenomenon occurred to the larger flange leading to the final failure of the specimen (Figure 36., Figure 37.).

Figure 34.: Distortional buckling.

Figure 35.: Distortional and flexural buckling.

Figure 36.: Failure.
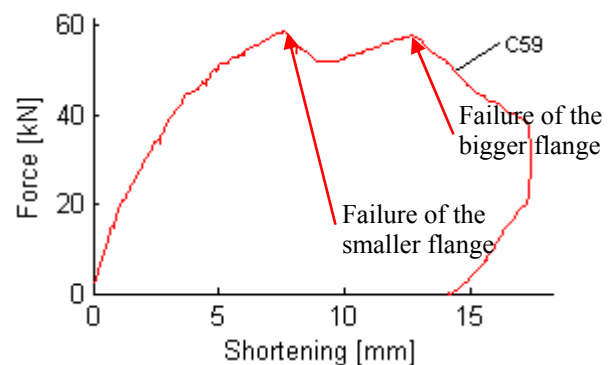
Figure 37.: Force-shortening diagram.

Group D

IC Brace specimens may be considered closely spaced built-up members of two Brace specimens in a back-to-back arrangement, connected at their webs. This arrangement is favourable, since the members tend to buckle towards their webs, thus they provide each-other lateral support resulting in a synergic effect. Due to this support and the symmetrical arrangement the specimen is in pure compression; local buckling of the webs was observed in all cases (Figure 38.). This was followed by the distortional buckling of the flanges of one of the members at the end or at the middle of the specimen (Figure 39., Figure 40.), which led to the forming of a yield mechanism in the flanges of this member. This was followed by the similar failure of the other C-section as it therefore lost its lateral support. The load level was maintained in this case as well after failure (Figure 41.), due to the restrained rotations at the end.

Figure 38.: Local buckling in the web.

Figure 39.: Distortional buckling.
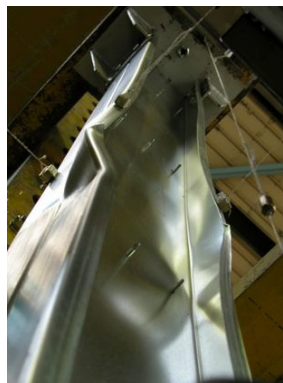
Figure 40.: Failure of one section.
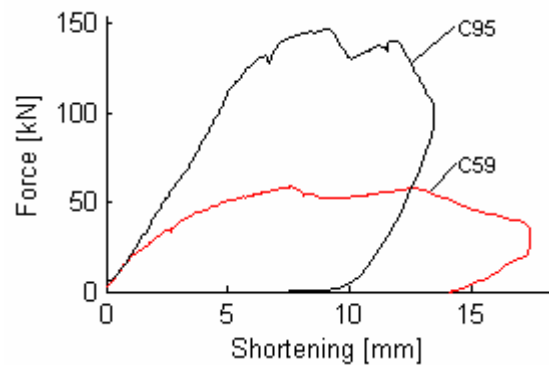
Figure 41.: Force-shortening diagrams.

Group E

IC Column specimens – two C-sections in back-to-back arrangement connected at the webs using self-drilling screws and with load introduction in the webs by means of metric bolts – may also be considered as closely spaced built-up cross-sections. During the loading process local buckling of the webs was observed. The buckling waves in the webs were not in unison, as the chords of this built-up section tended to move away from each other between the connecting self-drilling screws (Figure 42.); this can be considered as flexural buckling of the chord members about the minor axis. No significant global vertical deflections as indication of global flexural buckling were observed during the testing. The failure of the specimens was induced by a plastic yield mechanism at the position of the connecting screws (Figure 43.) leading to plastic plate buckling in one of the members (Figure 44.) at the web-flange junctions. This was followed by the failure of the whole specimen, as the failed member left the other one unbacked. A typical force-shortening diagram is shown on Figure 45.

Figure 42.: Members moving in opposite directions.

Figure 43.: Failure mechanisms at the screws.

20

Figure 44.: Yield mechanism.
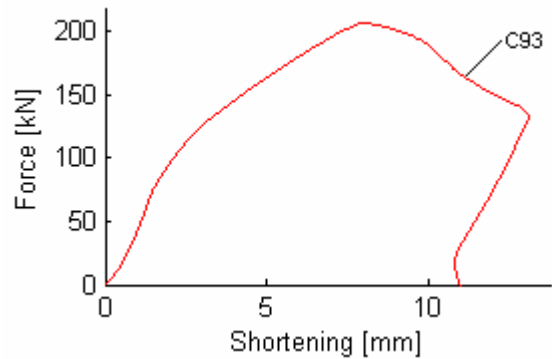
Figure 45.: Force-shortening diagram (C93).

Group F

HatC sections are the ones similar to SimpleC sections, but with lateral support provided by a hat section each 500 mm on one of the flanges. The first sign of the applied load on this type of specimens is the local buckling of the web of the section. The observed stability behaviour in the case of HatC specimens is the distortional buckling of the free flange; the hat sections restrained the displacements of the other flange (Figure 46.). The final failure was in all tests caused by a plastic mechanism in the web-flange joint above the load introduction zone with approximately equal measured load-bearing capacities for a given section; based on this, the failure mode is yield failure (Figure 47.).
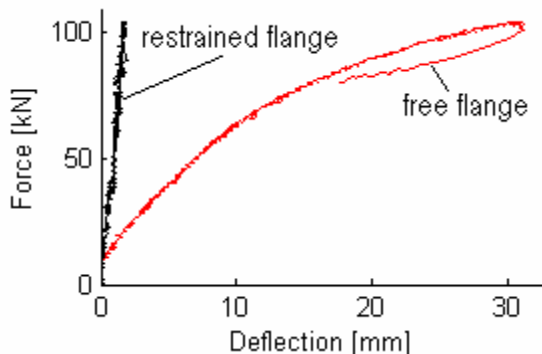
Figure 46.: Vertical in-plane deflections of the free and the supported flange.

Figure 47.: Failure of specimen.

Group G

All specimens exhibiting a local failure in the load introduction area causing the loss of load-bearing capacity are in this group; these are the specimens with a length of 800 mm and some longer specimens. Although being in the same group, this does not mean all local modes are similar, neither do they have the same cause.

Short specimens (all of them except for HatC and CompressionC types), due to the high expected load-bearing capacity are fitted with up to 98 self-drilling screws at one end of the specimen to avoid screw failure, resulting in a stub column. In the case of these specimens plastic plate buckling was observed in some cases in interaction with screw failure. On DoubleC specimens in most such cases plastic mechanisms with a complex shape were observed. In the case of CompressionC members, even if the failure was global mode, a certain amount of plastic deformation was usually observed at the load introduction (C02, C05, C16). SimpleC members, even if the number of screws was enough, if the screw layout

21

was short and wide (relative to the member length), local failure occurred (C68, C04). Figure 48 – Figure 51. show typical local failures.

Figure 48.: Plastic mechanism at the load introduction (SimpleC, C01).

Figure 49.: Plastic mechanism at the load introduction (DoubleC, C09).

Figure 50.: Plastic mechanism at the load introduction (CompressionC, C05).

Figure 51.: Plastic mechanism at load introduction (short screw layout, C68).

2.3. Evaluation of the test results

2.3.1. Test-based design resistances

In this Chapter the test-based design resistances calculated using the method provided by EC3 are presented and shortly discussed. Test based resistances are to be calculated as:

$$R_{adj} = R_{obs} / \mu_R \qquad (1)$$

where:

$$\mu_R = \left(\frac{f_{yb,obs}}{f_{yb}}\right)^{\alpha} \cdot \left(\frac{t_{obs,cor}}{t_{cor}}\right)^{\beta} \qquad (2)$$

R_{adj} the adjusted resistance of the load-bearing capacity,

R_{obs} the measured load-bearing capacity,

where:

$f_{yb,obs}$ the measured value of yield stress,

f_{yb} the nominal value of yield stress,

$t_{obs,cor}$ the measured value of plate thickness,

t_{cor} the nominal value of plate thickness (without coating),

$\alpha = 1$ if $f_{yb,obs} > f_{yb}$, otherwise $\alpha = 0$,

$\beta = 1$ if $t_{obs} \leq t$ or $b_p/t \leq (b_p/t)_{lim}$,

$\beta = 2$ $b_p/t > 1.5 \cdot (b_p/t)_{lim}$,

for intermediate values β is to be calculated using linear interpolation.

$$(b_p / t)_{lim} = 0.64 \cdot \sqrt{\frac{E \cdot k_\sigma}{f_{yb}}} \cdot \sqrt{\frac{f_{yb} / \gamma_{M1}}{\sigma_{com,Ed}}} \qquad (3)$$

where:

b_p nominal width of the plate,

k_σ value of the buckling factor,

$\sigma_{com,Ed}$ largest calculated compression stress in the element at failure.

The test-based design value: $R_d = \eta_{sys} \cdot R_k / \gamma_M$,   (4)

where:

η_{sys} =1.0, conversion factor for differences in behaviour under test conditions and service conditions.

γ_M the partial factor for resistance.

The characteristic value of design resistance, based on one test: $R_k = 0.9 \cdot \eta_k \cdot R_{adj}$ (5)

where:

η_k =0.9, if yielding failure,

=0.8, if local buckling,

=0.7, global stability phenomenon.

The following values apply to the tests carried out:

η_k =0.75 if in the test local and global phenomena was observed, 0.90 otherwise.

$\gamma_M = \gamma_{M1} = 1.0$,

$f_{yb} = 350$ MPa,

$\sigma_{com,Ed} = 350$ MPa.

The calculated test-based design resistances are to be found in Table 4.

Table 4: Test-based design values.

Test	R$_{obs}$ [kN]	μ$_R$	R$_{adj}$ [kN]	η$_k$	R$_d$ [kN]	Ratio R$_{obs}$/R$_d$	Test	R$_{obs}$ [kN]	μ$_R$	R$_{adj}$ [kN]	η$_k$	R$_d$ [kN]	Ratio R$_{obs}$/R$_d$
C01	85.92	1.09	78.70	0.75	53.12	1.62	C51	113.05	1.24	91.13	0.75	61.51	1.84
C02	133.57	1.09	122.34	0.75	82.58	1.62	C52	146.21	1.24	117.86	0.75	79.55	1.84
C03	18.05	0.98	18.43	0.75	12.44	1.45	C53	182.27	1.24	146.93	0.75	99.18	1.84
C04	21.86	0.98	22.20	0.75	14.99	1.46	C54	68.37	1.15	59.42	0.75	40.11	1.70
C05	35.91	0.98	36.47	0.75	24.62	1.46	C55	55.38	1.15	48.13	0.75	32.49	1.70
C06	94.19	1.09	86.27	0.90	69.88	1.34	C56	56.16	1.15	48.81	0.75	32.94	1.70
C07	21.90	0.98	22.36	0.90	18.11	1.21	C57	166.90	1.24	134.54	0.75	90.81	1.84
C08	19.36	0.98	19.66	0.90	15.92	1.22	C58	108.97	1.20	91.08	0.75	61.48	1.77
C09	200.78	1.09	183.90	0.75	124.13	1.62	C59	58.17	1.15	50.55	0.75	34.12	1.70
C10	55.27	0.98	56.44	0.75	38.10	1.45	C60	166.26	1.24	134.02	0.75	90.46	1.84
C11	47.28	0.98	48.02	0.75	32.41	1.46	C61	181.20	1.24	146.06	0.75	98.59	1.84
C12	71.11	1.09	65.13	0.75	43.96	1.62	C62	116.85	1.20	97.67	0.75	65.93	1.77
C13	104.34	1.09	95.57	0.75	64.51	1.62	C63	81.61	1.15	70.92	0.75	47.87	1.70
C14	12.50	0.98	12.76	0.75	8.62	1.45	C64	129.12	1.20	107.93	0.75	72.85	1.77
C15	24.16	0.98	24.54	0.75	16.56	1.46	C65	52.26	1.15	45.42	0.75	30.66	1.70
C16	25.62	0.98	26.02	0.75	17.56	1.46	C66	78.97	1.20	66.01	0.75	44.56	1.77
C17	93.81	1.09	85.92	0.90	65.60	1.43	C67	111.10	1.24	89.56	0.75	60.45	1.84
C18	20.49	0.98	20.92	0.90	16.95	1.21	C68	38.53	1.15	33.48	0.75	22.60	1.70
C19	22.14	0.98	22.49	0.90	18.22	1.21	C69	179.20	1.24	144.45	0.75	97.50	1.84
C20	219.02	1.09	200.60	0.75	135.41	1.62	C70	58.91	1.15	51.20	0.75	34.56	1.70
C21	45.78	0.98	46.75	0.75	31.56	1.45	C71	214.10	1.24	172.58	0.75	116.49	1.84
C22	58.66	0.98	59.58	0.75	40.22	1.46	C72	123.90	1.24	99.87	0.75	67.42	1.84
C23	46.77	1.09	42.84	0.75	28.92	1.62	C73	109.80	1.20	91.78	0.75	61.95	1.77
C24	53.16	1.09	48.69	0.75	32.87	1.62	C74	155.60	1.20	130.06	0.75	87.79	1.77
C25	9.47	0.98	9.67	0.75	6.53	1.45	C75	91.43	1.15	79.46	0.75	53.63	1.70
C26	17.24	0.98	17.51	0.75	11.82	1.46	C76	74.63	1.15	64.86	0.75	43.78	1.70
C27	24.65	0.98	25.04	0.75	16.90	1.46	C77	87.76	1.20	73.36	0.75	49.52	1.77
C28	104.25	1.09	95.48	0.90	77.34	1.35	C78	92.45	1.15	80.34	0.75	54.23	1.70
C29	21.81	0.98	22.27	0.90	18.04	1.21	C79	213.00	1.24	171.70	0.75	115.90	1.84
C30	23.55	0.98	23.92	0.90	19.38	1.22	C80	114.24	1.24	92.09	0.75	62.16	1.84
C31	150.87	1.09	138.18	0.75	93.27	1.62	C81	79.23	1.20	66.23	0.75	44.70	1.77
C32	26.04	0.98	26.59	0.75	17.95	1.45	C82	78.86	1.20	65.92	0.75	44.49	1.77
C33	58.00	0.98	58.91	0.75	39.76	1.46	C83	205.00	1.20	171.35	0.75	115.66	1.77
C34	46.67	1.09	42.75	0.75	28.85	1.62	C84	213.40	1.20	178.37	0.75	120.40	1.77
C35	56.17	0.98	57.05	0.75	38.51	1.46	C85	132.80	1.15	115.41	0.75	77.90	1.70
C36	140.44	1.09	128.63	0.75	86.83	1.62	C86	190.00	1.20	158.82	0.75	107.20	1.77
C37	180.67	1.09	165.48	0.75	111.70	1.62	C87	236.60	1.20	197.77	0.75	133.49	1.77
C38	-	-	-	-	-	-	C88	-	-	-	-	-	-
C39	-	-	-	-	-	-	C89	-	-	-	-	-	-
C40	41.02	1.15	35.65	0.75	24.06	1.70	C90	291.70	1.20	243.82	0.75	164.58	1.77
C41	63.99	1.20	53.49	0.75	36.10	1.77	C91	174.40	1.15	151.56	0.75	102.30	1.70
C42	94.34	1.24	76.05	0.75	51.33	1.84	C92	-	-	-	-	-	-
C43	62.76	1.15	54.54	0.75	36.82	1.70	C93	207.10	1.20	173.11	0.75	116.85	1.77
C44	131.80	1.15	114.54	0.75	77.31	1.70	C94	138.80	1.15	120.62	0.75	81.42	1.70
C45	53.76	1.15	46.72	0.75	31.54	1.70	C95	146.70	1.15	127.49	0.75	86.06	1.70
C46	98.87	1.15	85.92	0.75	58.00	1.70	C96	-	-	-	-	-	-
C47	97.23	1.15	84.50	0.75	57.04	1.70	C97	239.20	1.20	199.94	0.75	134.96	1.77
C48	98.61	1.20	82.43	0.75	55.64	1.77	C98	323.40	1.20	270.32	0.75	182.47	1.77
C49	111.45	1.20	93.16	0.75	62.88	1.77	C99	126.20	1.24	101.73	0.75	68.67	1.84
C50	146.41	1.20	122.38	0.75	82.61	1.77	C100	71.55	1.15	62.18	0.75	41.97	1.70

The calculated design resistances are based on the result of one test in each case. The obtained values of the ratio real/test-based resistances – which can be considered as the partial safety of the resistance – range from 1.21 to 1.86, with a mean of 1.67 – the lowest values belong to the HatC sections – , pointing to generally very conservative design.

2.3.2. Comparative analysis of the test results

In this Chapter the test results are evaluated by comparing them to each-other using the measured load-bearing capacities, force-dispacement curves and the test-based design resistances calculated in Chapter 2.3.1. Part of the comparisons aim the study of a given property to highlight the effects governing the behaviour of the studied arrangement. The majority of the comparisons are carried out to show the tendencies between two similar arrangements by comparing the test-based design resistances of members with the same cross-section and length but different arrangement, thus, provide a basis to the development of EC3-based design methods. The basis of these comparisons is in most cases arrangement SimpleC, Brace or CompressionC as these arrangements can be considered as primitives of the more complex arrangements. Note that meaningful comparisons are possible only between members of groups A to E according to the grouping of Chapter 2.2.4, since these all failed in a global mode. However, to give a full overview on the test results specimens with local failure modes are included in the comparisons; these tests are marked with an asterisk. Direct comparison of specimens with local failure modes are not carried out, as these are usually different (e.g. in the case of DoubleC and SimpleC specimens).

In the tables the measured ultimate load of the specimens is denoted with R_t; R_{t-b} stands for the test-based design resistance.

A comparison between specimens of arrangement SimpleC differing only in the number of screws used at load drive-in is shown in Table 5 with explanation in Figure 52. Force-shortening and force-horizontal deflection diagrams for the same specimens are shown in Figure 53. and Figure 54. It is observed, that the failure mode and the load-bearing capacity are not affected by the number of the screws used, but the axial rigidity of the specimen is increasing with the increasing screw number.

The comparison shows, that the number of screws does not affect the buckling length of the members, but the screws provide an elastic support in the axial direction; the stiffness of this support is proportional with the number of the screws.

Table 5: Effect of different screw numbers.

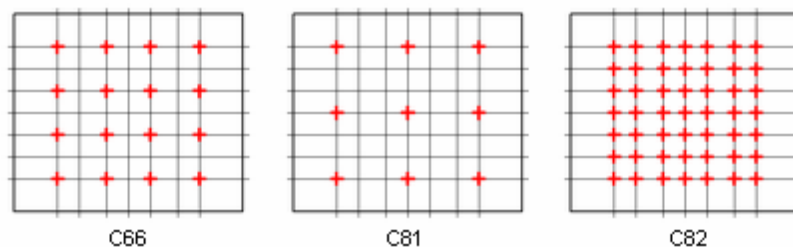| Test	Section	Length [mm]	R_t [kN]	Number of screws
C66			78.97	4x4
C81	C200/2.0	1500	79.23	3x3
C82			78.86	7x7

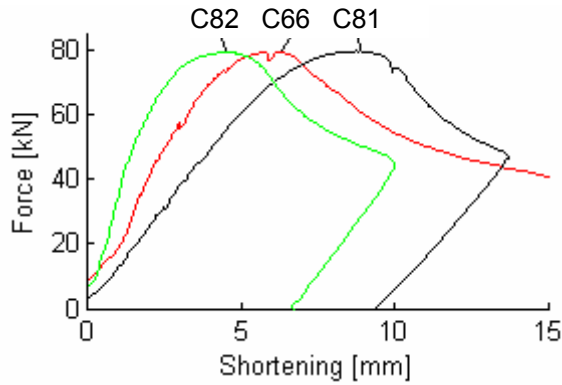Figure 52.: Positioning of the screws at load drive-in.

Figure 53.: Effect of screw number in the web; force-shortening diagrams.
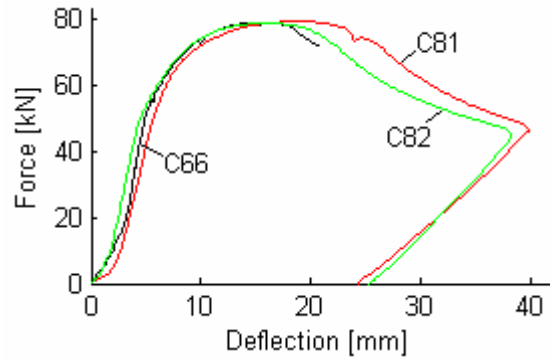
Figure 54.: Effect of screw number in the web – in-plane horizontal deflections.

Adding screws in the flanges results increased load-bearing capacity, as shown by the comparison of test results of specimens with SimpleC and C arrangement (Table 6). In case of 1500 mm long specimens the increase is ~10 %, 2500 mm long specimens with a C arrangement have 20 to 40 % higher load-bearing capacity than their SimpleC counterparts. The position and number of the screws (Figure 55.) in the flanges, once they are used has little effect on the load-bearing capacity, as shown by the design resistances in Table 7.

Table 6: Comparison of test-based load-bearing capacity of SimpleC and C specimens.

Length [mm]	Section	SimpleC		C		$R_{t-b,C}$ / $R_{t-b,SimpleC}$
		Test	$R_{t-b,SimpleC}$ [kN]	Test	$R_{t-b,C}$ [kN]	
1500	C200/1.5	C65	30.66	C70	34.56	1.13
	C200/2.0	C66	44.56	C77	49.52	1.11
	C200/2.5	C67	60.45	C72	67.42	1.12
2500	C200/1.5	C40	24.06	C45	31.54	1.31
	C200/2.0	C41	36.10	C48	50.56	1.40
	C200/2.5	C42	51.33	C51	61.51	1.20

Table 7: Effect of the number and position of screws used in the flange at load drive-in.

Length [mm]	Section	Test	R_t [kN]	Screws		
				Web	Flange (at web)	Flange (at lip)
2500	C200/1.5	C40	41.02	3x3	-	-
		C45	53.76	3x4	3x1	-
		C55	55.38	4x4	-	4x1
		C56	56.16	4x4	4x1	4x1

Figure 55.: Position of the screws.

The force-shortening diagrams show, that the initial stiffness of the specimens is not affected by the screws used in the flanges. However, the linear behaviour of the C specimens is maintained to a higher load level resulting in the higher load-bearing capacity (Figure 56, Figure 57).

26

Figure 56.: Effect of screw position in the flange; force-shortening diagrams.

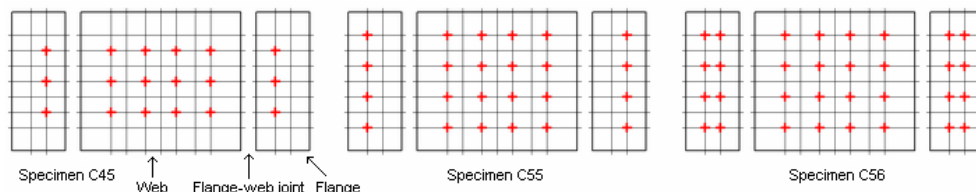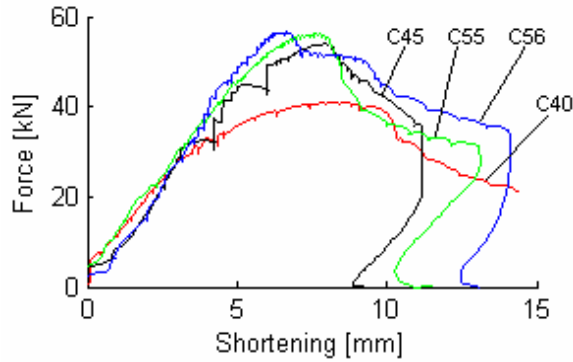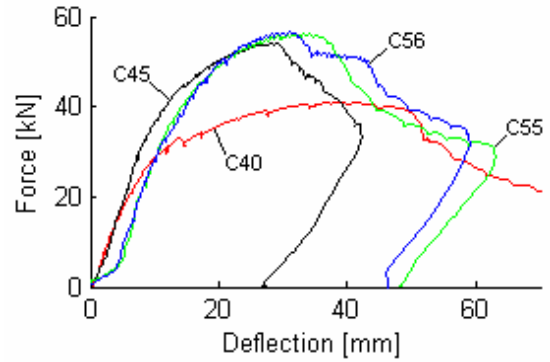Figure 57.: Effect of screw position in the flange – in-plane horizontal deflections.

Based on the comparisons above, the following statements can be made on members with a given section of C or SimpleC arrangement: i) the initial rigidity is not influenced by the number and position of the screws in the flanges, ii) the load-bearing capacity is higher by 10 to 40% if the load is introduced in the web and the flanges as well, compared to the arrangement where only the web is used to introduce load. Thus, neither in case of C, nor in case of SimpleC specimens, if screw failure is not dominant, the number of screws used does not increase the load bearing capacity. On the other hand, the load-bearing capacity of a single C-section can be increased by using C arrangement instead of SimpleC.

Comparing results of C, CU and CC specimens the increase of the load-bearing capacities resulting from the "added" U- and C-sections and screws in the flanges can be analyzed. According to the test results by strengthening a C-section with a U-section of same thickness increases the load-bearing capacity of the specimen by 13 to 45%. An added C-section provides an increase of 49 to 78% (Table 8). The relatively big scatter in the ratios is the result of the section geometries: C-sections are asymmetric but the difference in the flange size is bigger than the plate thickness, hence the assembled specimens may be less or more slender within limits.

Table 8: Effect of the number and position of screws used in the flange at load drive-in.

Length [mm]	Section	Test			Test-based design resistance [kN]			$R_{t\text{-}b,CU}$ / $R_{t\text{-}b,C}$	$R_{t\text{-}b,CC}$ / $R_{t\text{-}b,C}$
		C	CU	CC	$R_{t\text{-}b,C}$	$R_{t\text{-}b,CU}$	$R_{t\text{-}b,CC}$		
1500	C200/1.5	C70	C76	C75	34.56	43.78	53.63	1.27	1.55
	C200/2.0	C77	C73	C74	49.52	61.95	88.36	1.25	1.78
	C200/2.5	C72	C69	C71	67.42	97.50	116.49	1.45	1.73
2500	C200/1.5	C45	C54	C47	31.54	40.11	57.04	1.27	1.81
	C200/2.0	C48	C49	C50	55.64	62.88	82.61	1.13	1.49
	C200/2.5	C51	C52	C53	61.51	79.55	99.18	1.29	1.61

In tests on CU specimens two types of specimen arrangements were studied: by default, the load was introduced in the web of the C-section, but in two tests the load was introduced to the U-section. This inverse arrangement results in a 19 to 45% higher load-bearing capacity (Table 9, Figure 58.), hence this arrangement is favourable. The difference is the result of the stiffened flange of the C-section being on the compression side in the case of the inverse arrangement, whereas in the default arrangement it is the unstiffened flange of the U-section that is in compression.

Table 9: Comparison of normal and inverse CU arrangements.

Length [mm]	Section	Test arrangement		R_t [kN]		Ratio (Inverse/ Normal)
		Inverse	Normal	Normal	Inverse	
1500	C200/2.5	C79	C69	213.00	179.20	1.19
2500	C200/1.5	C46	C54	98.87	68.37	1.45

Two tests were carried out to investigate CU arrangements where the thickness of the C- and U-sections is not equal. Figure 59. shows the result of using the same C-section with a U-section of the same (C52) and smaller thickness (C99) resulting lower rigidity and load-bearing capacity (note that the number of screws used at load drive-in is the same).
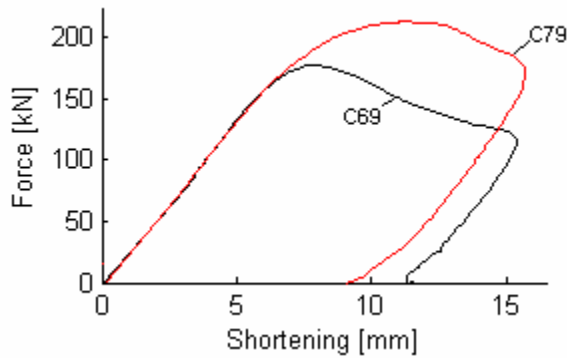
Figure 58.: Default (C69) and inverse CU arrangement (C79).
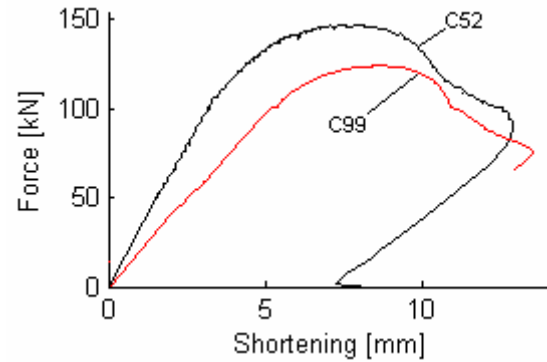
Figure 59.: Effect of non-equal plate thicknesses in case of CU arrangement.

The comparison of SimpleC and IC Column arrangements is shown in Table 10. The load-bearing capacity of the IC Column specimens is 141% to 224% higher (non-relevant failure modes are not taken into account) than that of the SimpleC specimens, the ratios increase with the increasing specimen slenderness.

Table 10: Comparison of SimpleC and IC Column arrangements.

Length [mm]	Section	Test		Test-based design resistance [kN]		$R_{t-b,IC Column}$ / $R_{t-b,SimpleC}$
		SimpleC	IC Column	$R_{t-b,SimpleC}$	$R_{t-b,IC Column}$	
1500	C200/1.5	C65	C85	30.66	77.90	2.54
	C200/2.0	C66	C86	44.56	107.20	2.41
	C200/2.5	C67	C88	60.45	*	-
2500	C200/1.5	C40	C94	24.06	74.61	3.10
	C200/2.0	C41	C93	36.10	116.85	3.24
	C200/2.5	C42	C92	51.33	*	-

* bolt shear failure

The comparison of Brace and IC Brace specimens is shown in Table 11 (non-relevant ultimate load values are omitted). The ratios show no clear tendencies, but doubling the cross-section yields double load-bearing capacity: IC Brace members have 196 to 250% of the load-bearing capacity of the pertinent Brace members.

The difference in the obtained tendencies of Brace/IC Brace and C/IC Column arrangements is the result of the behaviour modes obtained in the tests. In the case of both built-up sections the behaviour of the individual members is basically the same as that of their single counterparts. This leads in the case of IC Column specimens to the members trying to separate from each-other, but the connecting self-drilling screws keep them together, reducing the buckling length and second-order effects.

28

Table 11: Comparison of Brace and IC Brace arrangements.

Length [mm]	Section	Test		Test-based design resistance [kN]		$R_{t\text{-}b,\text{IC Brace}}$ / $R_{t\text{-}b,\text{Brace}}$
		Brace	IC Brace	$R_{t\text{-}b,\text{Brace}}$	$R_{t\text{-}b,\text{IC Brace}}$	
1500	C200/1.5	C63	C91	47.87	93.74	1.96
	C200/2.0	C62	C90	65.93	164.58	2.50
	C200/2.5	C61	C89	98.59	*	-
2500	C200/1.5	C59	C95	34.12	78.85	2.31
	C200/2.0	C58	C97	61.48	134.96	2.20
	C200/2.5	C57	C96	90.81	*	-

* insufficient hydraulic jack capacity

In the case of IC Brace members the connecting screws have little effect; the members of the specimen tend to move towards each-other and provide support – and so reduce the second-order effects – but the lips stiffening the flanges are unsupported, just in the case of the Brace specimen and the failure is caused by the same phenomenon, hence the higher load-bearing capacity is mainly the result of the doubled cross-sectional area.

The design resistances obtained in the tests with HatC arrangement show little variation for a given section type which points to yielding failure in case of these specimens. The test results are summarized in Table 12.

Table 12: Results of HatC specimens.

Length [mm]	Section	Test	$R_{t\text{-}b,\text{HatC}}$ [kN]	Mean of $R_{t\text{-}b,\text{HatC}}$ [kN]
800	C150/1.0	C07	18.11	17.70
2000		C18	16.95	
3600		C29	18.04	
800	C200/1.0	C08	15.92	17.84
2000		C19	18.22	
3600		C30	19.38	
800	C200/2.0	C06	69.88	70.94
2000		C17	65.60	
3600		C28	77.34	

The comparison of CompressionC and DoubleC specimens in Table 13 shows that in cases, where no local failure is observed DoubleC members have the 210 to 284 % load-bearing capacity of their counterparts. In case of local failure the ratio is much lower, as in the case of DoubleC members usually one of the C-sections failed, the deformations on the other section were a consequence of the composite action.

Table 13: Comparison of CompressionC and DoubleC arrangements

Length [mm]	Section	Test		Test-based design resistance [kN]		$R_{t\text{-}b,\text{DoubleC}}$ / $R_{t\text{-}b,\text{CompressionC}}$
		CompressionC	DoubleC	$R_{t\text{-}b,\text{CompressionC}}$	$R_{t\text{-}b,\text{DoubleC}}$	
800	C150/1.0	-	C10*	-	38.10	-
2000		-	C21	-	31.56	-
3600		-	C32	-	17.95	-
800	C200/1.0	C05*	C11*	24.62	32.41	1.32
2000		C16*	C22*	17.56	40.22	2.29
3600		C27	C33	16.9	39.76	2.35
800	C200/2.0	C02*	C09*	82.58	124.13	1.50
2000		C13	C20	64.51	135.41	2.10
3600		C24	C31	32.87	93.27	2.84

2.4. Application rule-based design approach

2.4.1. Introduction

As described in Chapter 1.3, the standard to design cold-formed members to date in Hungary is MSZ EN 1993-1-3:2006 (in the following: EC3-1-3:2006), which was preceded by ENV1993-1-3:1996 (in the following: EC3-1-3:1996), the pre-norm version of the currently operational standard. The basic principles of the two codes are the same, however, the method of calculating cross-sectional properties and application rules to design compression members have been changed on several points.

In Chapter 2.4 the basic principles of calculation are presented alongside with the application rules relevant for the laboratory tests for both versions of the standard. Design resistances calculated using these rules are compared to the test results, conclusions are drawn regarding the applicability of the formulae and accuracy of the results. Modifications on the formulae of the application rules are proposed to ensure a non-conservative yet safe design of the arrangements studied in the laboratory tests.

2.4.2. Summary of design principles

The application rules of both versions of EC3-1-3 for the design resistance of members in compression or compression and bending for ultimate limit state (ULS) is similar to the method provided by EC3-1-1 for class 4 cross-sections in its principles: the member resistances are to be determined using cross-sectional properties derived taking into account local stability phenomena of the cross-section. The properties are calculated in an often lengthy iterative process that takes into account local and distortional buckling of the cross-section and accounts for the change in stress distribution due to the change of the effective cross-section. Hence, two stability failure modes are taken into account on a cross-section level and included in all further checking procedures.

Both in case of cross-section and stability failure modes interaction formulae are used to calculate the utilisation of the members. The properties of the effective cross-section are to be determined for all pure cases of internal actions; in the case of a cross-section without symmetry this yields an effective area for compression, and four section moduli for bending about each principal axis. The shift of the centroid, that is, the distance of the centroid of the gross and the effective cross-section for pure compression resulting bending is always taken into account.

As the calculation of the effective cross-section and its properties is complex, in the practice these are pre-calculated and used in form of tables, or, as it is common practice in the case of building systems the load-bearing capacities are calculated for typical arrangements and provided to the designers as design tool or implemented in software.

The cross-sectional properties used in the calculations in this Chapter were determined by the program of Sándor Ádány; the values are included in the Annex, Table A13 – Table A14. Note, that the two versions of the standard allow different approaches to calculate these properties e.g. on how radii in the corners and iterations are carried out, resulting in slightly different numerical values of cross-sectional properties.

2.4.3. Relevant EC3 application rules

The application rules relevant from the laboratory tests point-of-view are presented in this Chapter: failure due to axial compression and bending moment, and interaction of flexural buckling and bending moment. Note that these do not cover all specimen arrangements – only

the arrangements where a single section is used are covered directly – and some failure modes (e.g. local failure modes of the load introduction area) are not handled.

Cross-section failure of members in compression and bending according to EC3-1-3:1996 are to be calculated as follows:

$$\frac{N_{Ed}}{f_{yb} \cdot A_{eff} / \gamma_{M0}} + \frac{M_{y,Ed} + \Delta M_{y,Ed}}{f_{yb} \cdot W_{eff,y,com} / \gamma_{M0}} + \frac{M_{z,Ed} + \Delta M_{z,Ed}}{f_{yb} \cdot W_{eff,z,com} / \gamma_{M0}} \le 1.0 \qquad (6)$$

$$-\frac{\psi_{vec} \cdot N_{Ed}}{f_{yb} \cdot A_g / \gamma_{M0}} + \frac{M_{y,Ed} + \Delta M_{y,Ed}}{f_{yb} \cdot W_{eff,y,ten} / \gamma_{M0}} + \frac{M_{z,Ed} + \Delta M_{z,Ed}}{f_{yb} \cdot W_{eff,z,ten} / \gamma_{M0}} \le 1.0 \qquad (7)$$

where:

$N_{Ed}, M_{y,Ed}, M_{z,Ed}$ — design internal actions in the member,

$\Delta M_{z,Ed} = N_{Ed} \cdot e_{Nz}$ — bending moment about the weak axis due to the shift of the centroid,

$\Delta M_{y,Ed} = N_{Ed} \cdot e_{Ny}$ — bending moment about the strong axis due to the shift of the centroid,

e_{Nz}, e_{Ny} — shift of the centroid of the cross-section along the strong and weak axis, respectively,

A_g — area of the gross cross-section,

A_{eff} — area of the effective cross-section,

$W_{eff,y,com}$ — section modulus for bending about the strong axis at the point with the greatest compression stress,

$W_{eff,z,ten}$ — section modulus for bending about the weak axis at the point with the greatest tensile stress (other moduli are notated analogously),

f_{yb} — characteristic value of the yield stress,

$\psi_{vec} = 0.8$ — reduction factor to incorporate vectorial effects,

$\gamma_{M0} = 1.0$ — partial factor.

Equation (7) is to be used only if $W_{eff,y,com} \ge W_{eff,y,ten}$ or $W_{eff,z,com} \ge W_{eff,z,ten}$.

Generally, the additional bending moment due to the shifting centroid is present, since $e_{Ny} = 0$ is true only if $A_g = A_{eff}$, or in the special case when the proportions of the C-section result the ineffective parts of the section have the same centroid as the effective parts.

The criterion of the application rule for these members in the case of EC3-1-3:2006 is slightly different from that of EC3-1-3:1996.

$$\frac{N_{Ed}}{N_{c,Rd}} + \frac{M_{y,Ed} + \Delta M_{y,Ed}}{M_{cy,Rd,com}} + \frac{M_{z,Ed} + \Delta M_{z,Ed}}{M_{cz,Rd,com}} \le 1 \qquad (8)$$

$$-\frac{N_{Ed}}{N_{c,Rd}} + \frac{M_{y,Ed} + \Delta M_{y,Ed}}{M_{cy,Rd,com}} + \frac{M_{z,Ed} + \Delta M_{z,Ed}}{M_{cz,Rd,com}} \le 1 \qquad (9)$$

where:

$$N_{c,Rd} = f_{yb} \cdot A_{eff} / \gamma_{M0} \qquad (10)$$

$$M_{cy,Rd,com} = f_{yb} \cdot W_{eff,y,com} / \gamma_{M0} \qquad (11)$$

The difference between the two application rules is partially formal: in the denominators of the addends the formulae have been substituted with a simpler expression. Quantitative changes are in the addend representing the contribution of axial actions: the Ψ_{vec} multiplier is

absent and the cross-sectional area to be taken into account here is the effective area instead of the gross area.

In the case of failure modes involving stability the application rules provide formulae to calculate the relative slenderness and derive reduction factors for various forms of global buckling. The basic formula for checking is the same in all cases, the χ reduction factors are to be calculated based on a relative slenderness calculated according to the failure mode. Here are only the global failure modes relevant to the laboratory testing presented: flexural buckling, and the interaction of flexural buckling and bending.

According to the application rules of EC3-1-3:1996 the design resistance against flexural buckling is to be calculated as:

$$N_{b,Rd} = \chi \cdot A_{eff} \cdot f_{yb} / \gamma_{M1}$$ (12)

where:

$\gamma_{M1} = 1.0$ — partial factor,

χ — reduction factor for buckling about the relevant axis, calculated using buckling curve "b" (general case), or curve "c", (provided $A_g = A_{eff}$).

$$\chi = \frac{1}{\Phi + \left(\Phi^2 - \overline{\lambda}^2\right)^{0,5}}$$ but $\chi \leq 1,0$ (13)

where:

$$\Phi = 0,5 \cdot \left(1 + \alpha \cdot \left(\overline{\lambda} - 0,2\right) + \overline{\lambda}^2\right)$$ (14)

where:

α — imperfection factor for buckling curve „b" $\alpha = 0.34$,

$\overline{\lambda}$ — relative slenderness about the relevant axis.

The relative slenderness for flexural buckling is to be calculated as:

$$\overline{\lambda} = \left(\lambda / \lambda_1\right) \cdot \left(\beta_A\right)^{0,5}$$ (15)

where:

$$\lambda = l / i$$ (16)

$$\lambda_1 = \pi \cdot \left(E / f_{yb}\right)^{0,5}$$ (17)

$$\beta_A = A_{eff} / A_g$$ (18)

where:

l — buckling length about the relevant axis,

i — radius of gyration about the relevant axis, calculated from the properties of the gross cross-section.

The interaction of flexural buckling and bending is to be calculated using the following equation:

$$\frac{N_{Ed}}{\chi_{min} \cdot f_{yb} \cdot A_{eff} / \gamma_{M0}} + \frac{\kappa_y \cdot (M_{y,Ed} + \Delta M_{y,Ed})}{f_{yb} \cdot W_{eff,y,com} / \gamma_{M0}} + \frac{\kappa_z \cdot (M_{z,Ed} + \Delta M_{z,Ed})}{f_{yb} \cdot W_{eff,z,com} / \gamma_{M0}} \leq 1.0$$ (19)

This formula is essentially the same as *(6)* with the difference of the addend representing axial actions is the utilisation for flexural buckling instead of axial compression, and the interaction of flexural buckling and bending moment is taken into account by the κ interaction factors. In the equations:

$\chi_{min} = (\chi_{TF}, \chi_z)$ — the smallest of the reduction factors for flexural and torsional-flexural buckling,

$$\kappa_y = 1 - \frac{\mu_y \cdot N_{Ed}}{\chi_y \cdot f_{yb} \cdot A_{eff}} \qquad \text{but} \qquad \kappa_y \leq 1,50 \qquad (20)$$

$$\kappa_z = 1 - \frac{\mu_z \cdot N_{Ed}}{\chi_z \cdot f_{yb} \cdot A_{eff}} \qquad \text{but} \qquad \kappa_z \leq 1,50 \qquad (21)$$

where:

$$\mu_y = \overline{\lambda}_y \cdot \left(2 \cdot \beta_{M,y} - 4\right) \qquad \text{but} \qquad \mu_y \leq 0,90 \qquad (22)$$

$$\mu_z = \overline{\lambda}_z \cdot \left(2 \cdot \beta_{M,z} - 4\right) \qquad \text{but} \qquad \mu_z \leq 0,90 \qquad (23)$$

where:

$$\beta_{M,i} = 1.8 - 0.7\psi \qquad \qquad \text{the equivalent uniform moment factor,} \qquad (24)$$

where:

ψ — the ratio of end moments about the relevant axis for linear moment distribution between adjacent lateral supports.

In EC3-1-3:2006 the calculation method has been changed. It allows two methods to use: to carry out a second-order analysis as specified in EC3-1-1 using the effective cross-sectional properties, or alternatively use the formula as follows:

$$\left(\frac{N_{Ed}}{N_{b,Rd}}\right)^{0.8} + \left(\frac{M_{Ed} + \Delta M_{Ed}}{M_{b,Rd}}\right)^{0.8} \leq 1 \qquad (25)$$

with:

$N_{b,Rd}$ — the design resistance (cross-section, flexural, torsional, or torsional-flexural buckling),

$M_{b,Rd}$ — the design bending resistance (cross-section failure or lateral-torsional buckling).

The main difference between the formula *(19)* and *(25)* is that the former handles bending about both axes, whereas in the latter it is not notated which axis is to be considered. In formula *(19)* the addition is linear but an interaction factor in function of the utilisation for axial actions is calculated, whereas in formula *(25)* the interaction is taken into account in the exponent that has a fixed value.

When using the application rules to calculate the design resistances of the tested members the following aspects need consideration: simplifications applied in modelling the cross-sections, internal actions to be taken into account in the calculations and potential stability failure modes.

The C-sections used in the tests are asymmetric, as the flange widths are different (Figure 4, Table 1). The asymmetry is small and therefore in the calculation of the cross-sectional properties it is neglected: the flange widths are taken to be equal to the mean of the real values, thus, instead of the originally asymmetric section a single-symmetric section is used. Due to this simplification there is no shift of the centroid along the weak axis for axial compression, hence no bending about the strong axis. The error caused by this approximation is small, since considering the gross sections i) the angle of the principal axis of the original section and that of the simplified section is cca. 1.5 degrees, ii) the difference of the second moments of inertia about the first principal axis is less than 0.1%, iii) the sections have an order of magnitude higher moment of inertia about the first principal axis than about the second. Based on this, considering a shift of the centroid along the weak axis with the same

magnitude as along the strong axis results an order of magnitude smaller contribution to the utilisation than the shift along the strong axis.

Due to this simplification in modelling the cross-section of the members, in the standard-based calculations no bending about the major axis is present: the members are in axial compression and bending about the weak axis. Hence, the design formulae of both versions of the standard can be directly used, the results are directly comparable.

Note, that lateral-torsional buckling was not considered in the calculations, as due to the simplified cross-sectional model there is no shift of the centroid along the weak axis, and there is no bending about the strong axis from loading in the members studied in the laboratory tests.

2.4.4. Comparison of test and standard

The application rules presented in Chapter 2.4.3 were used to calculate design resistances for SimpleC, CompressionC, C and Brace arrangements. The calculations were carried out using material properties derived from coupon tests and partial factors $\gamma_{M0} = \gamma_{M1} = 1.0$, to enable the direct comparison of test and standard; the ratios of test and design resistances present directly the safety of the application rules, that is, the safety of the resistance side of the design. Results of the coupon tests are presented in the Annex, Table A12.

In case of SimpleC, C and CompressionC specimens the buckling length was taken equal to the member length, Brace members were considered to have fixed supports on both ends. From the design method point-of-view these arrangements differ in the magnitude of the eccentricity of the load introduction. In case of CompressionC members the axial force was considered centric. In the case of SimpleC, C and Brace arrangements the eccentricity was calculated as the distance of the centroid of the screw layout and the centroid of the C-section, thus, a uniform distribution of the load between the screws was assumed. As a special case of the C arrangement, the eccentricity of the SimpleC specimens is equal to the distance of the section centroid and the web. Typical resulting eccentricities are shown in Figure 60. on a C200/2.0 section.
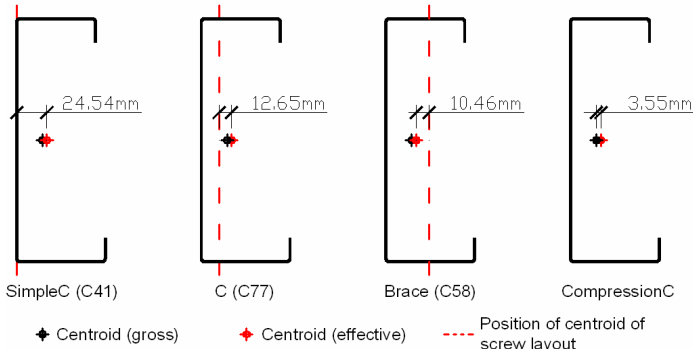
Figure 60.: Schematics of eccentricities resulting for a C200/2.0 section.

Note, that a direct calculation the design resistance in case of EC3-1-3:1996 is not possible, since the interaction factor depends on the value of the acting axial force. The design resistance was calculated with iteration and a maximum error of 0.001 kN. Although not necessary, the same algorithm was used to calculate the resistances according to EC3-1-3:2006. The obtained load-bearing capacities are shown in figures in the Annex, for each test; Figure 61. and Figure 62. show two examples. In the figures test resistance, test-based design resistance and the load-bearing capacities calculated according to the application rules of both versions of the standard for member lengths 100 to 10000 mm are shown. The ratio of the design resistances calculated according to the two version of the standard is also shown in

function of the member length, with minimum and maximum values. Note that the figures in the Annex show the results obtained using the formulae discussed in Chapter 2.4.5 as well.

Figure 61.: Comparison of test and design resistances (C16).
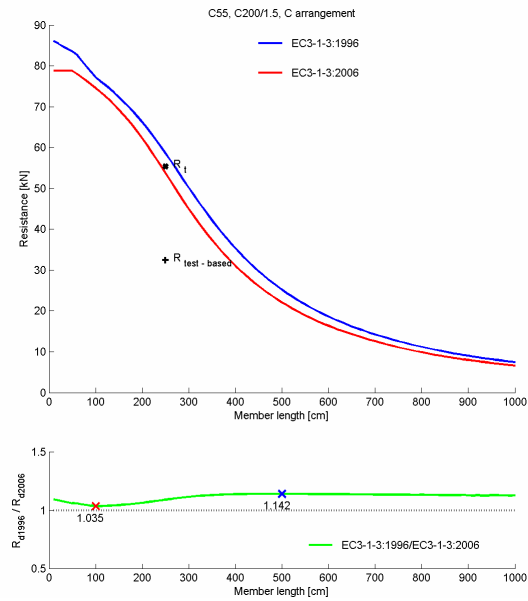
Figure 62.: Comparison of test and design resistances (C55).

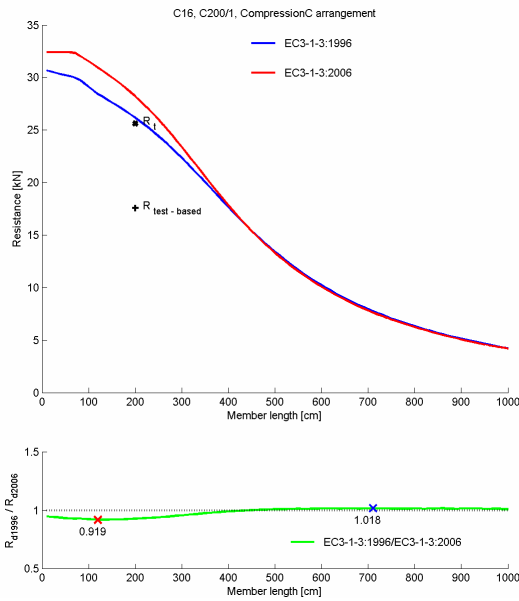In the following the comparisons of test and design resistances for both versions of the standard are presented in figures and tables for each test arrangement. In the figures the test and design resistances are shown as data points. The trend of the results is presented with a line obtained by linear regression, equation of the line and fitness are shown. The unity line drawn with black ($R_t = R_d$, with R_t standing for test resistance, R_d for design resistance) is shown as reference: the closer the data points and regression lines to this line are, the better the match of test and design resistance; regression lines over this line (R_d/R_t ratios greater than 1.00) indicate unsafe design. The tables containing the numerical values underlying the graphs are presented in the Annex, Tables A15 – A19.

The comparisons of test and design resistances of SimpleC specimens for both versions of the standard are presented in Figure 63. and the Annex, Table A15.

Figure 63.: Test and design resistances of SimpleC specimens.

In general, although the regression lines indicate slightly unsafe design, both versions of the standard provide good match to the test results, the scatter of the data is small. The design

resistances calculated according to EC3-1-3:2006 are more on the unsafe side relative to those calculated according to EC3-1-3:1996 and the scatter is also bigger in this case.

The comparisons of test and design resistances of CompressionC specimens for both versions of the standard are presented in Figure 64. and the Annex, Table A16. Both versions of the standard provide good match; EC3-1-3:1996 yields slightly unsafe, EC3-1-3:2006 yields safe design.
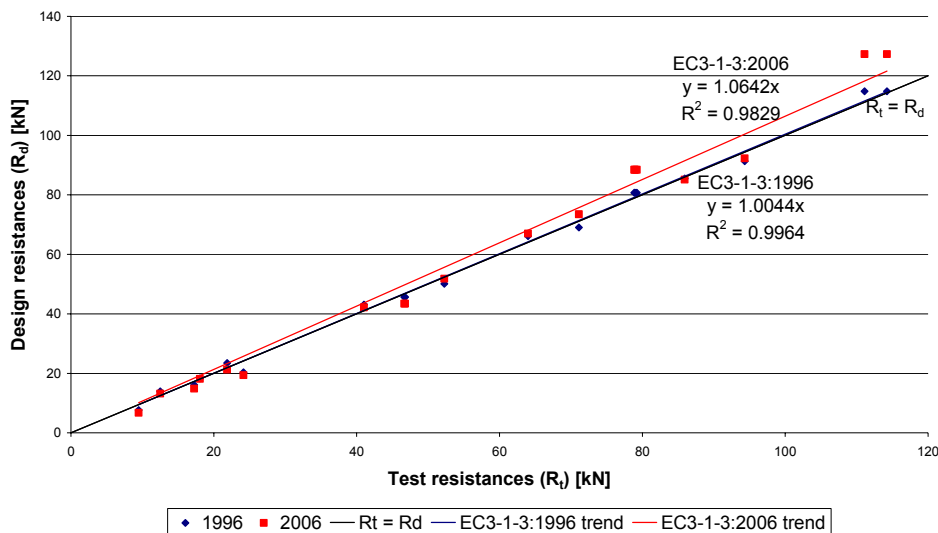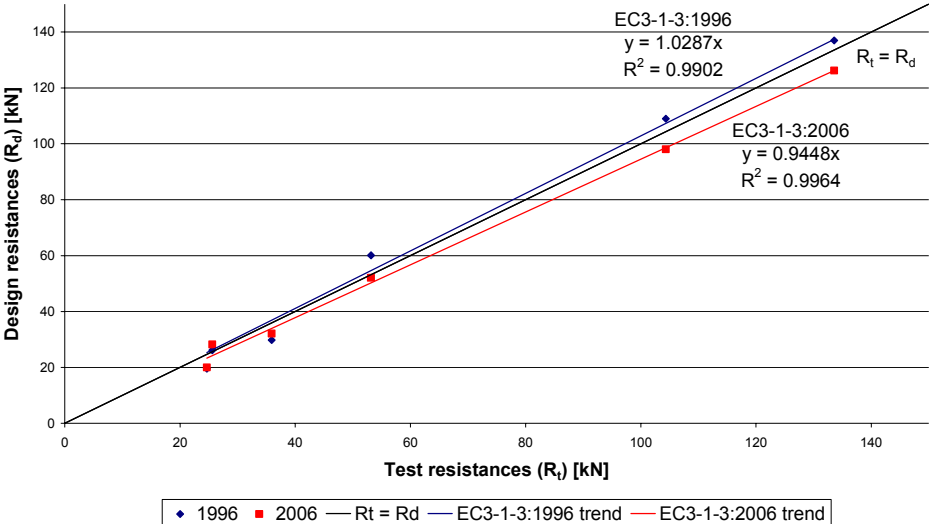

Figure 64.: Test and design resistances of CompressionC specimens.

The comparisons of test and design resistances of C specimens for both versions of the standard are presented in Figure 65. and the Annex, Table A17.

Figure 65.: Test and design resistances of C specimens.

For specimens with a C arrangement both version of the standard provide results with a significant scatter (+/- 15%), but the regression shows that the tendencies of the results are good. Considering the results of tests C45, C55, and C56 – same section and length, eccentricities: 12.25 mm, 5.58 mm, 3.08 mm in case of EC3-1-3:1996 – shows, that with decreasing eccentricity the match of test and standard-based results gets worse; this implies that assuming uniform force distribution between the screws may be not true for all cases, the load is transferred primarily by the screws in the web. For C200/2.0 and C200/2.5 the formulae of both standards yield unsafe design in case of the shorter specimens (C72, C77) and a safe design for longer specimens (C48, C51), however, a common property to explain this tendency is not found.

36

The comparisons of test and design resistances of Brace specimens for both versions of the standard are presented in Figure 66. and the Annex, Table A18.
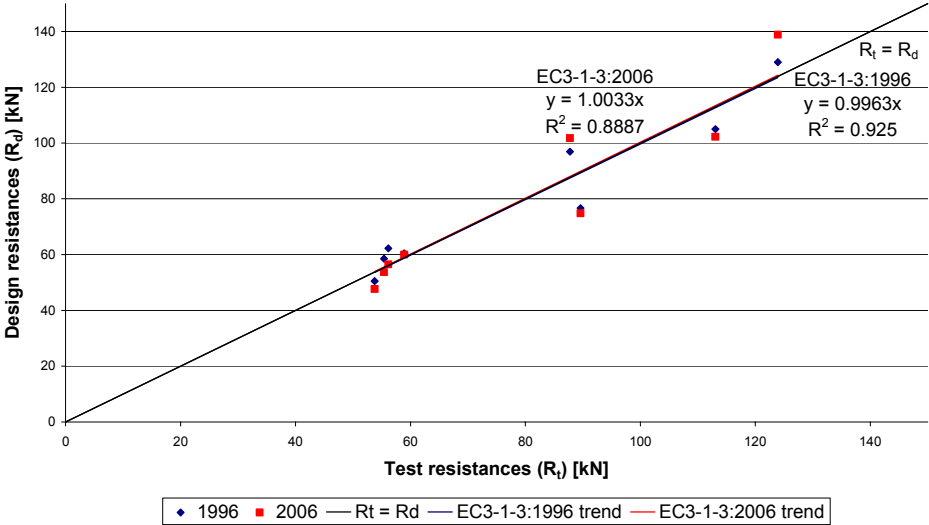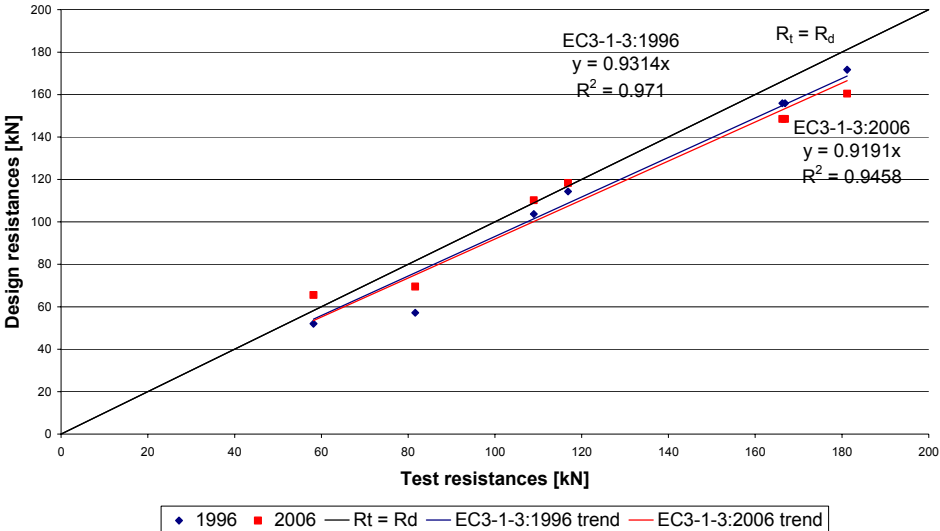

Figure 66.: Test and design resistances of Brace specimens.

Both versions of the standard provide satisfactory match of test and design resistances, with EC3-1-3:1996 providing results only on the safe side.

As all studied arrangements can be considered the same from the design method point-of-view (i.e.: the difference is the magnitude of the eccentricity), displaying all results in one figure provides a general overview on the accuracy of the application rules of both versions of the standard. An overview on the results is given in Figure 67., Table A19 in the Annex contains statistical data on the results for all types of specimens.
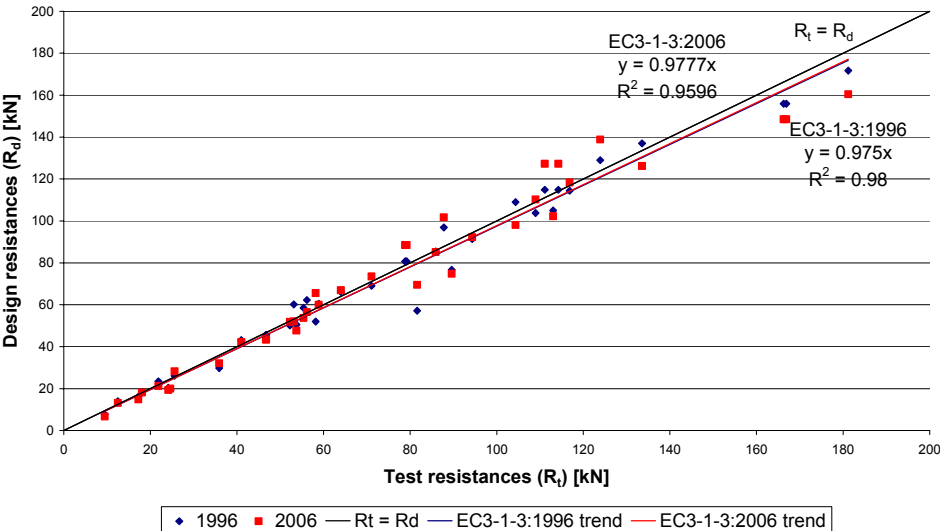
Figure 67.: Test and design resistances of all studied specimens.

The results of calculations carried out using the application rules was shown for each test arrangement made using a single C-section. Except for arrangement C a good agreement of test and design values and a relatively small scatter of the test/design resistance ratios were found. In case of the specimens with a C arrangement, significant scatter was observed, which is probably the result of a non-uniform load distribution between the self-drilling screws, a property that has not been taken into account in the calculations.

The failure mode of the members, according to the application rules is in most cases stability failure. In case of EC3-1-3:1996 this is due to the fact, that even in case of stub columns the

interaction coefficient in formula *(19)* is greater than 1.0, hence this yields the highest utilisation in all cases. In the case of EC3-1-3:2006 cross-section failure is the governing mode only for very short members.

Comparing the ratios of the design resistances obtained by the two versions of the standard (Figures presented in the Annex) shows that in case of SimpleC specimens for high web b/t ratios the design resistances from EC3-1-3:1996 are for all lengths higher than those from EC3-1-3:2006; with decreasing web b/t ratio the results of EC3-1-3:1996 are for short specimens lower, long specimens higher than those from EC3-1-3:2006; the transition length is higher for web smaller values of b/t ratio. In the case of Brace specimens the opposite of this tendency is observed, the results of EC3-1-3:1996 are in all cases lower than those from EC3-1-3:2006 for C200/1.5 members, and in all cases higher in case of C200/2.5 members. In case of C and CompressionC arrangements the tendency is the same as in the case of SimpleC specimens.

The minimum of the ratio of the design resistances calculated according to the two versions of the standard (EC3-1-3:1996/EC3-1-3:2006) is usually at cca. 1000-2000 mm member length, hence the biggest difference between the results of the two versions of the standard is approximately at the lengths important from the practical design point-of-view.

The comparison of the results clearly indicates that – due to the in some cases large differences between the values – in the checking formulae the contribution of the axial action and bending to the total utilisation is different, but as the results are in general in good agreement, both versions of the standard consist of a coherent method to calculate cross-sectional properties and design resistances over a wide range of parameters; however, the cross-sectional properties and formulae of the two versions of the standard may not be mixed.

Considering the slope and fitness of the regression lines and the standard deviations calculated, the application rules of EC3-1-3:1996 can be considered more accurate, although the differences between the results of the two versions of the standard are not significant. The comparison of test and design resistances also shows, that since the values of the partial safety factors is , according to the standard 1.0, the safety of the design method is equal to the safety of the material model.

2.4.5. Modified rules to handle the tested members

To eliminate results on the unsafe side from the design modified formulae have been derived for the arrangements discussed in Chapter 2.4.4 by calibrating the existing formulae to yield results only on the safe side. The calibration of existing application rules was done by modifying the eccentricity to be taken into account, thus raise the contribution of bending to the total utilization of the members.

In case of EC3-1-3:1996 the formulae *(6) (7) (19)* are to be used in design. In case of SimpleC, C and CompressionC members the eccentricity is to be calculated on the basis of the original method, that is, the distance of the centroid of the screw layout from the centroid of the effective cross section for axial compression is the base value. The modified eccentricity can be expressed as:

$$e_{\text{mod}} = 1.4 \cdot e_{nom} \qquad \text{but} \qquad e_{\text{mod}} \geq 0.4 \cdot y_S \qquad (26)$$

where:

e_{mod}	modified eccentricity,
e_{nom}	distance of the centroid of the screw layout from the centroid of the gross cross section for axial compression,
y_S	distance of the centroid of the gross cross-section and the web.

In case of members of Brace arrangement no modification on the original design method is necessary, as the design resistances calculated according to the original method yielded results rather on the safe side. The result of the modified design method is shown in Figure 68, for all affected specimen arrangements.
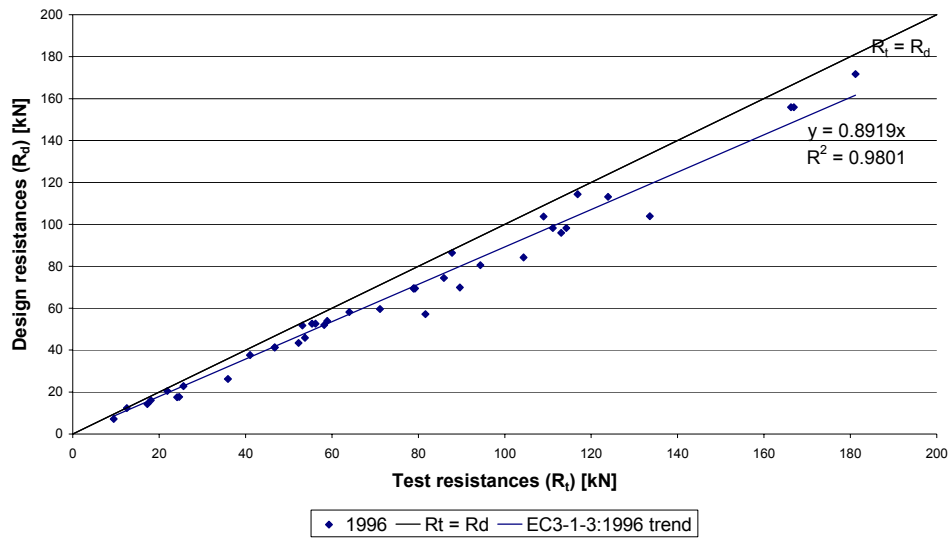
Figure 68.: Results of the modified design method.

In case of EC3-1-3:2006 two different approaches were utilized to modify the design formulae for stability checking. In the first approach *(27)* the exponent of the addend representing axial actions is set to unity, thus it is essentially the same as in EC3-1-3:1996, and the exponent modifying the utilisation for bending about the minor axis is changed; setting it to 0.47 provided results on the safe side in all cases.

$$\left(\frac{N_{Ed}}{N_{b,Rd}}\right)^{1.0} + \left(\frac{M_{z,Ed} + \Delta M_{z,Ed}}{M_{c,Rd}}\right)^{0.47} \qquad (27)$$

In the second approach *(28)* the exponents of the addends are equal – as in the original formula of EC3-1-3:2006 –, setting them to 0.65 provided results only on the safe side.

$$\left(\frac{N_{Ed}}{N_{b,Rd}}\right)^{0.65} + \left(\frac{M_{z,Ed} + \Delta M_{z,Ed}}{M_{c,Rd}}\right)^{0.65} \qquad (28)$$

The accuracy of the approaches has been analysed based on the comparison of the statistical evaluation of the results. The result of the evaluation is presented in the Annex, Table A20 and Figure 69.
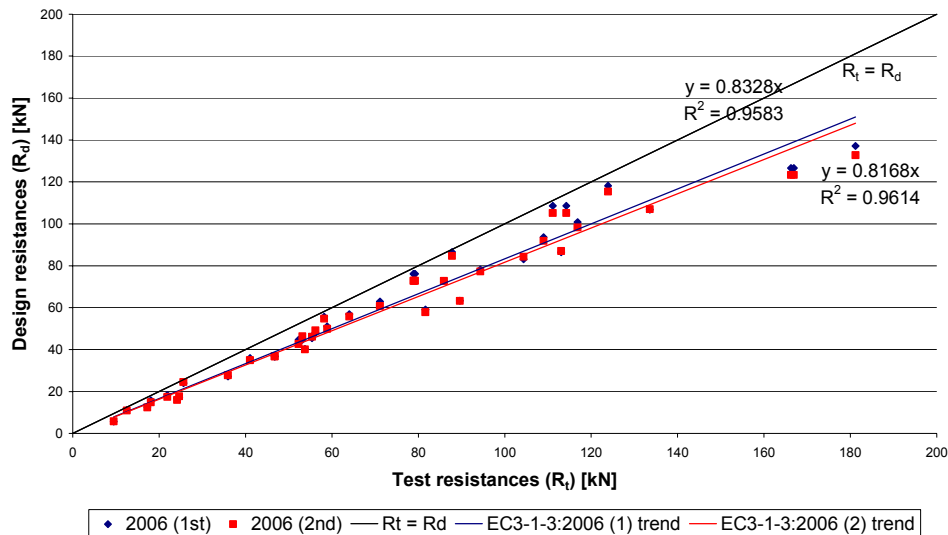
Figure 69.: Results of the modified versions of EC3-1-3:2006.

The analysis shows, that the two approaches yield in general results in good agreement; although the minima, maxima and averages show in many cases difference, the slope of the regression lines is close to each-other and the fitness of the lines is high in both cases. Based on this, both approaches can be used as modified design methods to design the studied members safely.

The comparison of the results of the modified design methods of both versions of the standard is shown in Figure 70. Based on the comparison the results of EC3-1-3:1996 are more accurate: the slope of the regression line is closer to unity, and the fitness of the line is higher.
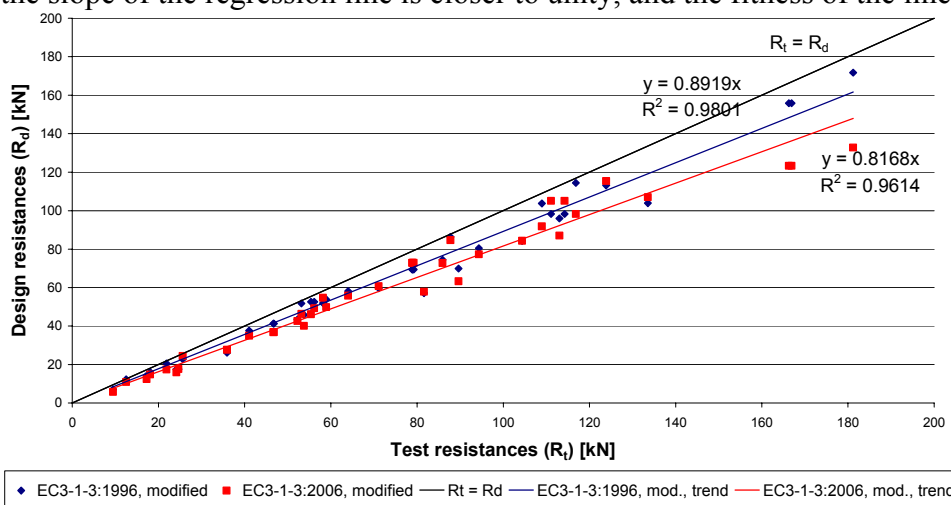
Figure 70.: Results of the modified design methods (EC3-1-3:1996 and EC3-1-3:2006).

Design methods for the specimens with complex cross-sections are to be based on the same basic principles as the ones with a simple arrangement; the design formulae for these arrangements can be derived from the existing ones, utilizing the results of the laboratory tests and the evaluation presented in Chapter 2.3.2. The formulae are derived from the application rules of EC3-1-3:1996, the notations used are the same as presented in Chapter 2.4.3.

The concept of the development was to rely on the formulae of the application rules of the standard, as the design resistances calculated with these are in case of the single specimens close to the test resistances. In the following the design methods developed for each complex arrangement are detailed.

In case of members with a HatC arrangement in all cases a cross-section failure was obtained. The design resistance of members with this arrangement are to be designed using the following formula:

$$\frac{N_{Ed}}{f_{yb} \cdot 0.5 \cdot A_{eff} / \gamma_{M1}} \leq 1.0 \qquad (29)$$

with A_{eff} being the effective cross-sectional area of the cross-section.

The comparison of the design and test resistances are shown in the Annex, Table A21.

The design resistance of IC Column, CC, and CU members are to be calculated based on the design resistance of a SimpleC member, by multiplying its resistance with a factor α shown in Table 14, depending on the arrangement to be designed. In each case the buckling length is to be taken equal to the member length. The design resistance of IC Brace members is to be calculated by multiplying the design resistance of a Brace member with the α factor. The supports are to be taken into account depending on the number of screws used, as shown in Table 15. The eccentricity is to be calculated as the distance of the screw position and the centroid of the effective cross-section for axial compression.

The following checks are to be performed:

Stability checks – interaction of flexural buckling and bending about the minor axis:

$$\frac{N_{Ed}}{\chi_{min} \cdot f_{yb} \cdot A_{eff} / \gamma_{M1}} + \frac{\kappa_z \cdot (M_{z,Ed} + \Delta M_{z,Ed})}{f_{yb} \cdot W_{eff,z,com} / \gamma_{M1}} \leq \alpha \qquad (30)$$

Strength checking – interaction of axial compression and bending about the minor axis:

$$\frac{N_{Ed}}{f_{yb} \cdot A_{eff} / \gamma_{M1}} + \frac{M_{z,Ed} + \Delta M_{z,Ed}}{f_{yb} \cdot W_{eff,z,com} / \gamma_{M1}} \leq \alpha \qquad (31)$$

if $W_{eff,y,com} \geq W_{eff,y,ten}$ or $W_{eff,z,com} \geq W_{eff,z,ten}$, then

$$-\frac{\psi_{vec} \cdot N_{Ed}}{\chi_{min} \cdot f_{yb} \cdot A_{eff} / \gamma_{M0}} + \frac{\kappa_z \cdot (M_{z,Ed} + \Delta M_{z,Ed})}{f_{yb} \cdot W_{eff,z,ten} / \gamma_{M0}} \leq \alpha \qquad (32)$$

where:

α factor depending on the arrangement.

Table 14: Values of α for different arrangements.

Arrangement	α
IC Column	0.8·L+1.0, with L being the member length in [m].
CC	1.8
CU	1.3, if C-section is loaded; 1.8 if U-section is loaded
IC Brace	2.5

Table 15: Column buckling length factor.

Number of bolts / flange	ν
1	1.00
2	0.75
> 2	0.50

The results of the modified method are presented in the Annex, Table A22 – Table A25.

The design resistance of a DoubleC member is to be calculated based on the design resistance of a CompressionC member for stability checking, and a SimpleC member for strength checking. The buckling length is to be taken equal to the member length. The eccentricity to be taken into account in case of the stability checking is the shift of the centroid of the cross section, in the case of strength checking the distance is calculated as the double of the distance of the web and the centroid of the gross cross-section, plus the shift of the centroid.

The following formulae are to be considered:

Stability checks – interaction of flexural buckling and bending about the minor axis:

$$\frac{N_{Ed}}{\chi_{min} \cdot f_{yb} \cdot A_{eff} / \gamma_{M1}} + \frac{\kappa_z \cdot (M_{z,Ed} + \Delta M_{z,Ed})}{f_{yb} \cdot W_{eff,z,com} / \gamma_{M1}} \leq 2.0 \qquad (33)$$

where:

$\Delta M_{zEd} = N_{Ed} \cdot e_{Nz}$ bending moment about the weak axis due to the shift of the centroid.

Cross-section checking – interaction of axial compression and bending about the minor axis:

$$\frac{N_{Ed}}{f_{yb} \cdot A_{eff} / \gamma_{M1}} + \frac{M_{z,Ed} + \Delta M_{z,Ed})}{f_{yb} \cdot W_{eff,z,com} / \gamma_{M1}} \leq 2.0 \qquad (34)$$

if $W_{eff,y,com} \geq W_{eff,y,ten}$ or $W_{eff,z,com} \geq W_{eff,z,ten}$, then

$$-\frac{\psi_{vec} \cdot N_{Ed}}{\chi_{min} \cdot f_{yb} \cdot A_{eff} / \gamma_{M0}} + \frac{\kappa_z \cdot (M_{z,Ed} + \Delta M_{z,Ed})}{f_{yb} \cdot W_{eff,z,ten} / \gamma_{M0}} \leq 2.0 \qquad (35)$$

where:

$\Delta M_{zEd} = N_{Ed} \cdot (e_{Nz} + 2 \cdot y_s)$ bending moment about the weak axis,

e_{Nz} shift of the centroid of the cross-section,

y_S distance of the web and the centroid of the gross cross-section.

The design resistances and results of the method are presented in the Annex, Table A26.

2.5. Summary

In two sets 98 laboratory tests were carried out on C-section members with various cross-sectional arrangements, loaded with centric or eccentric axial compression, resulting axial compression and bending about the weak axis as internal actions. A wide spectrum of specimens were tested in terms of member length, cross-section and arrangement. Four specimen types – those consisting of a single C-section – are covered by the application rules of EC3, whereas six specimen types with a complex arrangement, possible design solutions in case enhanced load-bearing capacity is necessary in structural members of cold-formed buildings, are not directly handled by standard design methods.

The test results provide a wide basis to analyse the stability behaviour of the tested members, to check existing design standards and to design method development: the failure modes obtained cover local, global and interacting stability behaviour of the specimens highlight the effect of load introduction on the load-bearing capacity and point out favourable structural detailing and arrangements.

Based on measurements and observations the stability behaviour and failure modes of the specimens have been identified and described. The method of EC3 was utilized to calculate the test-based design resistances of the specimens. This method yields conservative results when used to derive the design resistance of a member from one test; in the current study a safety of 1.21 to 1.86, with a median of 1.67 was obtained.

A quantitative study was carried out on members of the groups by comparing the test-based design resistances of members with the same length and cross-section, but different arrangement. The direct comparison of design resistances complementing the observations on the behaviour modes of the specimens provided numerical values to support the development of standard-based design methods for the arrangements directly not covered by codes.

The applicability and accuracy of the application rules of two versions of EC3-1-3 was studied by comparing test and design resistances of the simple arrangements directly covered by the standard. The specimens involved in this study differ from the design method point-of-view only in the magnitude of eccentricity to be taken into account. The application rules of both versions of the code yield results in good agreement with the test resistances; the formulae provide results on the safe and on the unsafe side as well, with mean values close to the test resistances, the scatter in three cases of the four is small. In general, both versions of the standard provide similar accuracy, the earlier version (EC3-1-3:1996) can be considered more accurate. To ensure safe design simple rules to calculate the eccentricity to be taken into account were derived to be used with the formulae of the application rules. The additional rules result in a higher contribution of the utilisation for bending to the total utilisation of the member, hence, to lower design resistance and results only on the safe side.

Using the results of the quantitative test evaluation simple methods to design the specimens with a complex arrangement have been derived from the application rules of EC3-1-3:1996. According to these the design resistance of these is to be calculated as a multiple of the design resistance of a single member with the same length and cross-section; the multiplier to be used depends on the type of arrangement to be designed.

The developed design methods may be used directly only for members with the examined arrangements using the same sections, but the observed behaviour modes provide basis to develop design methods for structural members with similar arrangement or standards other than EC3 as well. The test results may also be used as basis to develop FE models capable of simulating laboratory tests, providing a cheap and efficient tool to widen the basis of design method development.

3. Truss system made of cold-formed C-section members

3.1. Introduction

3.1.1. Background

In this Chapter results of a research and development work on a truss system made of cold-formed C-section members are summarized. The work was carried out in cooperation with an industrial partner (Lindab Ltd.) producing cold-formed members. The project aimed the development of a truss system, based on a list of requirements and specifications provided by the industrial partner. In confines of the work the structural arrangement and detailing, EC3-based design method and its validation by laboratory tests was to be carried out.

The requirements postulated by Lindab Ltd. were the following:
- all structural members should be cold-formed C-sections produced by the company,
- simple structural arrangement is to be developed enabling fast erection,
- a flexible system allowing single- or multi-span girders is to be developed,
- spanning 12...24 meters,
- roof slopes ranging 3 to 30%,
- short members are to be avoided.

The first step of the work was to develop the structural arrangement and an EC3-based design method enabling the evaluation of the thrift of the concept, and design the prototype of the trusses. A preliminary study on the possible structural arrangements was carried out. In this stage the structural arrangement was agreed upon and an EC3-based calculation was carried out to judge the thrift of the idea. As the solution proved to be viable, a preliminary design method based on the application rules of EC3 and utilizing advanced methods (FSM) was developed. This version of the design method was used to design the first trusses for selected spans and also, to gather experience on the specialities of designing such structures.

The second step of the research aimed the validation and refinement of the design method and the structural detailing of the system based on full-scale laboratory tests. Five tests were carried out on a 12-meter-span prototype of the truss designed using the first version of the design method. The tests were carried out in the Structural Laboratory of BME. The main aims of the tests were: i) to study the behaviour of the trusses, ii) to collect data regarding the characteristics of the behaviour, iii) to refine the design method and/or structural detailing of the truss. As a last act of the second development stage a detailed analysis of the primary test results was carried out. Based on this the design method and the structural arrangement has been refined at many points resulting in a less conservative design method and a more economical arrangement.

The development work was carried out by a team of researchers, most of who worked previously on similar development projects. The contribution of these members of the group confined to discussions on the fundamental questions of the project. As a sequel of the work a software implementing the design method was developed by the same research group to enable fast design, [41]. This work is not discussed in the thesis, but the software is used, primarily to illustrate and underpin certain aspects of the analyses and test results.

The author participated in the work as the member of the team responsible for the calculations connected to the design method development, laboratory testing and test evaluation, and shaping the final version of the design method.

3.1.2. Structural arrangement, fabrication

The structural arrangement of the truss is shown on Figure 71. and Figure 72. with details highlighted. The upper and lower chords of the truss consist of two C-sections in a back-to-back arrangement. The distance of the C-sections equals the web height of the brace members, which are stuck between the chord members and connected to them using fitted bolts. Brace columns are perpendicular to the upper chord and overhang its upper edge to provide support for the purlins. The orientation of the brace members, that is, whether they are "open" upwards or downwards is not defined. The main advantage of this arrangement is that similarly to other light-gauge systems no gusset plates are needed in the joint areas, hence a fast erection is possible. The main disadvantage of the arrangement is the fixed web width; however, brace members can be doubled in a back-to-back arrangement if higher load-bearing capacity is required e.g. near supports. Brace columns providing support are always doubled.

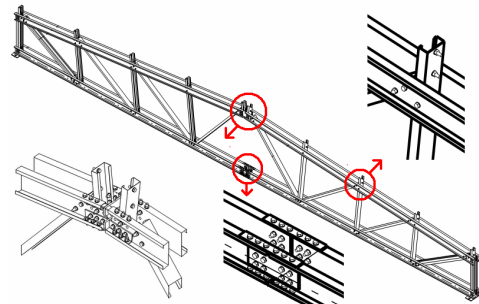Figure 71.: Prototype truss.   Figure 72.: Structural arrangement.

Members of the truss are fabricated by the conventional cold roll forming method; in the case of chord members in an additional step bolt holes are punched in the web in the positions defined in the manufacturing plan. Brace members are not pre-punched, but the holes are made during assembly using hand tools, after placing them to the correct position relative to the chord members. During assembly gusset plates are used only in the in-situ joints, the ridge (which is itself preferably an in-situ joint) and at the supports. The trusses can be pre-assembled and delivered to the building site for final assembly, but as no extra machinery is necessary for this, the whole work can be done on the site. Due to the low dead load of the truss no heavy crane is necessary to place them into final position.

Due to the arrangement the internal actions of the chord members are axial compression or tension and bending about both axes. The bending about the minor axis is the result of the out-of-plane eccentricity of the joints, that is, the result of the chord members being connected to the brace members at their webs. Major axis bending is the result of the in-plane eccentricity. Brace members, besides the axial action are subject to minor axis bending, as result of the in-plane eccentricity. As the truss is loaded only at the structural joints, the bending moment distribution is in all members linear, axial forces are constant along the length.

The members of the truss are similar in arrangement to the C-section members discussed in Chapter 2: compression brace members of the truss are similar to Brace members, compression chord members can be considered as SimpleC or C members. The results of the study presented in Chapter 2 cannot be directly applied to the truss system, as the bending moments acting in the truss members are different from the constant bending acting about the minor axis characteristic for the tested C-section members. However, the approach used to derive EC3-based design method for them can be utilized in this case as well. In Chapter 3, whenever appropriate the similarities between the behaviour of members with similar arrangement ad behaviour are highlighted.

3.2. Laboratory tests

3.2.1. Test setup

The laboratory tests were carried out in the Structural Laboratory of BME. In the tests 12.20-meter-span specimens were used. The truss girders were placed in upright position on the top of two columns of HEA-200 section, each four meters high (Figure 73. and Figure 74.). The specimens were tested using a gravity load simulator to apply uniformly distributed gravitational load using four jacks of 100 kN nominal capacity each in parallel circuit.

The lateral support of the upper chord of the specimens was provided by rods connected to the "wall" assembled from the elements of the frame system used in the laboratory for testing.

Figure 73.: Specimen No. 1 in the laboratory.

The measurement system consisted of five displacement transducers, two of which measured the horizontal deflections of the web of the upper chord, three the vertical displacements symmetrically at two structural joints and in the middle of the lower chord. Strain measurement was carried out in the chord and brace members in the cross-sections indicated with red numbers in Figure 74. The applied load was measured using a load cell.
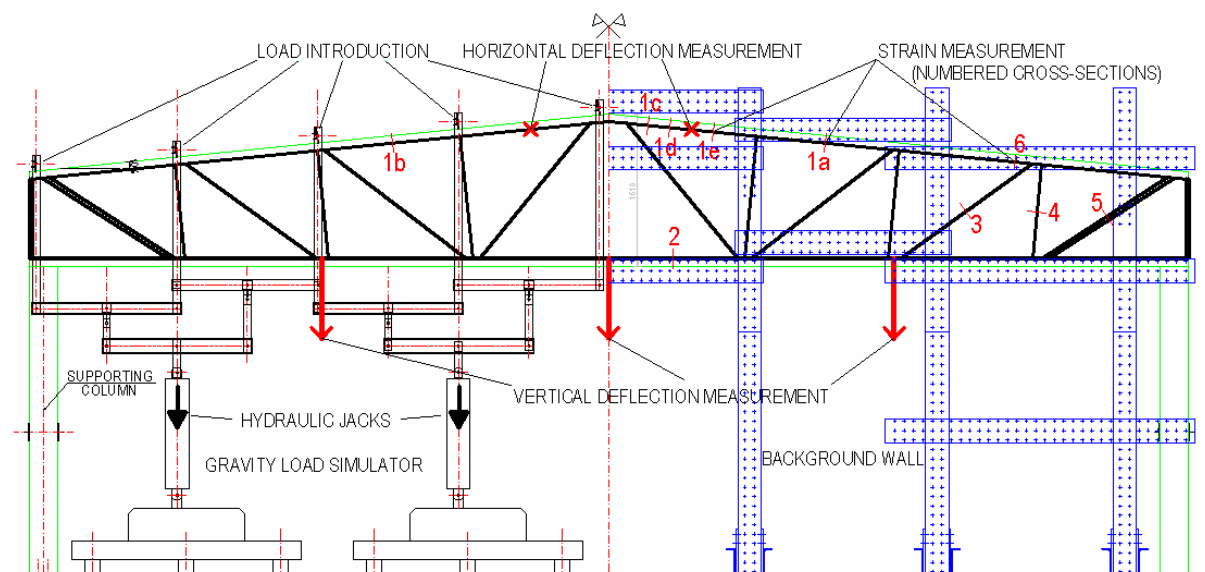

Figure 74.: Test setup – schematics of the loading and measurement system.

The arrangement of the strain gauges is shown in Figure 75. for upper chord members and two different arrangements for brace members in Figure 76. In all cases the gauges were used to measure in axial direction.
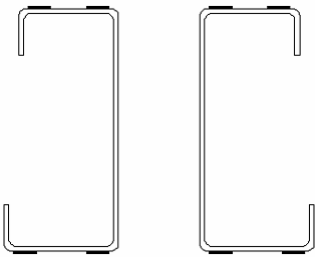

Figure 75.: Strain measurement points in the upper chord members' cross-sections.
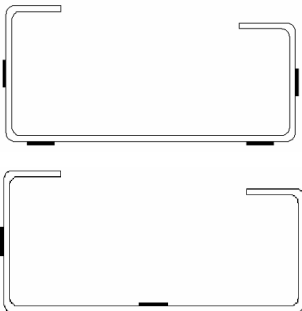

Figure 76.: Strain measurement points in the brace members' cross-sections.

The signals of the transducers and the load cell were recorded at 1 Hz sampling frequency using a HBM Spider8 amplifier and laptop PC running HBM CatmanExpress measurement software, enabling real-time data visualisation. Strain measurement was carried out using a system with devices not capable of real-time data transfer, hence during testing the increase of the load was stopped at certain levels for approximately one minute to measure strains. To enable comparison of the test specimen and design method, the SLS and ULS load levels were always included in these "stops"; the measurement data was used to calculate the internal actions in the members.

During testing the load was applied incrementally by the jacks operating the gravity load simulator. In the first part of the tests usually no deformations visible to the naked eye were present, due to the big span and linear behaviour of the structure. In this stage the global behaviour and current state of the specimen was followed on the force-displacement diagrams displayed on the computer screen. The specimens were first loaded and unloaded in a few cycles to a certain degree of the serviceability limit state (SLS) load level, staying in the range of the linear behaviour of the structure. Load- and unload cycles were repeated until no significant change of the residual deflections in two consecutive load cycles reaching SLS load level was observed, enabling the bolts to take their positions. Final failure was induced only after this process. In the following the testing procedures and the behaviour of the specimens are presented based on this last loading cycle.

3.2.2. Test specimens and observed behaviour

The first test specimen was designed by the designer of the industrial partner for 1.25 kN/m^2 (SLS) and 1.74 kN/m^2 (ULS) load, equivalent of 22.55 kN/jack and 31.63 kN/jack loading, respectively. In each subsequent test the detailing or the sections used were changed taking into account the proposals and demands of the industrial partner, but the global geometry and the topology remained the same, thus each test can be considered prototype test. The changes involved changing the sections to avoid the failure modes already obtained, thus produce a new and possibly different one.

In this Chapter the tests are presented in chronological order. The special properties of the specimens as well as behaviour and failure modes observed during the tests are presented in detail using figures and force-deflection diagrams. The presented values of the load-bearing capacities are in all cases include the weight of the loading system (3kN/jack) and friction of the hydraulic jacks (1 kN/jack). The force-deflection diagrams are presented as "raw" measurement results with a vertical line representing ULS load level modified to take into account the simulator and friction (29.63 kN/jack).

Test Number 1

The geometry and the sections used in the first test are presented in Figure 77. This test can be considered as testing the first prototype of the truss system. The most important special property of the specimen is the simple detailing of the ridge joint: the webs of the chord members are connected to each other but there is no connection in the flanges, resulting a joint easy to assemble. The joint is shown in Figure 78.
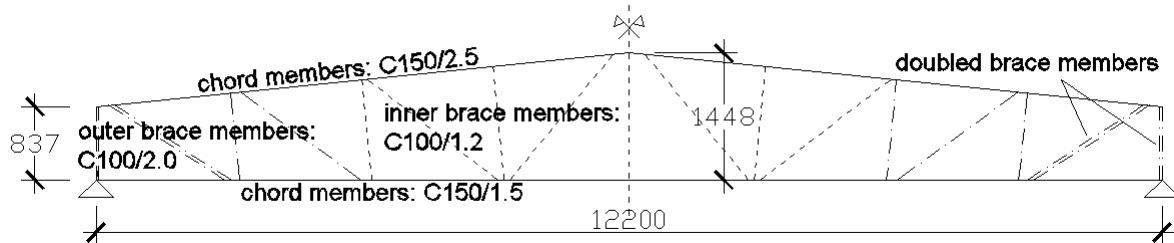

Figure 77.: Geometry and sections in the first test.

During the first – linear – part of the loading process no deformations visible the naked eye were observed on the truss. From 20.5 kN/jack load local buckling was observed in the web of the upper chord members next to the ridge; at this load level the gradient of the load-deflection curves dropped (Figure 79.). On further load increase the buckling waves in the chord and the out-of-plane deflection of the upper chord members next to the ridge gained on amplitude, and the slow decrease of the global stiffness of the truss was observed. The load increasing was stopped as the first signs of the imminent failure – pinches in the web and out-of plane flexural buckling – appeared (Figure 80., Figure 81.), to save the truss for a next test. The obtained failure mode in the first test is the interaction of local buckling, flexural buckling and bending at 28.5 kN/jack load, below the ULS load level.

The observed behaviour is practically the same as in the case of SimpleC members (Chapter 2.2.5, group A), even though the chord member is subject to bending about the major axis. The reason for this is that the load introduction is similar to that in the single-section test, and the stiffness of the section is an order of magnitude higher for bending about the strong axis than that for bending about the weak axis, hence no lateral-torsional buckling could occur.
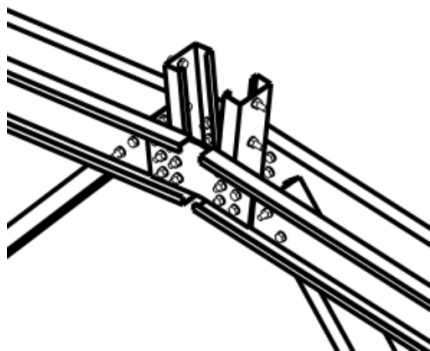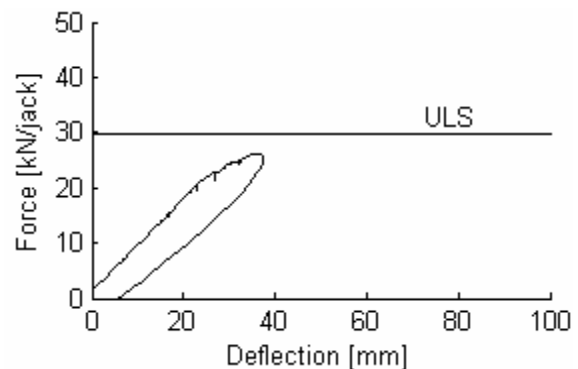

Figure 78.: Ridge joint in the first test.

Figure 79.: Force-deflection diagram – Test 1.

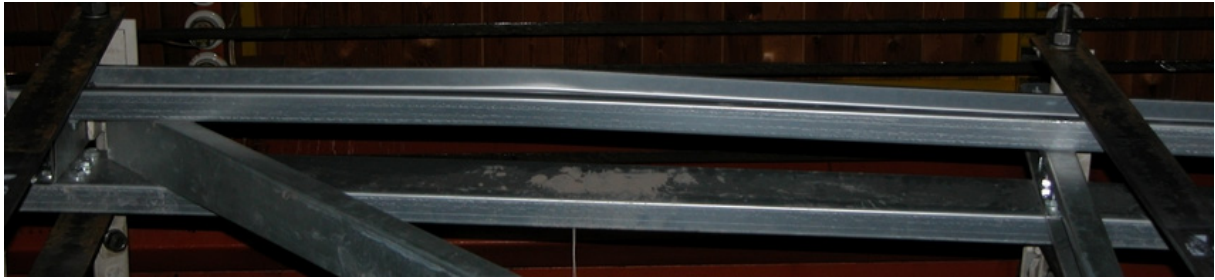Figure 80.: Buckling of the web in the upper chord.

Figure 81.: Out-of-plane deformations.

Test Number 2

In the second test the same specimen used as in the first one was used, strengthened to disable the failure of the chord members. The primary aim of the test was to check the load-bearing capacity of the ridge joint. On both sides, next to the ridge the upper chord members were connected to each-other along the whole length (Figure 82., left). Members second next to the ridge were connected at two points using two C-sections (Figure 82., right).

Figure 82.: Strengthening in the upper chord.

During the loading process the behaviour of the specimen was monitored on the real-time screening of deflections (Figure 83.). The failure occurred rapidly, shortly after the global behaviour becoming non-linear. The failure was caused by the buckling of the gusset plates in the ridge joint at 35.5 kN/jack load level, causing asymmetric plastic deformations in the whole ridge area escalating to the connecting brace members as well (Figure 84.).
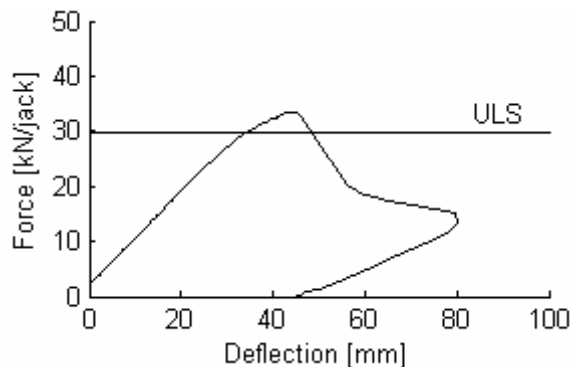
Figure 83.: Force-deflection diagram – Test 2.
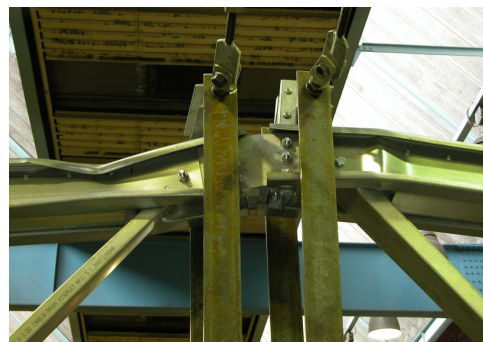
Figure 84.: Failure in the ridge.

Test Number 3

The third test specimen was fabricated by replacing the deformed members of the second specimen: the whole upper chord and the brace members connecting to them at the ridge. The sections of the members were unchanged. The members were connected to each other at half-lengths between the structural joints by means of two 150-mm-long C-sections to form a built-up member (Figure 85., Figure 87.). The configuration of the ridge joint was also changed: the gusset plates connected both the webs and the flanges of the upper chord members (Figure 86.).

Figure 85.: Connecting elements.
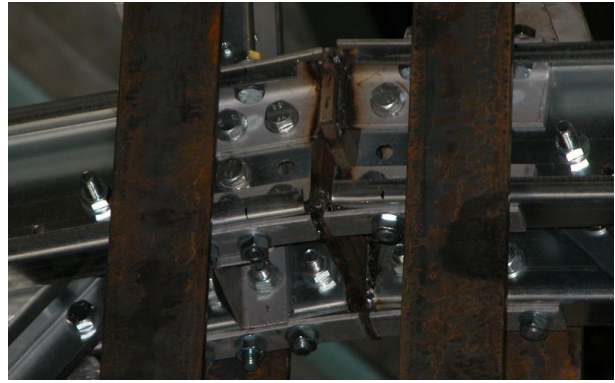
Figure 86.: Ridge joint configuration.
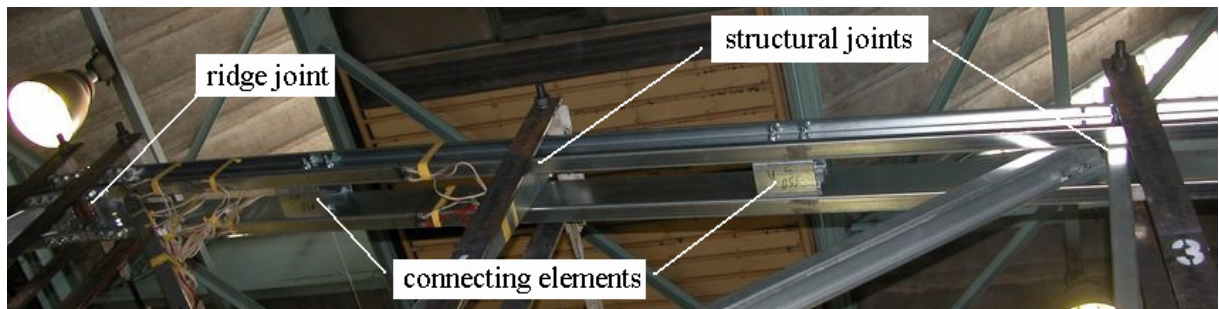
Figure 87.: Upper chord of the third test specimen.

During testing no out-of plane deformations in the linear part of the behaviour were observed. At the load level of 30 kN/jack local plate buckling in the upper chord members second next to the ridge was observed (Figure 88.).

Figure 88.: Local buckling in the upper chord.

The final failure of the specimen was a rapid out-of-plane flexural buckling of the member second next to the ridge (Figure 89.) at 36.4 kN/jack load, causing great plastic deformations and immediate, significant loss of load-bearing capacity (Figure 90.). The buckling length was approximately equal to the system length of the buckled member.
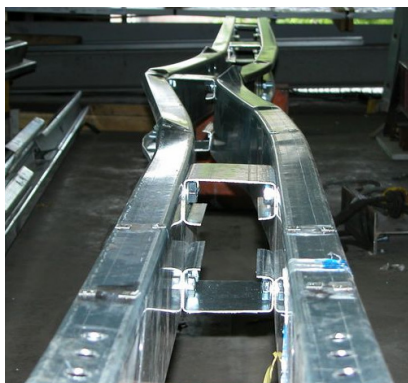
Figure 89.: Failure in the upper chord.
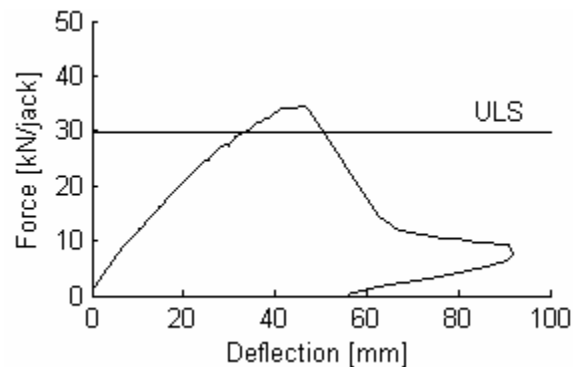
Figure 90.: Force-deflection diagram – Test 3.

50

Test Number 4.

For the fourth test a new specimen was used, with the same geometry as in the previous ones. Stronger sections were used as upper chord members – C150/2.5 instead of C150/2.0 –, and the ridge joint configuration was changed once again, to an end-plate type connection, similar to that used in the third specimen, but easier to assemble (Figure 91., Figure 92.).

During testing, based on the observed global vertical stiffness the behaviour of the truss was linear up to a load level of approximately 33 kN. The starting non-linear response was found to be induced by local buckling of the web of the brace members shown in Figure 92., on both sides of the truss, symmetrically.


Figure 91.: Ridge joint configuration.
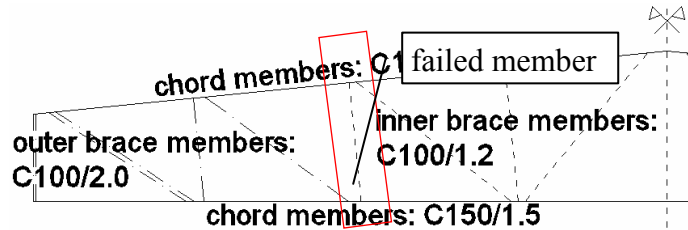
Figure 92.: Sections used in the fourth test.

Increasing the load resulted in dropping global stiffness and forming pinches in the brace member at the upper joint. The obtained failure mode is a failure due to the interaction of axial compression and bending; to avoid the collapse of the specimen, the loading process was stopped (Figure 94.). The measured maximum load was 38.0 kN/jack, the failure of the brace member occurred approximately at 35.4 kN/jack (including the weight of the simulator and jack friction). After disassembling the truss the bolt holes in the flange of the failed member were found to be placed towards the web relative to the planned position (Figure 93.), increasing the eccentricity to the member.

The failed brace member is similar in arrangement to the C-sections tested in the single-section tests in a Brace arrangement (Chapter 2.2.5, group C), especially to test C64. The difference is the specimen length, the number of bolts used in each flange and the moment distribution that is linear with different signs at the end in the case of the truss member and constant in the case of the single section tests.
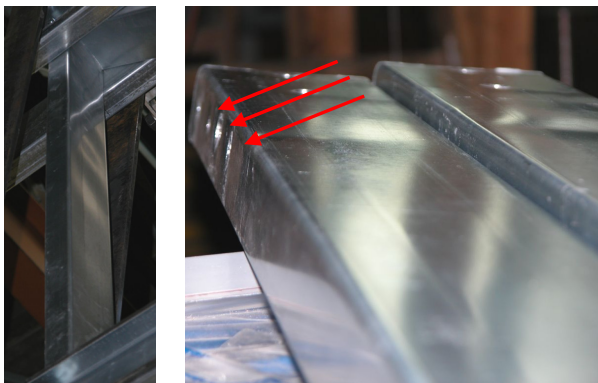
Figure 93.: Failure of the brace column.
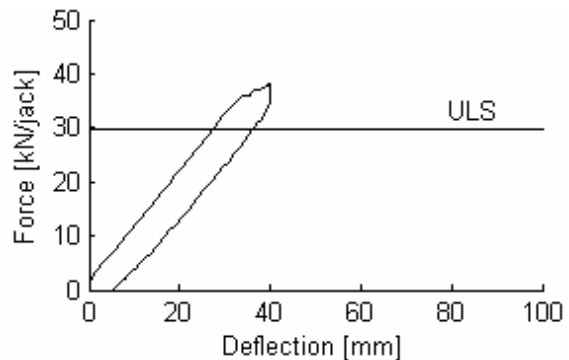
Figure 94.: Force-deflection diagram – Test 4.

Test Number 5

The fifth test was carried out on the same specimen as the fourth with the failed brace column members changed from C100/1.2 to C100/2.0 to avoid failure. The response of the fifth specimen was found to be linear up to a load level of approximately 37 kN/jack, where a continuously dropping stiffness was observed on the force-vertical displacement diagram. The

reason of the non-linearity was found to be a local failure in the lower chord at the structural joints next to the support, symmetrically on both sides of the truss (Figure 95.). Despite the local phenomenon no loss of load-bearing capacity occurred, but the truss showed to further load increase ever-decreasing stiffness. As the load was increased local buckling waves were observed in the upper chord member second next to the ridge joint, with forming pinches in the web and web-flange junctions (Figure 96.), similarly to the phenomena in the first test.

Figure 95.: Failure in the lower chord

Figure 96.: Local buckling in the upper chord.

The final failure of the truss was caused by the out-of-plane flexural bucking of the upper chord members second next to the ridge joint on one side of the truss (Figure 97.). Although not connected to each-other, both chord members buckled in the same direction similarly to the failure in the third test. The load-bearing capacity of the fifth specimen was 47.4 kN/jack (Figure 98.).

The failed upper chord member is similar in its arrangement to a member with a C arrangement in the single C-section tests (see Chapter 2.2.5, group A), at the ridge joint the load is introduced in the upper chord at the flanges and web as well. This results a more uniform stress distribution along the cross-section compared to the failed member of the first test; the difference is similar to that between a C-section with SimpleC and one with a C arrangement.
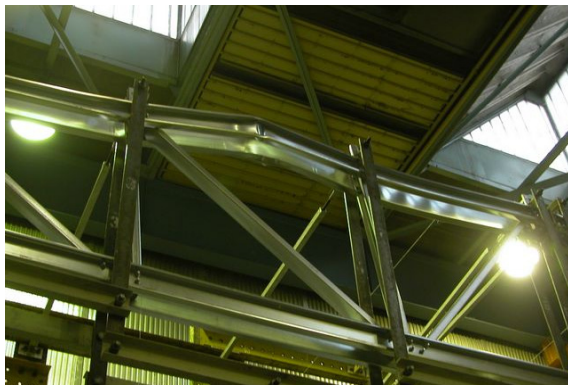

Figure 97.: Failure of the upper chord.
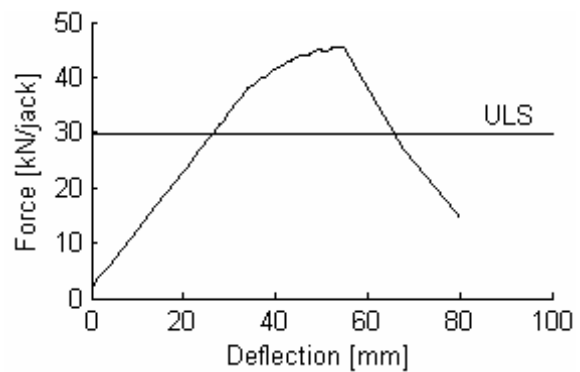
Figure 98.: Force-deflection diagram – Test 5.

3.2.3. Evaluation of the test results

Each test was comprehensively documented by photos or videos shot and notes taken during the testing process; the position of the strain gauges was measured after disassembling the trusses, etc. enabling an in-depth analysis of the test results to support design method validation. In this Chapter the analysis of the test results is presented based on the results of tests number 1, 4 and 5, as these are considered most important from the truss system point-of-view.

The primary aim of the in-depth analysis is to underpin the design method developed for the truss system. This includes checking the model(s) used for global analysis based on measured

deflections and acting internal forces calculated from results of the strain measurement. Comparisons involving the design method are presented in Chapter 3.3.

The direct results of the tests: load-bearing capacity, failure mode and force-deflections diagrams are summarized and compared in Table 16 and Figure 99.

Table 16: Summary of the test results.

Test	Initial stiffness [kN/mm]	Ultimate load [kN]	Failure mode
1	0.83	28.5	Interaction of flexural buckling and bending; upper chord
2	0.86	35.5	Joint failure; ridge joint
3	-	36.4	Flexural buckling of built-up member; upper chord
4	1.04	37.4	Interaction of axial compression and bending; brace member
5a	1.07	37.0	Joint failure; lower chord
5b	1.07	47.4	Interaction of flexural buckling and bending; upper chord

According to the measured initial stiffness two groups can be distinguished among the test specimen: the initial stiffness of first and second test specimens with a lower, and the fourth and fifth specimens with a higher value. The higher stiffness of the two latter is clearly a consequence of the stiffer upper chord. In the case of the third specimen the changing stiffness is caused by the slipping bolted connections, the slope of the curve is in this case approximately equal to that of the first two tests. A clear plateau cannot be observed on the force-deflection diagrams; partially because in some tests the loading process was cancelled to preserve the specimen for another test (Tests 1., 4.), in the other cases a rapid limit-point type failure was obtained, preceded only by ever-decreasing global stiffness.
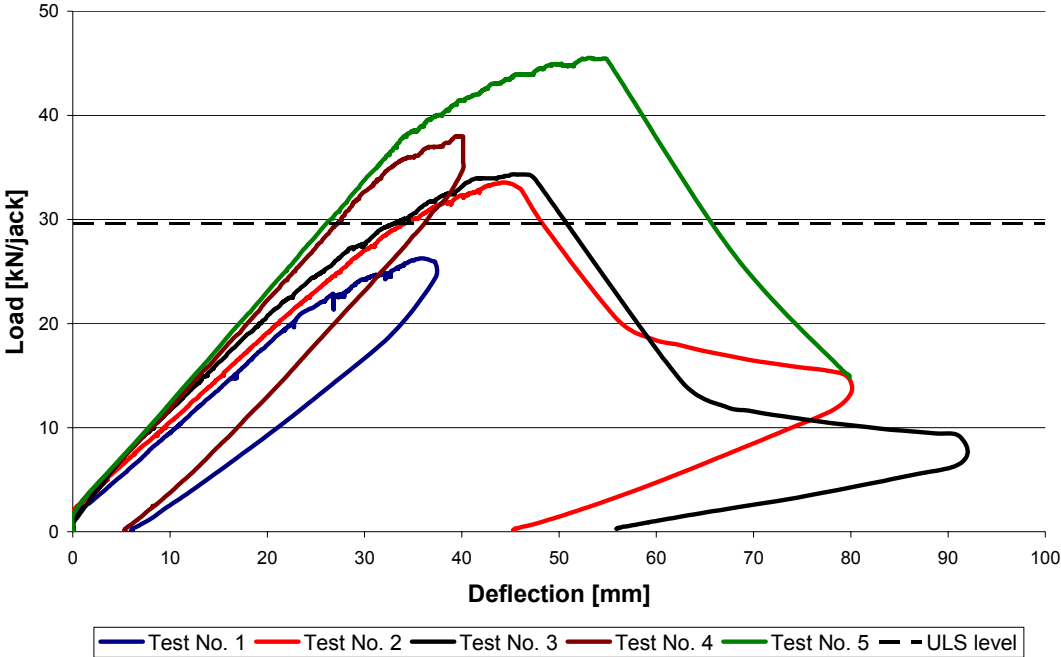

Figure 99.: Load-deflection diagrams of the tests.

The obtained load-bearing capacity is in the first test under the ULS load level. The premature failure of the truss is the consequence of the ridge joint configuration, resulting big out-of-plane eccentricity. In Tests 3, 4 and 5 the detailing of this joint was changed to result more favourable structural behaviour; in the last three tests no sign of failure was observed in this region, and the ULS load level was reached, in the last test the ULS level was exceeded by 50%.

The observed behaviour of the specimens follows the structural symmetry. This reflected in all tests in the symmetrical deflections and the failure modes obtained in Test 4, where brace columns in the same position on both sides of the truss failed, and in Test 5, where the failure in the lower chord was observed on both sides. The symmetric behaviour can be observed in the internal forces as well. Acting axial action and the biaxial bending were calculated in all cross-sections where at least three strain gauges were used; in the case of cross-sections with more than three gauges the forces are calculated by permutation the gauges used, the results are averaged. The calculation method is based on the basic assumptions of elasticity: rigid cross-sections, linear elastic material, hence it is not capable of following local buckling. In the evaluation the properties of the effective cross-section are used in case of compression members, for tension members the gross cross-section is used.

A complete list and position of the cross-sections used in the analysis is presented in Figure 100. and Table 17. The symmetrical behaviour is shown in Table 18 and Figure 101. Cross-sections with the same letter and different number indicate that measurement was carried out on both C-sections (i.e. chord members). Cross-section B1 is not shown in Figure 100., as it is on the opposite ("right") half of the truss, symmetric to cross-section A1. Although strain measurements were carried out in the lower chord as well, these are not used in the evaluation, as in these members only two strain gauges were used each cross-section. It is to be noted, that as in Test 4 and Test 5 the same specimen was used (with member 12 changed), hence the evaluation of the strains is based on the same gauge positions.

Figure 101. shows that the behaviour of the truss is symmetric and can be considered linear for loads smaller than 20 kN/jack, the limit where the global behaviour of the truss used in Test 1 becomes non-linear (Figure 99.). Note, that in this evaluation the elastic state of the material is not checked, hence internal actions for load levels higher than 20kN/jack are not valid, but included, to provide a complete overview.
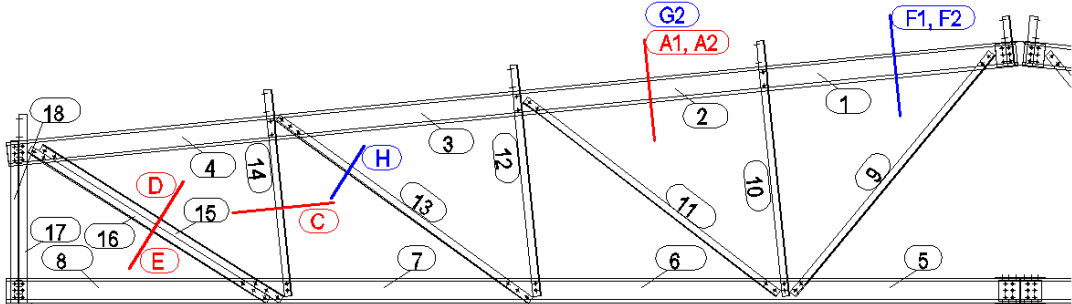

Figure 100.: Notation of cross-sections with strain measurement. Blue numbers indicate measurements in Test 4 and 5, red numbers in Test 1.

Table 17: Position of cross-sections with strain measurement.

Cross-section	Specimen	Section	Position
A1	1	C150/2.0	Member 2, 2250 mm from ridge
A2	1		
B1	1		Member 2, 2250 mm from ridge, opposite side
C	1	C100/2.0	Member 14, 540 mm from lower end
D	1		Member 15, 850 mm from upper end
E	1		Member 16, 880 mm from upper end
F1	4, 5	C150/2.5	Member 1, 820 mm from ridge
F2	4, 5		
G2	4, 5		Member 2, 2250 mm from ridge
H	4, 5	C100/2.0	Member 13, 540 mm from upper end

Table 18: Internal actions calculated from measured strains, A1, A2, B2 cross-sections.

Load [kN]	N [kN]			M_y [kNcm]			M_z [kNcm]		
	A1	A2	B2	A1	A2	B2	A1	A2	B2
0.0	0.00	0.00	0.00	0.00	0.00	0.00	0.00	0.00	0.00
10.0	-20.07	-21.56	-22.55	4.86	6.27	2.31	-10.94	-12.82	-8.55
15.0	-30.85	-33.16	-34.73	3.69	6.00	5.47	-16.93	-19.75	-12.60
20.0	-40.84	-43.98	-46.77	4.21	7.53	7.99	-23.09	-26.81	-16.82
22.5	-42.82	-46.73	-53.25	35.15	39.08	7.30	-28.76	-33.56	-20.46
22.7	-43.33	-47.29	-54.01	35.30	39.29	7.66	-29.15	-34.01	-20.99
24.6	-54.06	-58.35	-60.46	-29.36	-21.65	14.41	-32.27	-35.24	-26.62
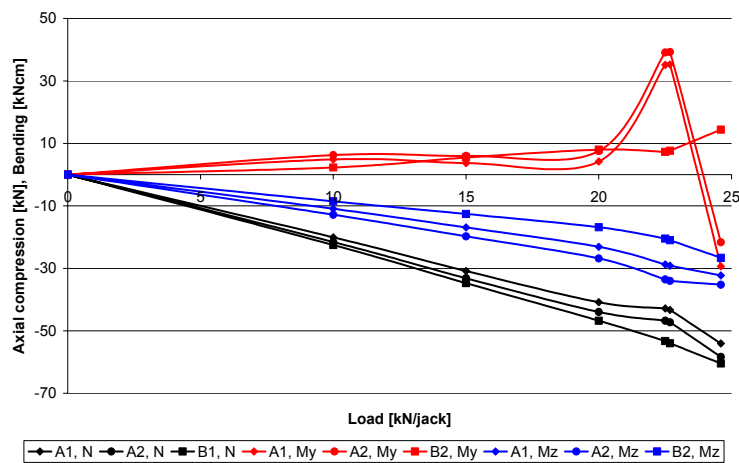
Figure 101.: Internal forces in function of the load – A1, A2, B2 cross-sections.

The structural symmetry results compression and bending actions in the two members of the upper chord (A1, A2) and in the members on the opposite side of the truss (A2, B2) with values in good agreement and tendencies. The peaks in Figure 101. also show that the failure in this test occurred on the side of the truss to that cross-sections A1 and A2 belong. It is to be noted, that the measured bending moments are small in value, the biggest absolute value is 0.35 kNm.

The comparisons show the coherence of the measurement data: deflections can be considered accurate, the calculated internal actions show satisfactory agreement when compared to each-other. Further analysis of the internal actions is to be found in Chapter 3.3.2.

3.3. Design method

3.3.1. Introduction

In this Chapter the design procedure is presented: global analysis, design methods of the structural members and joints are discussed in detail. In the presentation the application rules of EC3 and the final version of the design method are included, the differences are underpinned by laboratory test results.

The design method of the truss system follows the conventional method of Eurocode to design light-gauge structures: loads are calculated as described in Eurocode 1, the basis of design is Eurocode 3 Part 1-1 with application rules as defined in Eurocode 3 Part 1-3. According to this, all members, structural joints and bolted connections are to be checked for ultimate limit state (ULS), the deflections for serviceability limit state (SLS). In the thesis load calculation is not detailed as this in not considered as part of the design method. Methods of global analysis, the numerical model of the truss and verification is presented in Chapter 3.3.2.

As detailed in Chapter 2.4.1, two versions of EC3-1-3 are available for design, differing mainly in the formulae of the application rules as presented in Chapter 2.4.2. It was shown in Chapter 2.4.4, that the two versions yield results close to each-other in case of members in compression and bending. The application rules to design members in tension or tension and bending are essentially the same in both versions of the standard, with formal differences; so are the application rules for designing bolted connections. During the development the older version of the standard – EC3-1-3:1996 – was used, and the final version of the design method is also based on the formulae of this code. The design method of the truss members is presented in Chapter 3.3.3, design of structural joints, including the joint-chord interaction and the method of calculating bolted connections is presented in Chapter 3.3.4. In the following Chapters the design rules developed based on the test results are referred to as modified design method.

3.3.2. Global analysis

Global structural analysis of the trusses is based on linear analysis on a simplified 2D numerical model, thus the internal actions of the members can be calculated using commercial FE software. In the model the complex geometry is simplified by taking into account the in-plane eccentricity only: the doubly arranged chord members, as well as the brace members are modelled using single elements, out-of-plane eccentricity is taken into account on the structural member design level.

Due to the in-plane eccentricities beam elements, preferably 2-node 6 DOF beam elements are to be used in the model, as the simplifications utilized make the use of more advanced elements unnecessary. In the global analysis cross-sectional properties to be used are those derived from the gross cross-section of the members. All elements are modelled by their center lines; in-plane eccentricities of the joints result from the distances of these lines.

The simplifications in the model geometry are reflected in the definition of the cross-sections and the way internal forces are calculated during structural member design. The internal forces of brace members are the axial action, bending about the weak axis and in-plane shear. Doubled brace members can be modelled either with one or two elements; in the latter case cross-sectional properties are to be defined by doubling the respective values, taking no composite action of double members into account.

Bending due to the out-of-plane eccentricity is calculated based on the product of the axial force and the nominal value of the eccentricity, that is, the distance of the chord member's centroid and web, as detailed in Chapter 3.3.3. The model and the distribution of the internal actions resulting from the load applied in the laboratory tests are presented in Figure 102. – Figure 105.
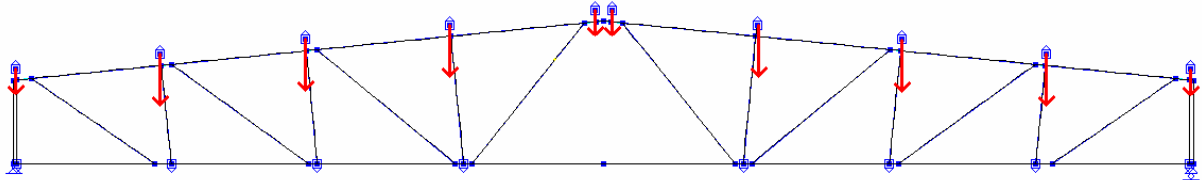
Figure 102.: Geometry and loads of the numerical model.
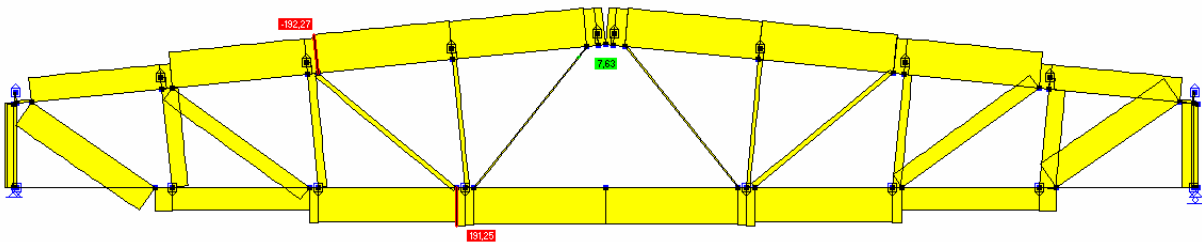
Figure 103.:Distribution of axial forces.
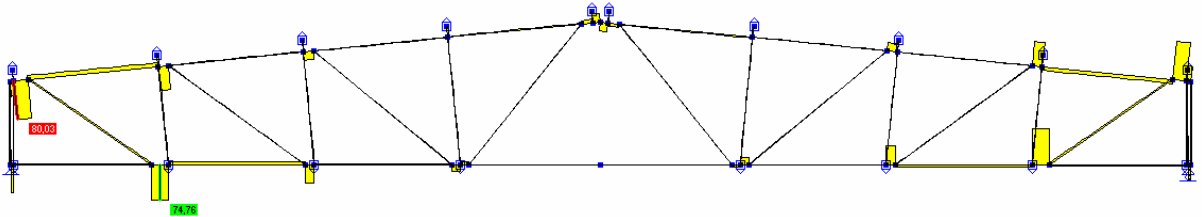
Figure 104.: Distribution of shear forces.
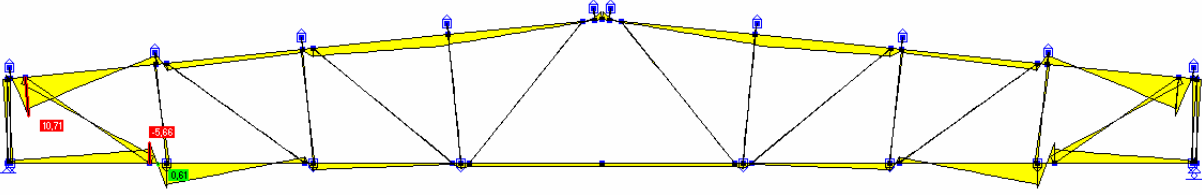
Figure 105.: Distribution of bending moments.

The global model was verified using the results of the laboratory tests: vertical deflections and internal actions calculated from measured strains. From the internal actions primarily the axial forces are considered relevant from the verification point-of-view; bending moments, especially in the brace members have small values and the strain gauges were placed in these members near the zero moment points, thus they may lead to misleading results.

Deflections measured and obtained from the FE model are compared in Table 19 for Test 1. and Test 5. The comparison shows, that the global model overestimates the initial stiffness of the truss, and the difference grows as the load increases. The reason of the differences is the overestimated rigidity of the joints and that the model is not capable of following the effect of local buckling. The specimen used in Test 5 maintains a constant ratio of measured and calculated deflections up to the ULS load level, which is most likely the result of the favourable ridge joint configuration and the higher web b/t ratio of the chord members.

Table 19: Measured and calculated deflections.

	Test 1.				Test 5.		
Load [kN/jack]	Deflection [mm]		Ratio (test/FE)	Load [kN/jack]	Deflection [mm]		Ratio (test/FE)
	test	FE			test	FE	
0.00	0.00	0.00	-	0.00	0.00	0.00	-
10.00	10.64	8.22	1.29	10.00	9.35	7.98	1.17
15.00	16.59	12.33	1.34	20.00	18.70	15.96	1.17
20.00	22.74	16.44	1.38	30.00	28.04	23.94	1.17
22.50	26.19	18.50	1.42	35.00	33.35	27.93	1.19
22.68	27.11	18.65	1.45	40.00	41.95	31.92	1.31
24.60	31.48	20.23	1.55	-	-	-	-

A summary on the comparison of internal actions obtained from the FE model and calculated from the measured strains is presented in Table 20, Table 21 and Table 22. In Table 20 results of Test 5, cross-section F1 is shown for all investigated load levels. In Table 21 results are presented for 20.0 or 30.0 kN/jack load level for each test; Table 22 summarizes the results: median values of the ratios of test and FE results (excluding results at 0.00 kN load level). M_z values for the FE results are calculated by multiplying the axial force with the nominal value of the out-of-plane eccentricity to enable comparison.

The result of comparing internal actions show a wide scatter, which is partially because of the uncertainties in the measurement and evaluation (mechanical model, position of strain gauges, etc.), hence no absolute statements on the accuracy of the model can be done.

Table 20: Comparison of test and model internal actions (Test 5, cross-section F1).

Load [kN/jack]	Test			FE model			Ratio (test/FE)		
	N [kN]	M_y [kNcm]	M_z [kNcm]	N [kN]	M_y [kNcm]	M_z [kNcm]	N	M_y	M_z
0.0	0.00	0.00	0.00	0.00	0.00	0.00	0.00	0.01	0.00
10.0	-16.26	0.21	-0.03	-21.74	0.17	-0.59	0.75	1.24	0.06
20.0	-34.82	0.43	-0.08	-43.48	0.33	-1.17	0.80	1.31	0.06
30.0	-54.03	0.63	-0.13	-65.22	0.50	-1.76	0.83	1.26	0.07
35.0	-63.60	0.71	-0.16	-76.09	0.58	-2.05	0.84	1.22	0.08
40.0	-72.85	0.69	-0.20	-86.96	0.66	-2.35	0.84	1.03	0.08
44.0	-81.53	0.58	-0.23	-95.66	0.73	-2.58	0.85	0.80	0.09
45.5	-83.46	0.49	-0.22	-98.92	0.76	-2.67	0.84	0.64	0.08

Table 21: Comparison of test and model internal actions (selected results).

Test	Cross-section	Load [kN/jack]	Test N [kN]	Test M_y [kNcm]	Test M_z [kNcm]	FE model N [kN]	FE model M_y [kNcm]	FE model M_z [kNcm]	Ratio (test/FE) N	Ratio (test/FE) M_y	Ratio (test/FE) M_z
Test 1	A1	20.0	-40.84	4.21	-23.09	-43.93	46.48	-57.73	0.93	0.09	0.40
	A2	20.0	-43.98	7.53	-26.81	-43.93	46.48	-57.73	1.00	0.16	0.46
	B1	20.0	-46.77	-7.99	-16.82	-43.93	-46.48	-57.73	1.06	0.17	0.29
	C	20.0	-33.54	18.78	18.12	-35.75	-	3.72	0.94	-	4.87
	D	20.0	33.59	-0.47	-3.62	31.25	-	-0.40	1.07	-	9.05
	E	20.0	36.42	1.51	-5.66	32.85	-	-0.76	1.11	-	7.45
Test 4	F1	30.0	-52.81	0.60	-0.17	-65.22	0.56	-1.76	0.81	1.07	0.10
	F2	30.0	-61.62	0.69	-0.18	-65.22	0.56	-1.76	0.94	1.23	0.10
	G2	30.0	-47.63	1.14	-0.13	-65.95	0.91	-1.78	0.72	1.26	0.07
	H	30.0	-55.98	-0.19	-0.13	-48.73	-	-0.08	1.15	-	1.76
Test 5	F1	30.0	-54.03	0.63	-0.13	-65.22	0.50	-1.76	0.83	1.26	0.07
	F2	30.0	-60.32	0.68	-0.13	-65.22	0.50	-1.76	0.92	1.37	0.08
	G2	30.0	-51.27	1.07	-0.08	-65.96	0.93	-1.78	0.78	1.15	0.05
	H	30.0	-55.86	-0.15	-0.11	-48.83	-	-0.10	1.14	-	1.11

The results of axial actions in chord members show -8 to +7% differences in the case of Test 1, which is acceptable result. In the case of Test 4 and Test 5 the differences are -28 to -6%, with values calculated from stain measurement a little closer to the ones calculated using the model in case of Test 5.

Table 22: Summary of the comparison of test and model internal actions.

Test	Cross-section	Median of ratios (test/FE) N	Median of ratios (test/FE) M_y	Median of ratios (test/FE) M_z
Test 1	A1	0.92	0.16	0.42
	A2	0.99	0.22	0.48
	B1	1.07	0.15	0.31
	C	0.94	-	5.23
	D	1.06	-	9.43
	E	1.11	-	7.68
Test 4	F1	0.81	1.01	0.10
	F2	0.94	1.16	0.10
	G2	0.72	1.27	0.08
	H	1.15	-	1.76
Test 5	F1	0.84	1.22	0.08
	F2	0.94	1.33	0.08
	G2	0.74	1.17	0.06
	H	1.14	-	0.98

The axial actions calculated from strain measurements in brace members are higher by 6-15% in case of tension members (cross-sections D, E, H), and 6% lower in case of compression members (cross-section C) than the values obtained from the numerical model. In the doubled member (cross-sections C, D) the measured axial force is approximately equal in the sections.

Note that – although not considered as a basis for verification – in-plane bending moments in the chord members calculated from the measured stains in the case of Test 1 are generally 20% that of the calculated values, and by up to 30% higher in the case of Test 4 and 5; this is assumed to be the result of the changed ridge joint.

Taking into account the uncertainties in measurement and evaluation and the limitations and simplifications of the model the results are acceptable, the global numerical model is valid.

3.3.3. Design of structural members

Structural members of the truss are to be designed taking into account all possible failure modes relevant for the given member. In the first phase of the development all failure modes included in EC3 were considered relevant; in the final version of the design method those corresponding to the observed stability behaviour and failure modes of the trusses are modified to provide less conservative design.

In this Chapter the design method is presented in light of the test results: the failure modes and load-bearing capacities of Tests 1, 4 and 5 are analysed and compared to the formulae of the application rules and the final version of the design method. It is understood, that the safety of the design – whether it is based on the formulae of the application rules or on that of the developed method – can not be judged based on the results of one test, but in Chapter 2.4.4 it was shown, that the studied application rules are accurate in the case of single structural members and the truss members are of similar arrangement. The design methods in light of the tests are judged based on the utilisations calculated for the members according to the application rules and the modified design method, that is, the design method of the truss.

In this Chapter both the application rules and the modified design method are used, and the calculated utilisations r_t, that is, the value obtained by evaluating the design formulae (e.g.: the ones presented in Chapter 2.4.3) for all members relevant are presented in tables. The internal actions used in the calculation of the utilisation are determined using the global FE model. Two load levels are considered: the ULS level and the ultimate load measured in the test in which the given member failed. In the tables the member failed in the given test is highlighted with bold setting; the results of this member are considered when changing the application rules to calibrate the design method. Considering a member, if r_t is greater or equal to 1.00, the design method is rather conservative, if r_t is less, than 1.00 it is rather conservative. If the member failed in the test, r_t calculated for the ultimate load indicates the safety of the design formula: r_t more than 1.00 indicates safe, less than 1.00 indicates unsafe design. It is understood, that the word safety is used in this context in a very simplified manner, as the uncertainties in e.g. the material properties are not included in the evaluation.

The numbering used in this section to distinguish members is shown in Figure 106. Due to the symmetry of the truss in the tables only the members on the "left" side are presented.
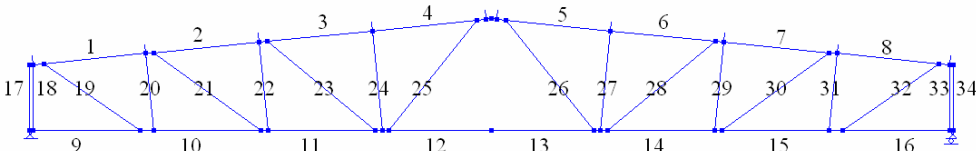
Figure 106.: Numbering of the truss members.

Design of compression chord members

Compression chord members are subject to axial compression, biaxial bending and shear. According to the standard, such elements are to be checked for interaction of axial compression and bending (in the following: N-M interaction), interaction of shear and axial force (in the following: N-V interaction) as cross-section failure modes, and the stability limit

states flexural buckling about both axes, flexural-torsional buckling, torsional buckling, lateral-torsional buckling, interaction of flexural buckling and bending (in the following: FB-M interaction) and interaction of flexural buckling and lateral-torsional buckling (in the following: FB-LTB interaction). From the numerous stability failure modes covered by the standard those not involving interaction are not relevant from the design point-of-view, as they provide lower utilisation (e.g.: flexural buckling) or cover phenomena not observed in the tests and not relevant for the cross-section (e.g.: torsional buckling). As relevant failure modes for compression chord members are the N-M, FB-M and FB-LTB interactions considered. The effect of shear in the members is neglected, N-V interaction is taken into account in the design of joints, as detailed in Chapter 3.3.4. The failure modes covered by the standard but not relevant from the structural behaviour point-of-view are not detailed in the thesis.

Due to the similar supporting conditions the internal actions of compression chord members are essentially the same as that of the single members tested in SimpleC and C arrangement, as presented in Chapter 2.2.5, with the difference that chord members are in biaxial bending, hence lateral-torsional buckling is a phenomena to be accounted for. The design formulae of the application rules for N-M and FB-M interactions are presented in Chapter 2.4.3.

The checking formula of the application rule for FB-LTB interaction is following:

$$\frac{N_{Ed}}{\chi_{min} \cdot f_{yb} \cdot A_{eff} / \gamma_{M0}} + \frac{\kappa_{LT} \cdot (M_{y,Ed} + \Delta M_{y,Ed})}{\chi_{LT} \cdot f_{yb} \cdot W_{eff,y,com} / \gamma_{M0}} + \frac{\kappa_z \cdot (M_{z,Ed} + \Delta M_{z,Ed})}{f_{yb} \cdot W_{eff,z,com} / \gamma_{M0}} \leq 1.0 \qquad (36)$$

Formula *(36)*, considering formulae *(6)* and *(19)* is the general case of checking slender members in compression and bending as it takes into account both flexural buckling and lateral-torsional buckling with reduction factors, and is formally the same as those. Hence, if the member considered has a low slenderness, or – as in the case of the single C-section members – one of the addends is zero, formula *(36)* yields the checking for FB-M interaction, thus it is not necessary to carry out checks for this as well. Since the orientation of the chord member is fixed and therefore the bending about the weak axis results compression in the web, this formula also covers strength checking on the compression side.

In formula *(36)* the factors are as follows:

N_{Ed}	axial compression from the global analysis,
$M_{y,Ed}$	bending about the strong axis from the global analysis,
$M_{z,Ed} = N_{Ed} \cdot y_c$	bending about the weak axis,
y_c	distance of the centroid and the web of the cross-section,
$\chi_{min} = min(\chi_z, \chi_{TF})$	reduction factor for flexural buckling, in the case of the truss system $\chi_{min} = \chi_z$,
χ_{LT}	reduction factor for lateral-torsional buckling,

$$\kappa_{LT} = 1 - \frac{\mu_{LT} \cdot N_{Ed}}{\chi_z \cdot f_{yb} \cdot A_{eff}} \qquad \text{but} \qquad \kappa_{LT} \leq 1.0 \qquad (37)$$

$$\mu_{LT} = 0.15 \cdot \lambda_{lat} \cdot \beta_{M,LT} - 0.15 \qquad (38)$$

$\Delta M_{y,Ed}$ and $\Delta M_{z,Ed}$ bending moments about the strong and weak axis, respectively, due to the shift of the centroid.

The factor $\beta_{M,LT}$ is to be calculated depending on the shape of the bending moment distribution. The calculation of χ_{LT} follows the same pattern as the calculation of the reduction

factors in EC3: it is derived from the pertinent relative slenderness, using buckling curve "a". To calculate relative slenderness the following formula is to be used:

$$\overline{\lambda_{LT}} = \sqrt{\frac{f_y \cdot W_{eff}}{M_{cr}}} \qquad (39)$$

where M_{cr} stands for the critical moment of the member calculated based on the gross cross-section. As no closed formula is provided in the design code for the calculation of M_{cr}, this was derived utilizing the finite strip method.

The calculation of buckling lengths is based on the values provided by the standard, the values used are presented in Table 23.

Table 23: Buckling lengths.

Factor	Buckling mode
$\nu_y = 0.9$	Flexural buckling about the y-y axis (in-plane flexural buckling)
$\nu_z = 1.0$	Flexural buckling about z-z axis (out-of-plane flexural buckling)
$\nu_{LT} = 0.9$	Lateral-torsional buckling about z-z axis
Buckling length is calculated as $\nu_i \cdot l_0 = l$, with l_0 being the system length.	

The utilisations calculated using formula *(36)* for the upper chord members of the specimens used in the tests for the ULS and ultimate load levels are presented in Table 24 with the failed member highlighted.

It is to be noted, that during the design of the first test specimen the out-of-plane eccentricity was neglected, as its value was considered small; the results presented in the tables are calculated taking it into account.

Table 24: Utilisations of the compression chord members.

Load level	Test	Member			
		1	2	3	4
ULS	1	1.31	1.39	1.56	**1.52**
	5	0.97	0.99	**1.12**	1.09
Ultimate load	1	1.18	1.25	1.40	**1.37**
	5	1.45	1.50	**1.69**	1.64

The test results show, that the neglected out-of-plane eccentricity and unfavourable joint arrangement yields an unsafe structure, as in the first test the ultimate load level was less than the ULS level. Changing the ridge joint configuration to enable force transfer in the flanges of the chord members the load bearing capacity is enhanced. The utilisation of the specimen used in Test 5 is over 100% at the ULS level and is 169 % at failure, although the ratio of the ultimate load and the ULS load is 1.5; this indicates that the application rule for this arrangement yields conservative design and can be changed to provide more economic results.

The application rule of EC3 to design the upper chord members of the trusses was changed by reducing the out-of-plane eccentricity to be taken into account in the design by 50% to reflect the favourable ridge joint detailing as follows:

$$\frac{N_{Ed}}{\chi_{min} \cdot f_{yb} \cdot A_{eff} / \gamma_{M1}} + \frac{\kappa_{LT} \cdot (M_{y,Ed} + \Delta M_{y,Ed})}{\chi_{LT} \cdot f_{yb} \cdot W_{eff,y,com} / \gamma_{M1}} + \frac{\kappa_z \cdot (0.5 \cdot M_{z,Ed} + \Delta M_{z,Ed})}{f_{yb} \cdot W_{eff,z,com} / \gamma_{M1}} \le 1 \qquad (40)$$

The utilisations for the ULS load level calculated using *(40)* are presented in Table 25.

Table 25: Utilisation of the chord members (modified design method).

Load level	Test	Member			
		1	2	3	4
ULS	1	1.15	1.15	1.30	**1.26**
	5	0.85	0.83	**0.94**	0.91
Ultimate load	1	1.03	1.04	1.17	**1.14**
	5	1.27	1.25	**1.41**	1.37

The results show, that if the ridge joint provides full force transfer, the modified design formula yields utilisations under 100% for the ULS load level, the safety against failure is over 1.4, thus the method can be considered valid.

Design of compression brace members

According to the standard compression brace members are to be checked for N-M interaction, flexural buckling about both axis, torsional buckling, torsional-flexural buckling, FB-M interaction. Stability failure modes involving lateral-torsional buckling can be omitted, since in these members no bending about the strong axis is present. Signs of torsional-flexural behaviour modes were not observed during the testing, due to the supporting conditions, hence the design method of these members can be reduced to checking FB-M and N-M interactions. The checking formulae of the application rules are presented in Chapter 2.4.3.

In the development version of the design method these members were handled as members in centric compression and bending, as it was suspected, that the eccentricity of the load introduction is small.

The utilisations calculated according to *(6)*, *(7)* and *(19)* using this approach for the ULS load level and the ultimate load of Test 4 are presented in Table 26, with the member failed in Test 4 highlighted.

Table 26: Utilisation of the compression brace members.

Load level	Test	Member				
		17	18	20	22	24
ULS	4	0.62	0.80	0.85	**0.77**	0.42
	5	0.62	0.80	0.85	0.41	0.40
Ultimate load	4	0.77	0.99	1.04	**0.94**	0.53
	5	0.91	1.18	1.24	0.59	0.61

The member failed in Test 4 had at failure an utilisation of 94%, which points to unsafe design. However, the highest utilisation among the brace members was 124%; this points to the failure is caused by the inaccurate assembly as presented in Chapter 3.2.2. To avoid premature failure due to such reasons, an additional eccentricity was defined to be taken into account in the cross-section checkings of all – compression and tension – brace members, excluding the doubled columns at support.

According to the modified design method, the eccentricity to be taken into account is

$$\frac{N_{Ed}}{A_{eff} \cdot f_y / \gamma_{M0}} + \frac{N_{Ed} \cdot e_{add} + M_{z,Ed} + \Delta M_{z,Ed}}{W_{eff} \cdot f_y / \gamma_{M0}} \leq 1 \qquad (41)$$

where:

$$e_{add} = \max(8mm, 0.2 \cdot b_1) \qquad \text{the additional eccentricity,} \qquad (42)$$

and b_1 being the width of the smaller flange of the section as defined in Figure 4.

The utilisations obtained using the modified formula *(41)* are summarized in Table 27.

Table 27: Utilisation of the compression brace members (modified design method).

Load level	Test	Member				
		17	18	20	22	24
ULS	4	0.62	0.80	1.10	**0.99**	0.55
	5	0.62	0.80	1.10	0.52	0.53
Ultimate load	4	0.77	0.99	1.39	**1.25**	0.69
	5	0.91	1.18	1.66	0.75	0.79

The utilisation of the member failed in Test 4 at the ULS load level is 99% if calculated with the modified formula and over 124% for the ultimate level, the highest utilisation is 166%. Based on this the safety of the modified design method is over 1.66, the method is valid.

Design of tension chord and brace members

According to the application rules tension members are to be checked for the cross-section failure modes plastic failure, ultimate failure and combined tension and bending. As in the tests no such failure modes were obtained, the same formulae are used in the modified design methods those of the application rules. The following formulae are to be used in the checkings:

$$\frac{N_{Ed}}{A_g \cdot f_{ya} / \gamma_{M0}} \leq 1 \qquad\qquad \text{plastic resistance} \qquad\qquad (43)$$

$$F_{n,Rd} = \left(1 + 3 \cdot r \cdot \left(d_0 / u - 0.3\right)\right) \cdot A_{net} \cdot f_u / \gamma_{M2} \quad \text{ultimate resistance} \qquad (44)$$

where:

d_0	bolt hole diameter, equal to the bolt diameter,
A_{net}	net cross-sectional area,
f_{ya}	average yield stress,
f_u	ultimate stress,

$u = max(2e_2, p_2)$ $\qquad\qquad\qquad\qquad$ e_2, p_2 bolt distances, $\qquad\qquad$ (45)

$r = $ *[number of bolts in the cross-section/number of bolts in bolt layout]*,

and

$$F_{n,Rd} \leq A_{net} \cdot f_u / \gamma_{M2} \qquad\qquad\qquad\qquad\qquad\qquad\qquad\qquad (46)$$

The interaction of tension and bending is to be checked using

$$\frac{N_{Ed}}{A_g \cdot f_{ya} / \gamma_{M0}} + \frac{M_{z,Ed}}{W_{eff,z,ten} \cdot f_{yb} / \gamma_{M1}} + \frac{M_{y,Ed}}{W_{eff,y,ten} \cdot f_{yb} / \gamma_{M1}} \leq 1 \qquad (47)$$

and if $W_{eff,y,ten} \geq W_{eff,y,com}$ or $W_{eff,z,ten} \geq W_{eff,z,com}$, then

$$-\frac{\Psi_{vec} \cdot N_{Ed}}{A_g \cdot f_{ya} / \gamma_{M0}} + \frac{M_{z,Ed}}{W_{eff,z,com} \cdot f_{yb} / \gamma_{M1}} + \frac{M_{y,Ed}}{W_{eff,y,com} \cdot f_{yb} / \gamma_{M1}} \leq 1 \qquad (48)$$

is also to be checked.

In case of tension brace members, similarly to the compression brace members, due to the same reasons the smallest value of $W_{eff,z}$ is used in the checkings. $M_{z,Ed}$ is the bending about the weak axis as calculated using the numerical model and the additional eccentricity is taken into account as defined in *(42)*.

In case of tension chord members in the checkings for the interaction of axial tension and bending $M_{z,Ed}$ is to be calculated as the product of the acting axial force and the reduced value of the out-of-plane eccentricity.

The utilisations of the tension members in Test 5 for the governing checkings listed are summarized in Table 28 with the chord members highlighted.

Table 28: Utilisation of the tension members.

Load level	Test	Member						
		5	9	**15**	16	**22**	23	**31**
ULS	5	0.24	0.95	0.78	0.65	0.77	0.40	0.77
Ultimate load	5	0.36	1.43	1.17	0.98	1.16	0.60	1.16

The highest utilisation among the brace members is present in the diagonal member next to the support, with a value over 142%; the chord member with the highest utilisation is 116% at the middle of the lower chord. As no failures involving tension members were obtained in the tests, these values can be considered as minimum safety of the pertinent design methods.

3.3.4. Design of connections and structural joints

The design of joints is a field not fully covered by the standard. Application rules for designing connections with various types of fasteners are present; however, on the design of structural joints only guidelines are given concerning strength and stiffness. The design method of the truss system dealing with structural joints and connections are derived partially from the application rules; the end connections of the brace members and the in-situ joints of the chord members are covered by these. The design method for the structural joints is derived from the application rule for N-type RHS joints as described in EC3-1-8, and validated using the results of Test 5.

The design of the in-situ connections consists of checking the load-bearing capacity of the bolted connection for shear and bearing resistance; the checking of the net cross-section for ultimate failure is described in Chapter 3.3.3. The design method of the complex structural joints consists of four separate checkings: the end connection of the brace members is to be checked for bearing resistance and bolt shear, the web of the chord member is to be checked for shear buckling and the interaction of axial force and shear; in both checkings, if the structural joint is in the compression chord, the effect of local buckling is included.

Checking bolted connections for shear is to be carried out according to the application rule of EC3-1-3 by calculating the design shear resistance of the bolts:

$$F_{v,Rd} = \alpha \cdot f_{ub} \cdot A_s / \gamma_{M2} \qquad (49)$$

where:

f_{ub} — the ultimate stress of the bolt,

A_s — the tensile stress area of the bolt,

α — reduction factor depending on the bolt grade.

The bearing resistance is to be calculated as:

$$F_{b,Rd} = 2.5 \cdot f_u \cdot d \cdot t / \gamma_{M2} \qquad \text{but} \qquad F_{b,Rd} \leq f_u \cdot e_1 \cdot t / (1.2 \cdot \gamma_{M2}) \qquad (50)$$

where:

d	the diameter of the bolt shaft,
t	smaller of the summa thickness of the plates moving in the same direction,
e_1	edge distance perpendicular to the direction of the force.

For the two design resistances the inequalities $1.2 \cdot F_{b,Rd} \le F_{v,Rd}$ and $1.2 \cdot F_{n,Rd} \le F_{v,Rd}$ must be true. Similar all other bolted connections the design resistance of long joints is to be reduced, and the formulae are valid only if the limits of edge- and bolt distances are kept.

The checking of the structural joints affects primarily the short sections of the members at the supports where due to the in-plane eccentricity the intensity of the shear force is an order of magnitude higher than in the members, hence the following checkings are to be performed only on the short elements of the numerical model representing these areas.

The resistance of the web of the chord members is to be calculated considering the web as an infinitely long unstiffened panel. The design checking is to be completed as follows:

$$V_{b,Rd} = \frac{\chi_w \cdot f_y \cdot A_{v,eff}}{\sqrt{3} \cdot \gamma_{M5}} \ge V_{Ed} \tag{51}$$

where:

$V_{b,Rd}$	design shear resistance of the section,
χ_w	reduction factor for shear buckling, considering an infinitely long panel $(k_\tau = 5.34)$,
$A_{v,eff}$	the gross area of the web if the joint is in the tension chord, the effective area of the web for uniform compression stress if the joint is in the compression chord $(k_\sigma = 4)$,
V_{Ed}	the maximum shear force in the joint.

The interaction of the chord member and the joint is calculated using the following formula:

$$N_{0,Rd} = \left[\left(A_{0,eff} - A_{v,eff} \right) \cdot f_y + A_{v,eff} \cdot f_y \cdot \sqrt{1 - \left(V_{Ed} / V_{b,Rd} \right)^2} \right] / \gamma_{M5} \tag{52}$$

where:

$A_{0,eff}$	the gross cross-sectional area of the chord member if the joint is in the tension chord, the effective area of the cross-section of the chord member for axial compression if the joint is in the compression chord,
$V_{b,Rd}$	calculated according to *(51)*.

In contrary to the usual approach where the design resistance of a member is compared to the internal forces acting in the member, formula *(52)* provides and upper limit for the axial force acting in the chord member, thus, although detailed in this Chapter, it is a checking to be carried out alongside with those presented in Chapter 3.3.3.

The utilization of the chord members for this failure mode calculated using *(52)* is presented in Table 29. The results show, that this failure mode is not governing in any member of the truss.

Table 29: Utilizations for the interaction of joint and member.

Load level	Test	Lower chord				Upper chord			
		5	15	22	31	10	17	24	30
ULS	5	0.01	0.29	0.44	0.46	0.23	0.34	0.37	0.37
Ultimate load	5	0.01	0.44	0.66	0.70	0.35	0.51	0.56	0.55

The most utilized joints in the trusses are those near the supports, as shown in Figure 104. The utilisations according to *(51)* of the joints based on the results of Test 5 are presented in Table 30 (joints with less than 10% utilization at ULS level are omitted), the joint failed in Test 5 is highlighted. The results show, that the utilisation of the failed joint is near 150% at the collapse of the specimen.
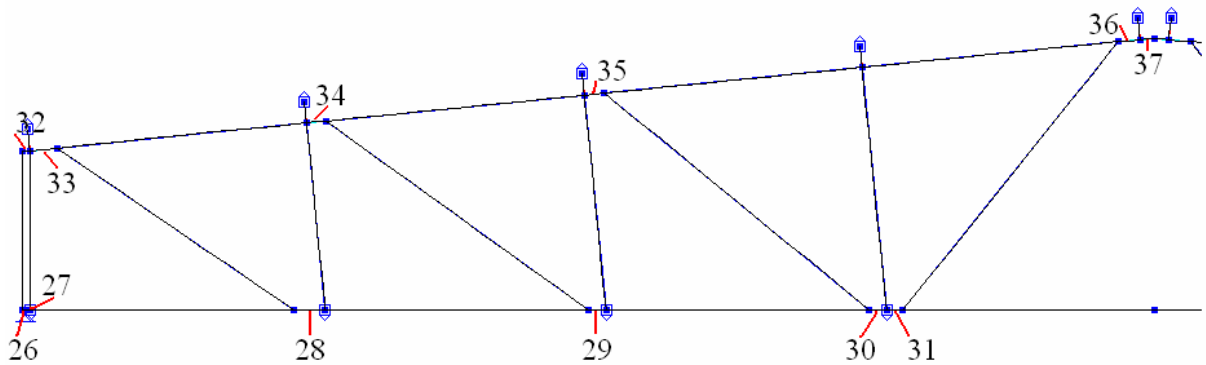

Figure 107.: Numbering of the joints.

Table 30: Utilisation of the joints.

Load level	Test	Member							
		26	27	28	29	30	32	33	34
ULS	5	0.41	0.77	**0.98**	0.52	0.18	0.15	0.38	0.24
Ultimate load*	5	0.48	0.90	**1.15**	0.60	0.21	0.17	0.44	0.28
Ultimate load**	5	0.62	1.16	**1.48**	0.78	0.28	0.22	0.57	0.36

* the load level of the failure of the lower chord joint, 37.0 kN/jack

** the load level of the failure of the upper chord members, 47.4 kN/jack

3.4. Summary

In this Chapter the process and main results of the development of a truss system made of cold-formed C-section members was presented.

In the first stage of the development the structural arrangement and a preliminary version of its EC3-based design method was developed, which was used to design the prototype of the truss. Five laboratory tests were carried out on the truss with the aim to enhance its performance by changes in detailing, and to refine and validate the design method. The result of the development is a system of design rules and instructions forming the basis of the truss system.

The test results: obtained failure modes and the pertinent load-bearing capacities were used to refine the formulae of the application rules of the standard, and to derive new ones from existing design methods of similar structural arrangements.

The global analysis of the truss is to be carried out using a 2D beam model; in the model the cross-sectional properties are to be taken into account as the properties of the gross cross-section of the members; in case of doubled members (chord members, double brace members) no composite action is to be taken into account.

The design method of the upper chord members was derived from the application rule of EC3 for members in compression and bending by changing the value of eccentricity to be taken into account to calculate bending about the weak axis by 50%. The modified formula yields cca. 15% reduction in the utilisation of the member failed in Test 5 and sets the utilisation at the ULS load level to 94%, at failure to 141%.

To account for misplacing the brace members during the assembly of the truss, the design formulae of these members has been modified to take into account an additional eccentricity, thus an increased bending about the weak axis. Brace members, if necessary, may be doubled to enhance the load-bearing capacity. The doubled members are to be designed without taking into account composite action, that is, if modelled with one element the internal actions are to be halved.

A new design formula for N-type structural joints made using cold-formed C-section members has been derived from the existing application rule provided by the standard for N-type joints of RHS or H-sections. The design method developed accounts for the shear buckling utilisation of the web of the chord members and reduces the axial resistance of them. This checking is complemented by a shear checking of the webs of the chord sections. These two design formulae not only provide additional checking of these structural elements, but take into account the interaction between the truss members and structural joints.

The design method summarized can be used to design trusses made of cold-formed C-section members if the detailing corresponds that of the last specimen tested: the ridge joint configuration enables load transfer between the upper chord members in the webs and the flanges as well.

The laboratory tests and standard-based analysis provides information on the critical parts of the trusses. The upper chord is sensitive to out-of-plane eccentricities; the detailing of the joint ridge plays a major role in the behaviour of these members; the flanges and the webs of the chord members connecting in this joint are to be connected to each-other to enable load transfer through the whole cross-section. The structural joints near the support are most utilized of all joints in the truss and the resistance of these can be governing regarding the size of the C-section to be used in the chord.

4. Numerical modelling of cold-formed structures

4.1. Introduction

The laboratory tests summarized in the previous Chapters provide a basis for design method development, but their major shortcomings: being expensive and time-consuming calls for the use of alternative approaches.

In this Chapter numerical models developed to complete the laboratory tests are presented. As mentioned in Chapter 1.5, the calculation method for the numerical modelling of cold-formed members capable of simulating laboratory tests is available; almost any major FE program supports shell elements, nonlinear material behaviour and large strains/displacements. The computational power needed to carry out such analyses on models with sizes up to a few million DOF is available off-the-shelf, thus the preconditions for modelling large-scale structures are given. However, the use of advanced numerical models to simulate experiments on structures or parts of structures made of cold-formed members is rare, for two reasons.

First, due to the high imperfection sensitivity of cold-formed structures imperfections must be included in the model to obtain the real behaviour and load-bearing capacity. Imperfections may be incorporated in the model based on real imperfections, or by applying equivalent geometrical imperfections. The former method poses difficulties, especially in the case of larger structures, for the latter no unified approach suited for cold-formed members similar to that included in Eurocode 3 Part 1-5 for plated structures [37] is present.

Second, the connector elements used in cold-formed structures – frames, trusses, etc. – result semi-rigid structural joints that influence the global behaviour of these, and in most cases cause interaction between the joints and the connected members. However, no generally applicable model of the connector elements exists that can be incorporated in shell FE models to accurately predict both global and local behaviour of cold-formed structures. Nevertheless, a consistent solution for the question of equivalent imperfections may only be provided once the problem of modelling the semi-rigid structural joints is solved, and vice versa.

From the numerical modelling point-of-view cold-formed members can be considered as shell structures, as the proportions of the plates of the cross-section and strains resulting from the load are similar to those. Eurocode 3 Part 1-6: Strength and stability of shell structures [42] defines seven levels of numerical modelling to be used in design procedures; the most sophisticated approach is to take into account both geometrical and material nonlinearities, and perform the analysis on a structure with initially imperfect geometry (Geometrically and Materially Non-linear Analysis with Imperfections, GMNIA). In the current study this level of modelling is utilized, considering two more aspects: the real material properties and thickness of the plates. This level of modelling is called virtual experimenting, as it enables carrying out laboratory tests using purely numerical methods instead of real ones, either to reproduce the results of a real test – to verify the model – or to obtain the load-bearing capacity of a structure using the verified model without carrying out a test in reality. Note, that virtual experimenting can be used only to complete laboratory tests, as tests are necessary for the verification. However, if virtual experimenting is utilized e.g. in design method development, the number of tests can be greatly reduced if a verified model is available.

In this Chapter the numerical models of single C-section members with C200 section in SimpleC arrangement and of the truss are presented. The models are developed with a coherent approach regarding modelling the geometry of the members, contact surfaces, material properties, etc. Connector elements are modelled using the same basic approach; however the differences in the structural behaviour of bolts and self-drilling screws are

reflected in the models. Equivalent geometrical imperfections are modelled by two approaches: in the case of C-section members these are generated based on results of a constrained finite strip method analysis of the section, in the case of the truss model the shape of the imperfections is derived from the eigenshape of the model. The models are calibrated and verified with the results of test specimens to provide the same rigidity, load-bearing capacity and failure mode.

The computer program used for development is the finite element software package Ansys 11.0 [43], however, the presented techniques can be adapted to other general purpose finite element programs as well.

4.2. Numerical model of SimpleC members

4.2.1. Global numerical model

The geometrical model of the specimens, including the dimensions of the C-section and the gusset plate as well as plate thicknesses and position and diameter of the screw holes is generated corresponding to the real test specimen.

The geometrical model is generated to be perfect, the radii in the corners of the C-section are modelled according to the real geometry. The C-section member and the gusset plates are modelled using 4-node 24-DOF shell elements (SHELL181) with a bilinear (linear elastic – kinematic hardening plastic) material model derived from coupon tests. The material properties applied to the models are derived from the coupon tests presented in the Annex, Table A12. In accordance with the recommendations in [37] the modulus of elasticity was set to 210000 MPa; the modulus of plasticity to 2100 MPa. The material properties measured and those applied in the model are shown in Figure 108. and Figure 109. for t=1.0 mm.
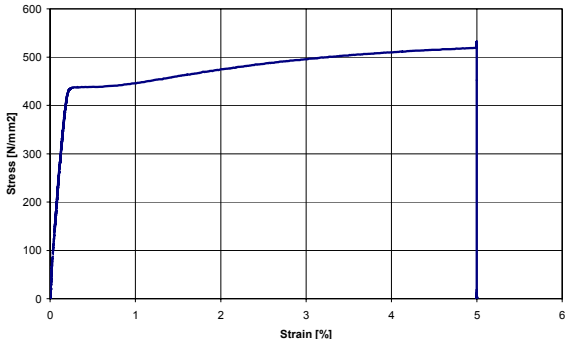

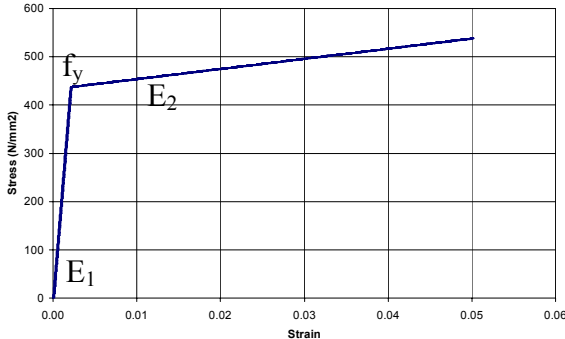Figure 108.: Measured σ-ε diagram ($f_y = 437$ MPa).

Figure 109.: Material model ($f_y = 438$ MPa, $E_1 = 210000$ MPa, $E_2 = 2100$ MPa).

The applied average element edge lengths are summarized in Figure 110. and Table 31; the flat parts of the members (e.g.: flanges, web, etc.) are meshed with the automatic mesh generator of Ansys, the radii are divided in three segments of equal length. Geometrical imperfections are added by the appropriate change of node locations after mesh generation, details on this are given in Chapter 4.2.3. Contact surfaces at the gusset plate are modelled using CONTA173 and TARGE170 surface-to-surface contact and target elements in a symmetric arrangement. To achieve better numerical stability the mesh on the contacting surfaces are congruent and the contact is assumed to be frictionless. The connector elements are modelled using beam elements detailed in Chapter 4.2.2. Load is applied through the nodes of the sole of one of the gusset plates as kinematic constraint – 20 mm displacement in the axial direction to cause compression in the member. Vertical and horizontal supports are applied at all corners of the gusset plate soles. The model details are shown in Figure 111.
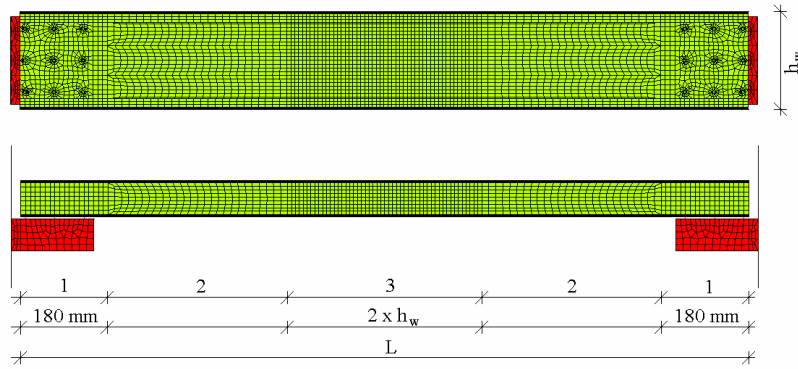
Figure 110.: Zones with different element sizes.

Table 31: Zones with different element sizes.

	Zone 1	Zone 2	Zone 3
Position of zone	From end of specimen to 180 mm	From 180 mm to L/2-h_w	Between L/2-h_w and L/2+h_w
Average element edge length	10 mm	15 mm	8 mm

To solve the model a static analysis was carried out taking into account large deformations, the default Newton-Ralphson iteration procedure was used with the sparse matrix solver chosen automatically by the Ansys solver routine, tolerance of the iteration was 0.5% both for moment and force error.

A MATLAB-based [44] pre- and post-processing program was developed to generate input macros enabling fast model generation and result evaluation.

4.2.2. Numerical model of self-drilling screws

The screw model developed consists of 2-node 12-DOF beam elements (BEAM4): one element represents the shaft of the screw; this is connected to the rim of the screw hole by radial elements, as shown in Figure 112. The material model of each element is linear elastic. The rim of the screw hole is divided in 16 segments of equal length. The shaft element's cross-sectional properties (area, moments of inertia) are derived from the screw shaft diameter. Shear deformations of the shaft element are taken into account; radial elements are set to have no shear deformations. The model can be calibrated by choosing the appropriate values of the cross-sectional area and moments of inertia of the radial beam elements and the shear area of the shaft element as detailed in Chapter 4.2.4.
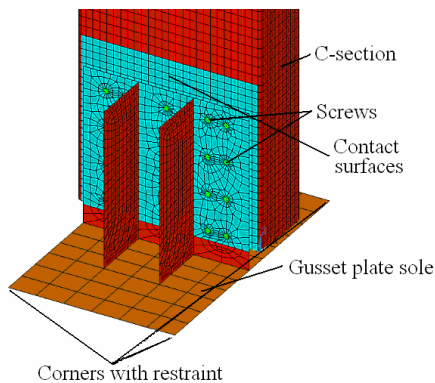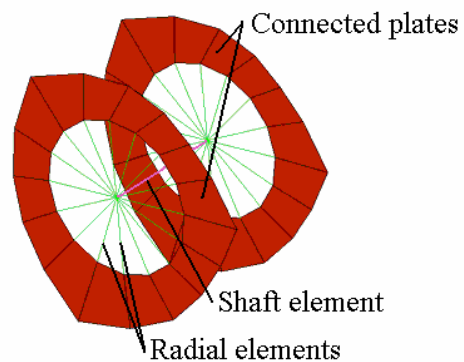

Figure 111.: Detail of the FE model.

Figure 112.: Screw model.

71

As in the screw model no contact elements are used, failure modes involving separation of the screw and the connected plates are not covered by the model. However, the phenomena observed in the joint area during the tests on SimpleC members can be followed using the model as it has all basic properties necessary for this: the shaft is more rigid than the plates and the radial elements are connected to the shell elements similar to that in the reality. The separation of the connected plates is allowed, as the bending deformation of the radial elements makes the pull-out of the screws possible. The tilting of the screw is modelled by the shear deformations of the shaft element. This way, the model is capable of following the change of eccentricity resulting from the relative displacements of the connected plates. Note that modelling the screw behaviour would pose considerable difficulties if spring elements or constraint equations were used.

4.2.3. Modelling of imperfections

Imperfections of the real specimen are applied as equivalent geometrical imperfections with the aim to reproduce the behaviour and load-bearing capacity of the test specimens. It is typical to apply the model eigenshapes for geometrical imperfections, however, in the case of the studied problem, these are mainly coupled modes, thus they do not provide the possibility of an imperfection sensitivity analysis, as the weights of the pure – local, distortional, global – buckling modes in the eigenshapes of the model are not known. Furthermore, any finding regarding the behaviour of the numerical model of a given test cannot be directly applied to another test's model.

The imperfections applied to the models are derived from results of analyses carried out using the constrained finite strip method (cFSM). This method is an extension to the finite strip method (FSM) presented in Chapter 2.2.3 that decomposes the buckling shapes obtained using FSM based on mechanical criteria and yields the weights of the pure buckling modes in the shape as result. The results of the analysis are shown in Figure 113. The upper figure shows the change of the critical stress in function of the buckling length. On the bottom graph in Figure 113. the contributions of the pure modes to the total are presented using curves; the local maxima of these curves show at which buckling length the given mode has the biggest modal weight. Figure 114. shows the buckling shapes belonging to the maxima of the modal curves: local, distortional and global mode.
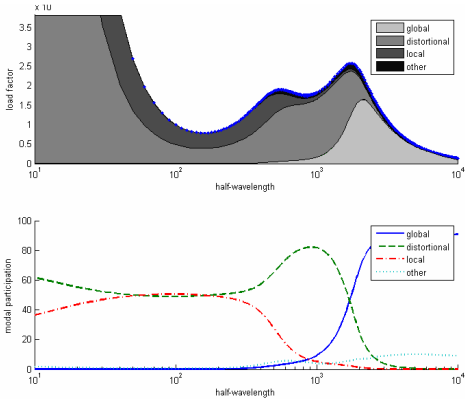

Figure 113.: Buckling curve with modal participation (top), curves of modal weights (bottom).
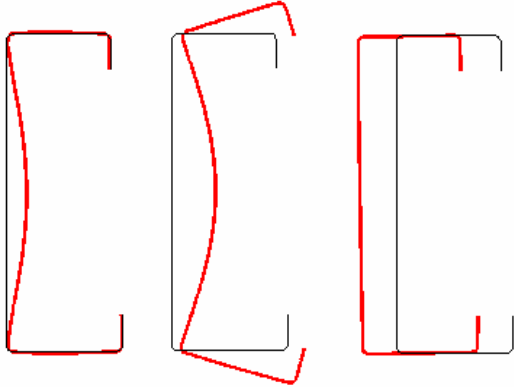

Figure 114.: Local, distortional and global buckling shapes (left to right).

The imperfect shape applied to the numerical model is generated using the shapes generated using FSM analysis by dragging these along the member using a sinusoidal line as path to modify the coordinates of the nodes of the mesh. The FSM model of the test specimens – the

cross-section, including the radii in the corners – is defined using CUFSM's built-in template to be the same as that of the FE model. The stress distribution applied to the FSM model to obtain the buckling shapes is uniform, since the method is merely used to generate an imperfect shape, thus it does not need to be conforming to that of the FE model. The shapes used are to ones belonging to the local minima of the local and distortional modes in the buckling curve – the buckling lengths where the mode gives most part of the shape. As global buckling has no local minimum, in this case a buckling length long enough to provide pure mode – ten times the member length – is used.

It is to be noted, that the procedure is not entirely correct, as the cFSM classification requires the section to be modelled without radii at the edges to provide exact results. However, the method, if applied consequently can be considered as a possible approach to easily generate imperfections in a controlled way.

As in a real test only full buckling half-waves appear, during modifying the perfect geometry care must be taken to have only full half-waves in the imperfect geometry. This needs different considerations in the case of each buckling mode as follows.

In the case of global buckling one sinusoidal half-wave is applied as dragging path, and all nodes of the FE model are re-located.

In the case of local buckling only a portion of the nodes is modified, those between the end supports. The position of the waves is calculated based on this length to fit the highest number of half-waves in the region (Figure 115.). This method does not generate local buckling waves at the end supports of the member and leaves a portion (shorter than the half of the buckling length applied at each end) of the sections perfect.

In the case of distortional buckling the member length is divided by the half-wavelength derived from cFSM as the buckling length to that the local minimum of distortional buckling belongs and the result is rounded towards the nearest integer. This way the number of half-waves to be applied is set, resulting in a new buckling length – that is, the one providing full-waves and being close to the real minimum of the curve of pure distortional buckling. To have the pertinent buckling shapes and buckling lengths cFSM is once again used to determine the buckling shape for this new length. The nodes of the FE model are then modified using the newly calculated buckling shape and a sinusoidal wave with the calculated number of full half-waves to generate the imperfect shape.

The total imperfect shape to be applied to the C-section member is generated by a weighted superposition of the shapes generated for the individual buckling modes. The resulting shape is almost symmetric; a slight asymmetry is present due to the different flange sizes. Figure 115. shows an imperfect shape generated from local, distortional and global shapes applied to the model.

local shape
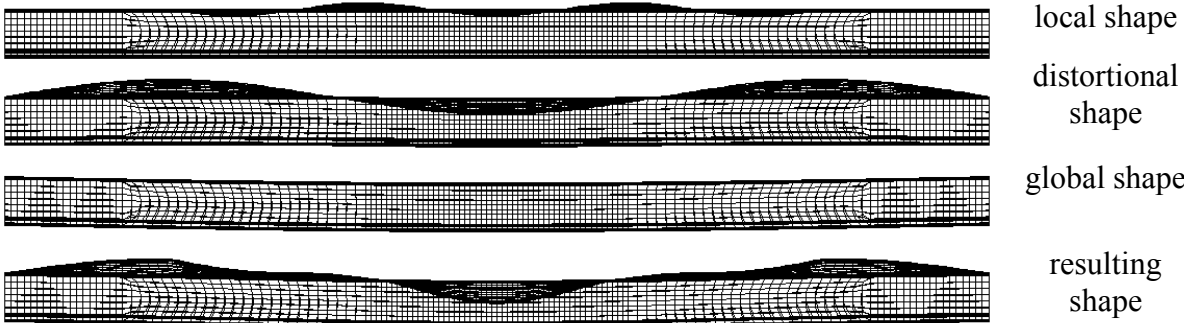
distortional shape

global shape

resulting shape

Figure 115.: Applied local, distortional and global shapes and the resulting shape.
For illustration, amplitude is in all cases 10 mm.

The main advantage of this approach is an easy implementation (as CUFSM is an open-source software it can be integrated in the pre-processor) and a certain level of consistency regarding the otherwise usually arbitrary choice of imperfect shape. The shapes generated this way are similar to those obtained from an eigenvalue analysis of the FE model and the applied pure shapes and their magnitudes are known and can be controlled. This makes studying the imperfection sensitivity of the members possible, as the properties (amplitude, wavelength) of the pure shapes applied to the model may be treated as parameters.

The effect of imperfections with different shapes on the behaviour of cold-formed lipped channel members using FE models was recently published in [45]. Recent research on eigenshape classification using FEM [46] shows great promise to determine the weights of pure buckling modes in eigenshapes. A comparison of the proposed approach and the eigenshape-based approach is out of scope of this paper, but is definitely worth investigating.

4.2.4. Calibrating the model

Calibration of the connector elements

The calibration of the model was carried out in two steps. First, without taking into account geometrical imperfections the screw model was calibrated, as it was suspected that imperfections change the rigidity of the model. This step also served as proof of the concept, that is, the screw model can be used to predict the real specimens' rigidity over a wide parameter range.

The settings used during the parametric study are listed in Table 32. Figure 116. and Figure 117. show the resulting force-axial shortening diagrams. Figure 118. shows the deflected shape of a screw for different settings to provide insight how different settings influence the behaviour. Figure 119. shows the failure mode obtained from the analysis with the settings listed in Table 34.

Table 32: Settings of the elements of the screw model.

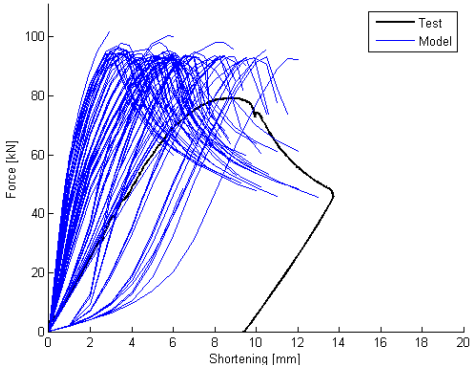|	Area [mm^2]	Shear area divider[1]	Moments of inertia (bending) [mm^4]	Moment of inertia (torsion) [mm^4]
Shaft element	$r^2\pi$	1; 10; 100; 1000	$r^4\pi/4$	$r^4\pi/2$
Radial elements	0.1; 1; 10; 100	0	0.0001; 0.001; 0.01; 0.1; 1; 10; 100	1

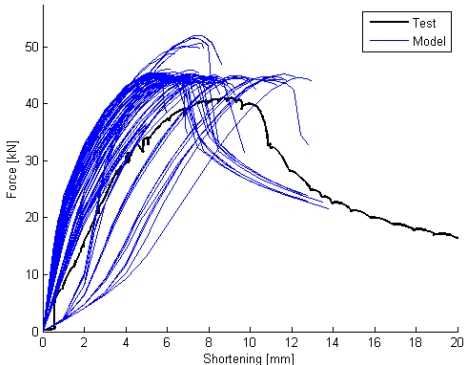Figure 116.: Results of the parametric study (C81).

Figure 117.: Results of the parametric study (C40)

---

[1] Ansys defines shear stiffness by the ratio A/A$_w$ with A being the full cross-sectional area, A$_w$ the shear area; zero means no shear deformation.

From the results the following conclusions can be drawn: i) by changing the properties of the elements in the model, the connection rigidity can be tuned within wide range, ii) the failure mode of the member is in all cases the same as the one obtained in the laboratory test, iii) connection rigidity is primarily governed by the shear stiffness of the shaft element, iv) rigidities of the radial elements influence the non-linear behaviour, v) the numerical stability and convergence speed of the model is sufficient.

Load-bearing capacities obtained from the parametric study scatter, but are little affected by the connection rigidity, as shown in Table 33.
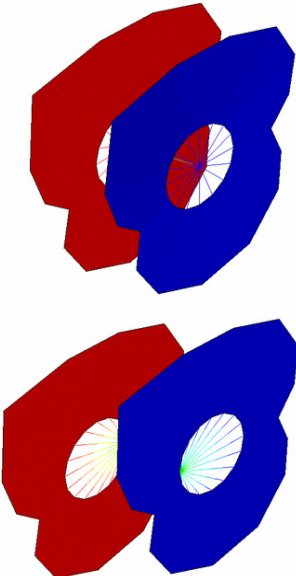

Figure 118.: Deflections of the screw models for different settings (C81).
Top: rigid radial elements, shaft tilting
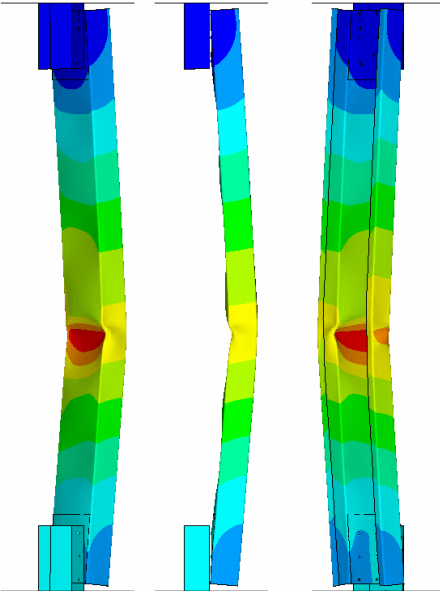Bottom: rigid shaft, radial elements with small area

Figure 119.: Failed shape of the model (structural displacement vector sum, C81).

Table 33: Effect of screw rigidities on the calculated ultimate load.

Test	Measured load-bearing capacity [kN]	Calculated load-bearing capacities [kN]			Standard deviation of the results
		minimum	maximum	mean	
C40	41.02	43.75	51.97	45.31	0.0428
C81	79.23	90.67	101.63	93.93	0.0257

Similar parametric studies – although in a narrower parameter space – were carried out using results of more tests to find the settings resulting in conforming force-displacement diagrams of the test and models. Among the suiting parameter sets for the further studies a choice was made based on the speed of convergence.

The settings chosen are presented in Table 34. The force-shortening diagrams resulting using these settings for tests C40 (C200/1.5, 9 screws, L = 2500 mm) and C82 (C200/2.0, 49 screws, L = 1500 mm) are in good accordance with the measured diagrams (Figure 120. and Figure 121.). Note that both diagrams are obtained using the same settings of the elements of the screw model, regardless of the number of screws and thickness of the C-section member.

Table 34: Settings of the elements of the screw model.

	Area [mm^2]	Shear area divider	Moments of inertia (bending) [mm^4]	Moment of inertia (torsion) [mm^4]
Shaft element	$r^2\pi$	100	$r^4\pi/4$	$r^4\pi/2$
Radial elements	100	0	0.01	1

It is to be noted, that the calibration of the screw model should be based on tests on structural members; single lap shear tests on connections containing one to three self-drilling screws are not well suited for this purpose, as the rigidities of the screws may scatter (i.e.: different torques applied during fastening) and local effects may also strongly influence the behaviour of an individual screw, but such phenomena have less effect if screw groups are used.
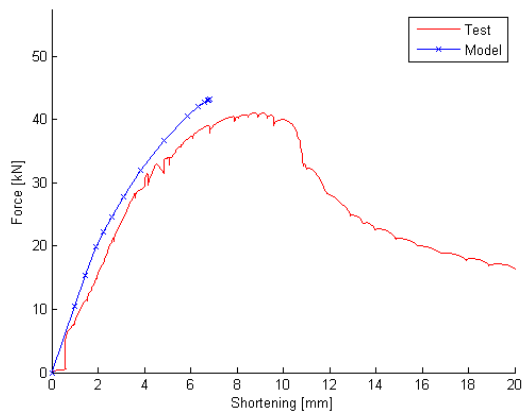

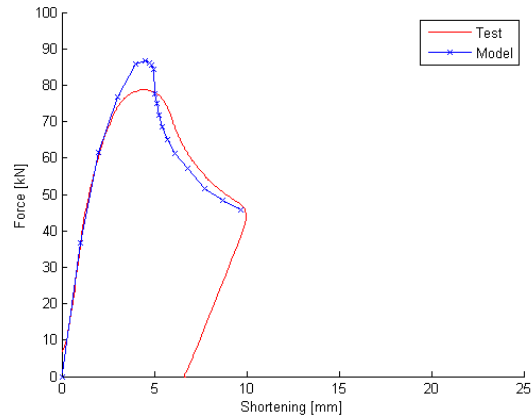Figure 120.: Force-shortening diagram resulting from the chosen settings (C40).

Figure 121.: Force-shortening diagram resulting from the chosen settings (C82).

Calibration of the imperfections

An imperfection sensitivity study was carried out on the numerical models of the laboratory tests with the aim to find a set of imperfect shapes and their amplitudes that lead to an accurate reproduction of the load-bearing capacity obtained in the tests, while not affecting the failure mode and stiffness. The study was carried out by applying local, distortional and global shape imperfections to the perfect model derived from cFSM analyses as detailed in Chapter 4.2.3. The magnitudes applied with the shapes are listed in Table 35.

Table 35: Amplitude values used in the study.

Shape	Local	Distortional	Global
Values [mm]	0; 1; 2; 3; 4	0; 1; 2; 3;	0; 2; 4; 6; 8; 10; 12

Applying imperfections to the perfect model results a decrease of the initial stiffness of the model; hence the settings of the screw model elements presented in Table 34 had to be modified in order to maintain the accordance of test and numerical results. As shown by the parametric study on screw model behaviour this can be done by increasing the shear stiffness of the screw shaft element.

To avoid a time consuming full parametric study involving most of the tests, a wide range of imperfection amplitudes and shear stiffness, the method of successive approximation was used to determine the values providing best fit using primarily the results of test C66, C81 and C82, other tests were involved in the process only once a set providing satisfactory accordance with these three was found. This also means that a systematic parametric study was not carried out on the imperfection sensitivity of the members.

76

The observations made on the models' behaviour and load-bearing capacities in the study are listed as follows: i) all three types of imperfections reduce both load-bearing capacity and the stiffness of the model, ii) the amplitude of the global shape has major influence on the initial stiffness, iii) the amplitude of the local shape affects the behaviour of the model near limit point more than that of the global shape, iv) the failure mode is not affected by the imperfections with amplitudes within the studied range, v) for a given value of global imperfection the decrease of the load-bearing capacity due to the presence of distortional shape is smaller if local shape is applied than that if no local imperfection is present; the phenomenon is stronger for higher amplitude values of the local and/or global shapes, vi) the direction of the imperfection plays key role in the case of global imperfections, but has no effect in case of local imperfections. As during the tests no signs of distortional deformations were observed, distortional shape imperfections have been excluded from the investigations.

Note that the above statements are observed overall tendencies and the quantitative values of the pertinent changes depend on which test's model is studied.
The settings of the screw model found to provide good accordance of results of test and numerical model are listed in Table 36 – only the shear stiffness of the shaft element has been changed. The imperfections to be applied are summarized in Table 37. In the case of global imperfections the direction in which it is to be applied is in accordance with the stability behaviour observed in the laboratory tests.

Table 36: Settings of the elements of the screw model in case of the imperfect model.

Position	Area [mm^2]	Shear area divider	Moments of inertia (bending) [mm^4]	Moment of inertia (torsion) [mm^4]
Shaft element	$r^2\pi$	70	$r^4\pi/4$	$r^4\pi/2$
Radial elements	100	0	0.01	1

Table 37: Geometrical imperfections to be applied.

Shape	Local	Distortional	Global
Value [mm]	3	-	6
Length of sinusoidal half-wave	150 mm	-	Member length

Note, that the settings presented in Table 36 and Table 37 are to be used together obtain good accordance of test and model. The proposed values of the amplitudes listed in Table 37 are fixed values determined by the calibration of the model to yield best match of test and model results; in the studied cases the amplitude for the global imperfection it is between L/250 (L = 1500 mm) and L/416 (L = 2500 mm), for local imperfection $h_w/67$, with h_w being the web width of the section.

4.2.5. Virtual experiments on SimpleC members

The calibrated model was used to carry out virtual experiments on all laboratory tests with a C200 section with the settings of the screw model and by applying imperfections with the shapes and amplitudes described in Chapter 4.2.4. The resulting force-displacement diagrams are presented in Figure 122. and Figure 123. The obtained diagrams show, that the load-bearing capacities obtained using the calibrated numerical model are in very good accordance with the measured ones, the failure modes obtained are the same as those obtained in the tests. The comparison of test and model results is summarized in Table 38. The difference of test and model result is between +2.6 % and -5.6 % from the basis of the test result, the average is 98.9%, thus the model slightly underestimates the load-bearing capacity of the test specimen.

Table 38: Specimen characteristics and test results.

| Test	Section	Length [mm]	Load-bearing capacity [kN]		Ratio Test/Model
			Test	Model	
C12	C200/2.0	2000	71.10	70.63	1.006
C15	C200/1.0		24.20	22.85	0.944
C23	C200/2.0	3600	46.80	47.27	0.990
C26	C200/1.0		17.20	17.57	0.979
C40	C200/1.5	2500	41.02	40.27	1.018
C41	C200/2.0		63.99	66.26	0.966
C42	C200/2.5		94.34	91.93	1.026
C66	C200/2.0	1500	78.97	81.49	0.969
C67	C200/2.5		111.10	108.32	1.026
C80	C200/2.5		114.24	113.97	1.002
C81	C200/2.0		79.23	80.79	0.981
C82	C200/2.0		78.86	81.64	0.966
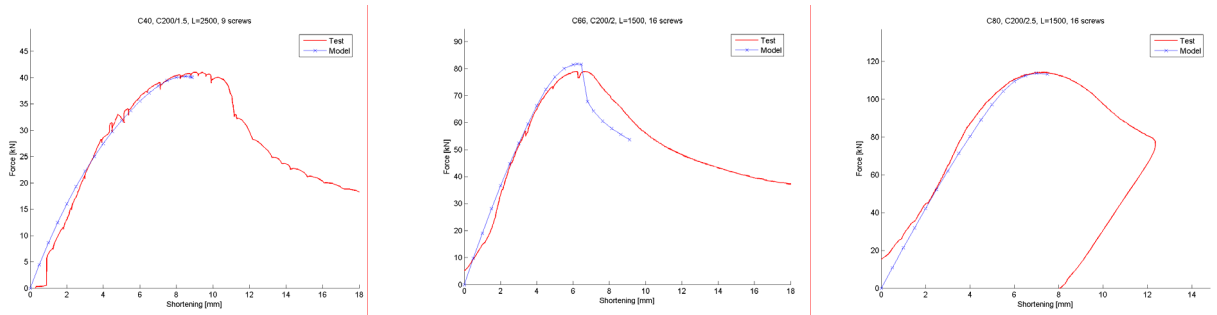
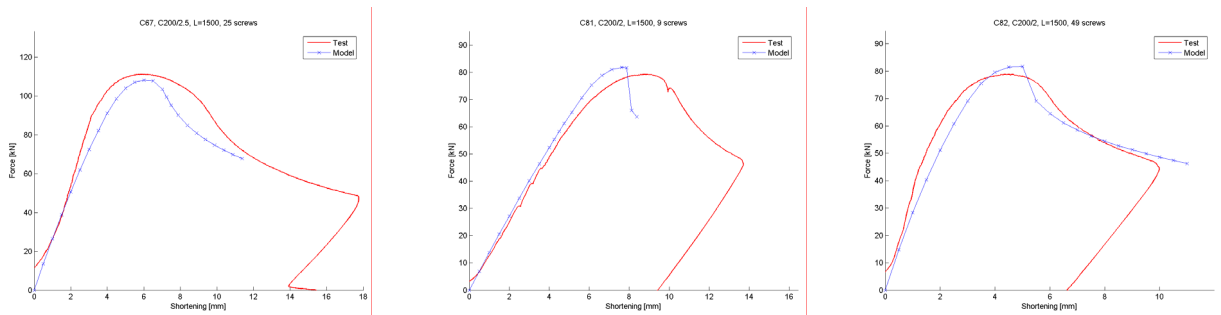Figure 122.: Force-shortening diagrams; left: C40; middle: C67; right: C80.

Figure 123.: Force-shortening diagrams; left: C66; middle: C81; right: C82.

Comparing the obtained rigidities the accordance is not uniformly good in all cases, although the majority of the tests are reproduced quite accurately. By comparing the descending branch of test specimens and the pertinent models similar differences can be observed; this is partly the result of the geometry of the plastic mechanism in the model is different from that in the reality partly of local effects at load introduction – in case of a denser screw layout an interaction between the screws is possible, which is a phenomenon not fully covered by the numerical model.

4.3. Numerical model of the trusses

4.3.1. Global numerical model

The global numerical model of the truss was developed based on the same approach as the model of the SimpleC members. Shape, dimensions and positions of the C-sections members, bolts, gusset plates, etc. are generated in the model according to reality, with perfect geometry. The full model is presented in Figure 127., details are shown in Figure 124. The element types and material models used in the members and contact areas are also the same: SHELL 181 elements with linear elastic − hardening plastic material model with material properties derived from coupon tests as shown in Table 39 and measured plate thicknesses. The majority of the contact regions are modelled using the CONTA173 – TARGE170 pair in a symmetrical arrangement. Despite the similarities of the two structures modelling connector elements, certain contact regions, loading and boundary conditions needed special considerations.
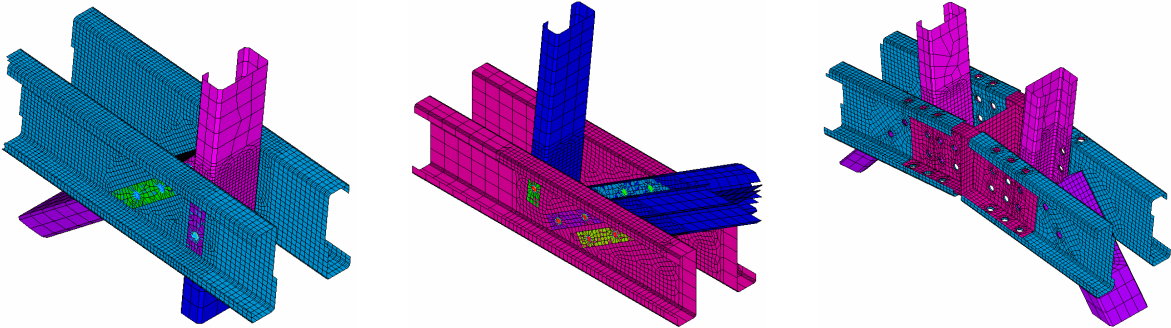

Figure 124.: Details of the model. Joint in the upper chord, joint in the lower chord, ridge joint in the model of Test 5 (left to right).

Table 39: Results of material tests.

| Specimen | Coupon | | Yield stress [MPa] | Ultimate strength [MPa] |
	Thickness (without zinc coating) [mm]	Width [mm]	$R_{p0,2}$	R_m
RT-1	2.01 (1.98)	19.7	418	481
RT-2	1.11 (1.08)	19.8	419	483
RT-3	1.11 (1.07)	19.7	416	485
RT-4	2.02 (1.99)	19.8	417	478

In the trusses 8.8 grade M14 metric bolts were used as connector elements. The numerical model developed for the bolt is similar to that of the self-drilling screws, however, the differences in the structural behaviour are needed changes relative to that. The model of the bolt is detailed in Chapter 4.3.2.

Discretization of the geometrical model is carried out taking into account the structural behaviour of the given part of the truss, hence the mesh in contact regions and structural joints is denser, whilst members have a relatively coarse mesh, as seen in Figure 124. The size of the model of Test 5 is approximately 1.41 million DOF.

Contact regions, where three plates are in contact, that is, the one in the middle has contacting plates on both sides pose difficulties, since due to the limitations of Ansys shell elements can have regular contact surfaces only on one side. To overcome this, on one side of such elements a regular contact is defined using CONTA173 and TARGE170 elements, on the other side LINK10 compression only 2-node 2 DOF spar elements are used to connect the nodes on the opposite plates. Since the meshes in the contact areas are generated to be congruent, this results spar elements perpendicular to the contacting plates. This arrangement works properly only if there is no relative slide between the surfaces, but since in all contact areas connector elements are present, the slide can be considered small enough to make this solution work effectively.

Boundary conditions were defined according to the real supporting conditions by restraining the displacements of the respective nodes. Figure 125. shows the hinge at one of the supports with the vertical and the horizontal, out-of-plane displacements restrained. Figure 126. shows the lateral supports at the load introduction points.
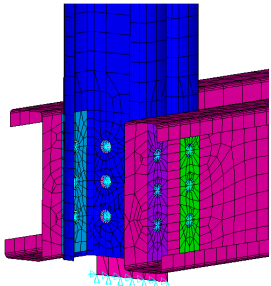

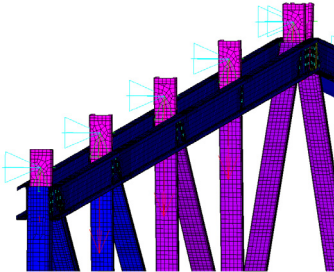Figure 125.: Hinge at the support column.

Figure 126.: Lateral support at load introduction.

To avoid convergence problems, an extended version of the gravity load simulator was included in the model to enable using displacement as load; this solution provides the same loading conditions as those were in reality. The vertical members of the loading system are modelled by tension-only LINK10 elements with a cross-section area of 10 cm^2, the horizontal members using BEAM4 elements with the second moment of inertia calculated to yield less than 0.01 mm deflection for a concentrated load of 25 kN, thus the deformations of these members are negligible. The material model used in the case of these elements is linear elastic, module of elasticity is 210000 MPa. The arrangement is shown in Figure 127. The LINK10 elements connect to the purlin supports at a single node; to avoid local failure in this region the plate thickness is set to 6 mm. Note that in the linear static and bifurcation analyses the model of the gravity load simulator was not used, in these analyses concentrated forces were used instead.
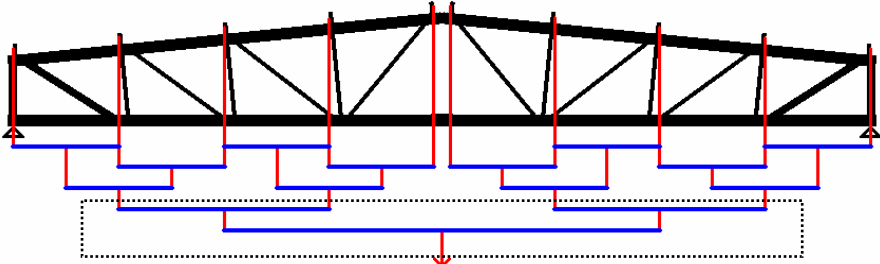

Figure 127.: Model with gravity load simulator with the added elements highlighted.

A MATLAB-based pre-processor was developed to speed up the modelling process; the input of the program are the positions and sections of the members including bolt positions, hence the truss is defined by a few parameters enabling easy and effective model generation.

4.3.2. Numerical model of bolts, calibration

The fitted bolts used in the tests carry the loads by shear and bearing. Similarly to the model of self-drilling screws the bolts consist of the bolt holes in the connected plates, one element placed in the centre of the holes to represent the shaft and radial elements connecting it to the rim of the hole. The rim of the bolt hole is discretized in 16 segments of equal length, the cross-sectional properties of the shaft element are derived from the diameter of the bolt shaft.

To incorporate the effect of bearing in the model the radial elements are doubled: the nodes of the rim and the shaft element are connected by compression only LINK10 spar elements and overlaid 2-node 12 DOF BEAM44 elements. BEAM 44 elements are essentially the same as BEAM4 elements, with the major difference that components of its stiffness can be released at the nodes, thus an incomplete displacement transfer can be achieved between the connected nodes. In the radial elements of the bolt model the axial stiffness of the BEAM44 element is released, thus the LINK10 and BEAM44 elements together represent an element having full bending stiffness but capable of carrying only compression axial forces. The bending stiffness of the BEAM44 elements associated with the out-of-plane displacements, that is, the axial direction of the shaft is set "rigid", the in-plane stiffness "flexible", as the BEAM44 elements are merely used to provide out-of-plane stiffness to the LINK10 elements. This way, the effect of bearing is modelled by the compression only spar elements, shear is transferred by the shaft element. The model needs calibration to provide the same stiffness to the connection as that is in reality, which can be done by choosing the appropriate value to the cross-sectional area of the spar elements. The connection stiffness depends on the thickness of the connected plates, hence the radial LINK10 elements should have the areas defined according to the plate thickness. However, in the model of the truss all of these elements are set to have the same area, thus the differences are averaged.

The bolt model was calibrated using the results of deflection measurement from Test 1 and Test 5. The bolt model is presented in Figure 128., the applied settings resulting a good agreement of test and model stiffness are summarized in Table 40.
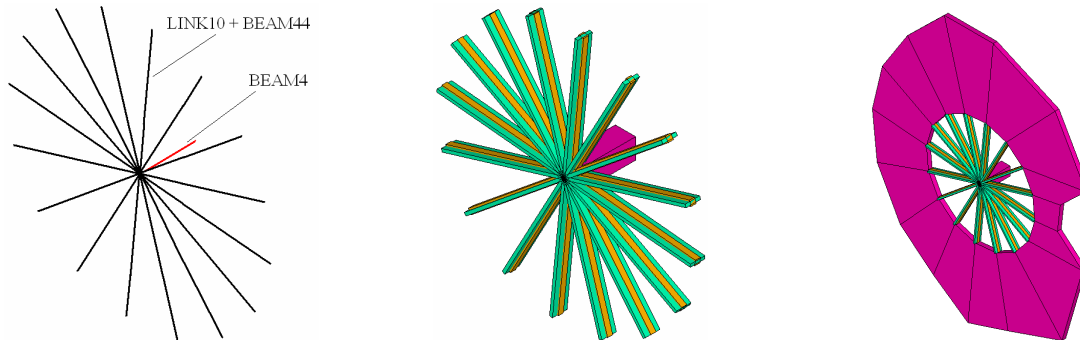

Figure 128.: Bolt model.

Table 40: Settings of the elements of the bolt model.

	Element	A $[mm^2]$	Shear area divider	I_z $[mm^4]$	I_y $[mm^4]$	I_x $[mm^4]$
Both tests	BEAM4	$r^2\pi$	0	$r^4\pi/4$	$r^4\pi/4$	$r^4\pi/4$
	BEAM44	10^{-3}	0	100	0.1	0
Test 1	LINK10	0.4	-	-	-	-
Test 5	LINK10	1.0	-	-	-	-

A – area; I_z – out-of-plane bending relative to the plate; I_y – in-plane bending relative to the plate; I_x – torsion.

The deflected shape of the calibrated model of Test 5 is presented in Figure 129., results are summarized in Table 41 alongside with the deflection obtained from the global beam model presented in Chapter 3.3.2, and from the "non-calibrated" shell model, that is, with the radial spar elements of the bolt model set have a cross-sectional area of A = 200 mm^2 and to work for compression and tension as well.
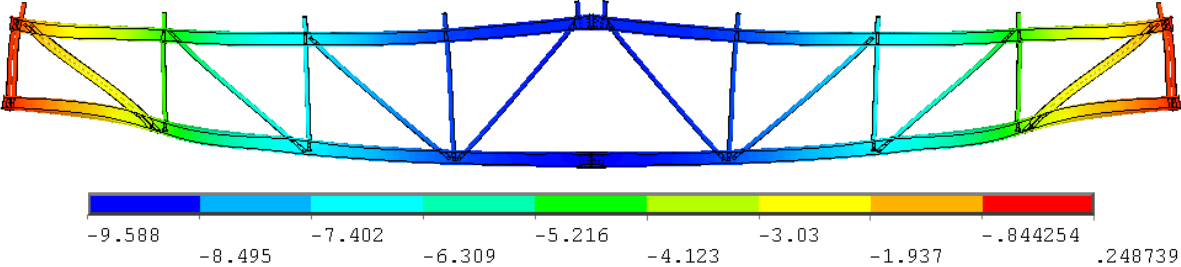

Figure 129.: Vertical deflections at 10 kN/jack load level. Test 5, deflections in 60x magnification.

Table 41: Measured and calculated deflections.

Model type	Load [kN/jack]	Test 1.			Test 5.		
		Deflection [mm]		Ratio (Test/FE)	Deflection [mm]		Ratio (Test/FE)
		Test	FE		Test	FE	
Calibrated			12.06	0.998		9.59	0.993
Non-calibrated	10.00	12.04	9.77	1.232	9.52	8.35	1.140
Beam			8.22	1.465		7.89	1.207

The comparison of the deflections calculated using different models shows, that the stiffness of the shell model, without calibration is higher than that of the beam model, as it follows the deformations in the joints more accurately, but underestimates the real deflections.

4.3.3. Linear static analysis

The calibrated model was used to study the stress distribution in the members of the truss based on a linear static analysis. Figure 130. and Figure 131. show details of the model of Test 5, with the von Mises stresses resulting from the equivalent of 10kN/jack load applied as concentrated forces at the purlin supports.

The stresses in the chord members – except for the joint areas – are moderate, the distribution is similar to that expected from axial force and bending.
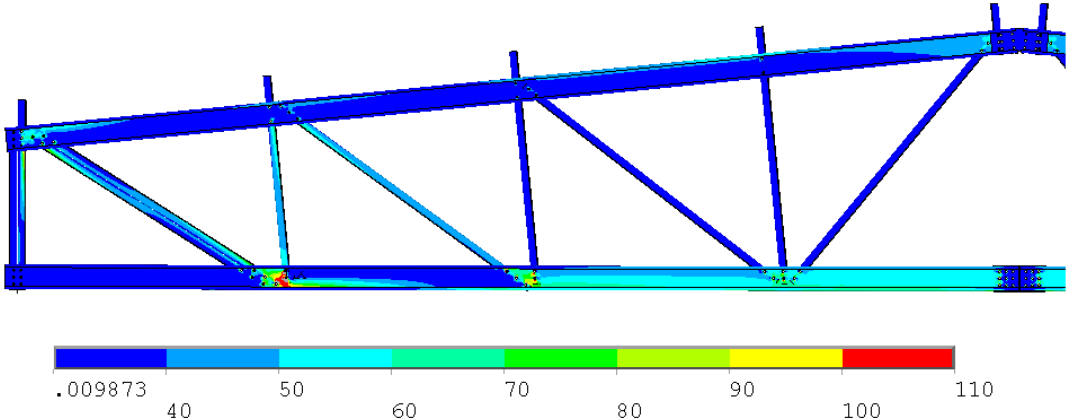

Figure 130.: von Mises stress distribution in the truss at 10kN/jack load level, Test 5 [MPa].

In accordance with the results of the laboratory test and of the global beam model used in design, the highest stresses can be found in the webs of the lower chord members at the joint

areas especially near the support, and, as expected, high stress gradients are present at the bolts. The reason for the joints being the places of stress concentration is the in-plane eccentricity of the joints and the thin plates (t = 1.50 mm) of the lower chord members. The stresses at 10 kN/jack load level – slightly under the third of the ULS load level – exceed the third of the nominal yield stress 350 MPa. Based on this it is suspicible that the first failure in the fifth test was cross-section failure due to the interaction of shear and bending.
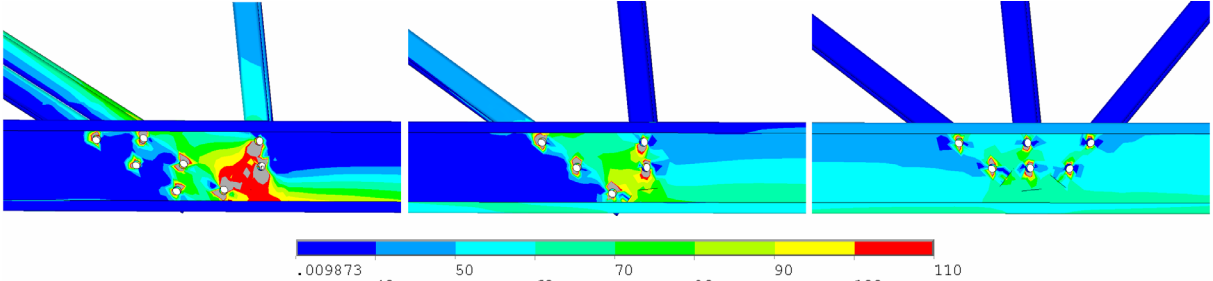

Figure 131.: von Mises stresses in the joints of the lower chord, Test 5 [MPa].

4.3.4. Linear bifurcation analysis

Bifurcation analysis is applied to obtain the eigenmodes of the models with the aim to apply them on the perfect model as geometrical imperfections, thus enable virtual experimenting. However, the results of this analysis can be used to explore the possible stability failure modes of the truss, similar to the way a linear static analysis provides results regarding the stress distribution in the members. In contrary to the model of SimpleC members, the eigenshapes of the trusses can be distinguished and classified within certain limits based on the location and shape of the buckling. The analysis is carried out based on the stress state stored in a static analysis carried out by applying 10kN/jack load to the trusses as detailed in Chapter 4.3.2. Note that the ULS load level is 31.63 kN/jack; considering 10 kN/jack as load eigenvalues under 3.16 indicate critical loads lower than the ULS load level.

In the following the typical eigenshapes and the pertinent load factors are presented for Test 1 and Test 5, with the failure modes classified. The eigenshapes of the model of Test 1 are presented in Figure 132. with load factors and classification in Table 42, those of Test 5 are presented in Figure 133. and Table 43; in the tables, in case of interacting modes the governing mode, that is, the mode that contributes more to the displacements is highlighted.

Figure 132.: Typical eigenshapes of the model of Test 1.

Table 42: The first 100 eigenshapes and load factors of the model of Test 1.

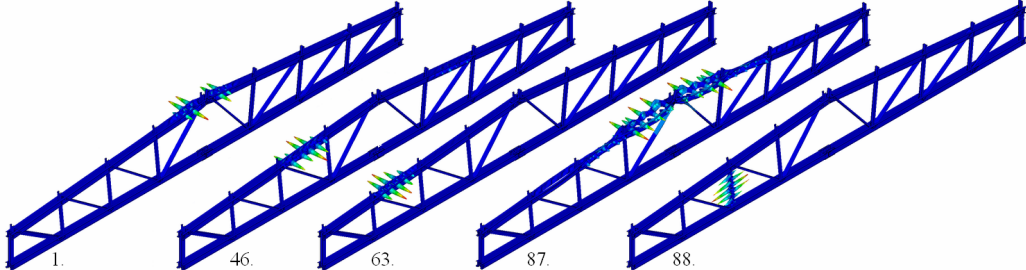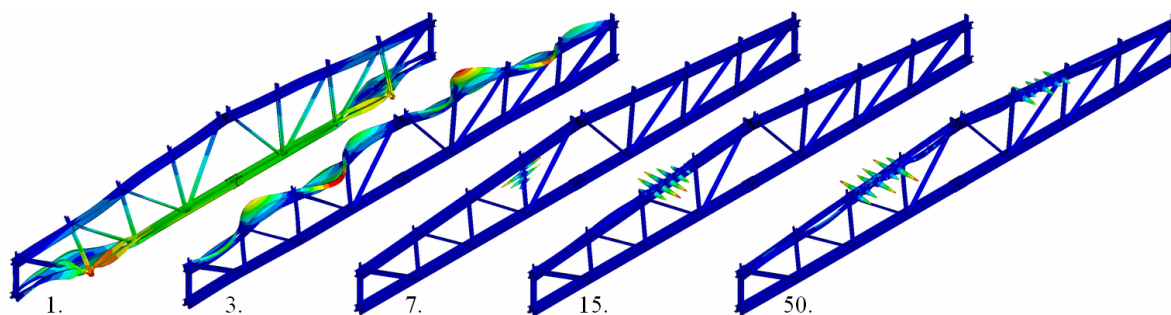| Range of eigen-mode number	Range of eigenvalue	Failure mode
1 – 87	3.320 – 4.501	Interaction of **local buckling** and flexural buckling (upper chord, different locations).
88 – 92	4.502 – 4.504	Local buckling (brace).
93 – 100	4.515 – 4.530	Interaction of **local buckling** and flexural buckling (upper chord).

Figure 133.: Typical eigenshapes of the model of Test 5.

Table 43: The first 50 eigenshapes and load factors of the model of Test 5.

Range of eigen-mode number	Range of eigenvalue	Failure mode
1 – 2	6.141 – 6.159	Lateral-torsional buckling (lower chord).
3 – 6	7.529 – 7.626	Lateral-torsional buckling (upper chord).
7 – 10	7.916 – 7.978	Local buckling (brace).
11 – 46	8.036 – 8.506	Local buckling (upper chord).
47 – 48	8.537	Local buckling (brace).
49 – 50	8.562	Interaction of **local buckling** and flexural buckling (upper chord).

In the case of Test 1 among the first 100 eigenshapes covering load factors between 3.32 to 4.53 almost only modes showing the local buckling of the upper chord are present, the interaction with a global mode e.g.: flexural buckling is rare and weak, which is clearly the consequence of the high web b/t ratio and the unfavourable joint ridge arrangement. The eigenshapes obtained correspond the observed behaviour of the test specimen.

In the case of Test 5 the first 50 eigenshapes provide five different failure modes, with eigenvalues ranging 6.141 to 8.562. Te higher eigenvalues are partly the result of the lower b/t ratio of the chord member (a C150/2.5 section is used instead of a C150/2.0) and partly that of the established load transfer in the ridge joint through the flanges of the chord members. The variety of failure modes in the first 50 eigenshapes points to more economic design.

The high eigenvalues show the reserves in the members that resulted the high load-bearing capacity measured in the test. The failure mode obtained in the test corresponds to the interaction of the second and third group of eigenshapes. Signs of lateral displacements or lateral-torsional buckling were not observed in the lower chord during testing; the failure of the lower chord joint occurred presumably due to the high stress concentration in this part of the truss.

4.3.5. Virtual experimenting using the truss model

Based on the results of the bifurcation analysis equivalent geometrical imperfections have been added to the model to enable reproducing the fifth laboratory test as virtual experiment using the developed model. In the analysis the load was applied using the model of the gravity load simulator.

The imperfect shapes chosen to be applied were the 3rd and 15th eigenshapes (Figure 133.) with maximum amplitude of 7.5 mm and 1.5 mm, respectively. The applied amplitudes are an equivalent of L/200 global, and $h_w/60$ local imperfections, with L being the system length and h_w the web width of the upper chord members. The former value corresponds the recommended value for global bow imperfection to be taken into account for columns in a

plastic analysis as detailed in EC3-1-1; the latter is higher than the value of $h_w/200$ recommended in EC3-1-5 Annex C, Finite Element Method analysis of plated structures.

Using the imperfect model with the setting introduced previously a static analysis was carried out taking into account large deformations. The sparse matrix solver was used to solve the problem with the default Newton-Ralphson iteration procedure.

The primary results of the virtual experiment are the same as those of a real one: force-deflection diagram, load-bearing capacity and failure mode; these provide the basis to judge the goodness of the model. The force-displacement diagram obtained using the model is presented in Figure 134., the failed shape is shown on Figure 135., details are presented in Figure 136. and Figure 137. Note that on the figures non-relevant details (bolts, gusset plates, contacts etc.) are not shown. Grey areas indicate areas with off-scale values; in the case of displayed stresses the material in these areas yields.
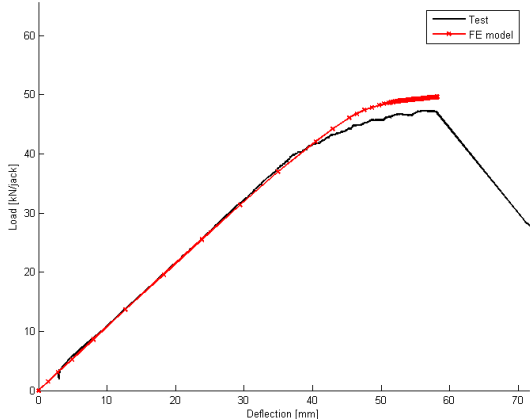

Figure 134.: Force-vertical deflection diagrams.
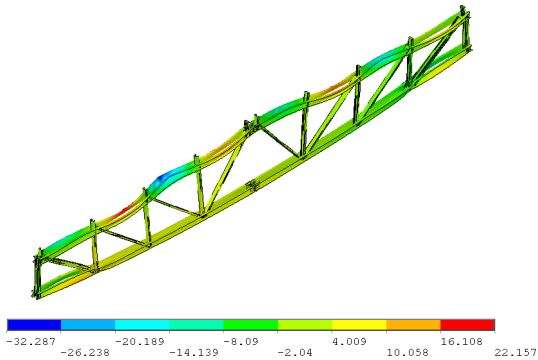
Figure 135.: Shape of the failed model. Out-of-plane deformations [mm].
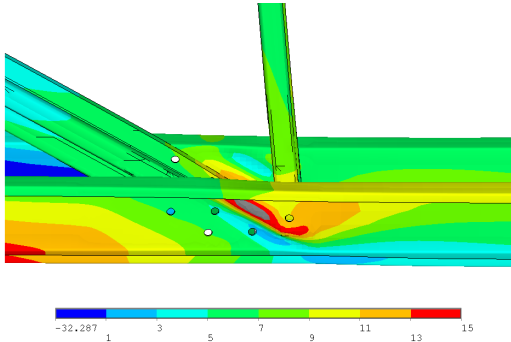
Figure 136.: Failure in the lower chord. Out-of-plane deformations at failure [mm].
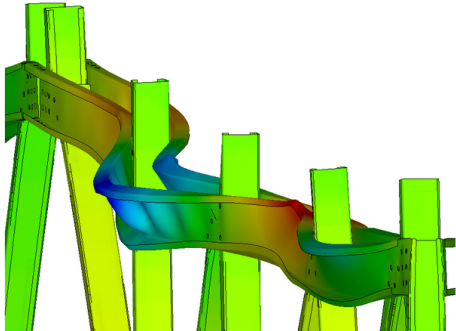
Figure 137.: Failure of the upper chord. 6x magnified out-of-plane deformations.

The obtained force-vertical deflection diagram shows, that the rigidity and the load-bearing capacity of the real test are reproduced in the model with a good accuracy; details show remarkable similarity with the real failure modes. Based on this, the model can be used to study the truss and draw conclusions regarding parts of it not investigated in the laboratory tests.

The stress distribution in the truss at the ULS load level is shown in Figure 138., with details in Figure 139. to Figure 142. All displayed stresses are von Mises stresses in MPa calculated at the midplane of the members.

Figure 138.: Stress distribution in the truss members at the ULS load level.
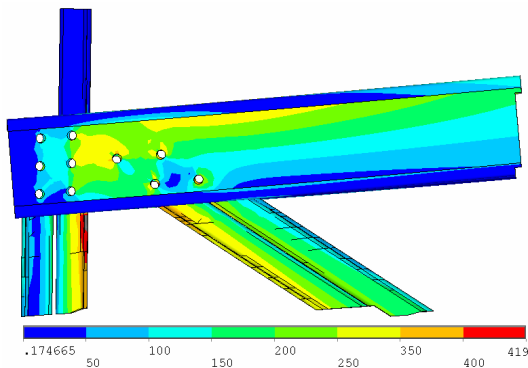
Figure 139.: Stress distribution in the upper chord joint at the support. ULS load level.
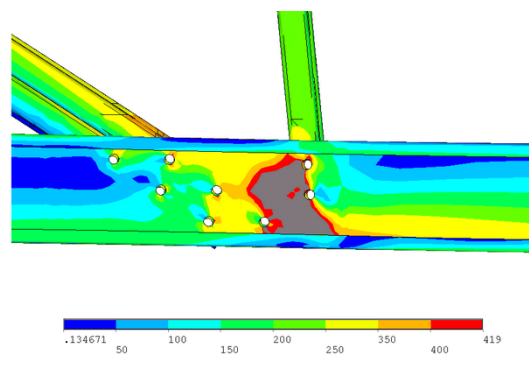
Figure 140.: Stress distribution in the lower chord joint. ULS load level.

At ULS load level the stress distribution in the members show that the critical parts of the structure are primarily the joint regions near the support where the material is in plastic state primarily due to shear and bending. The web of the lower chord yields in great area the lower chord joint closest to the support.

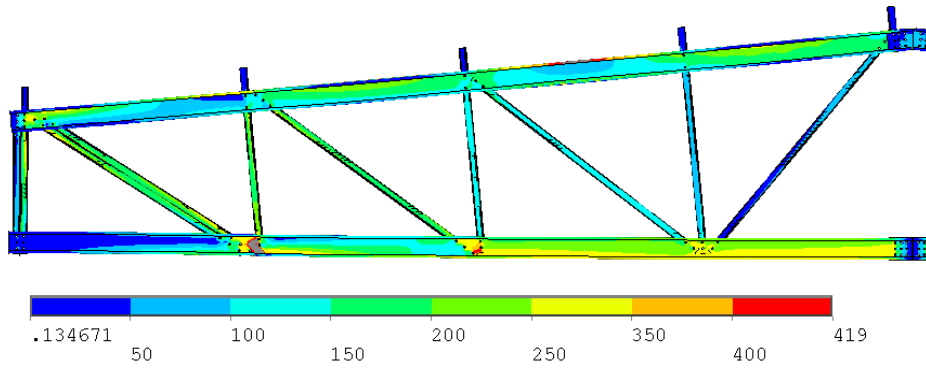The stresses in the lower chord correspond the expected smooth distribution. On contrary in the upper chord members the top fibre is overloaded compared to the lower fibre as a consequence of the compression force and the bending about the strong axis (in-plane bending). The material in some spots of the member second next to the ridge (Figure 141.), that is, the member failed in the tests yields, as a consequence of the out-of-plane bending developing due to the deformations.

The stress distribution of the joints in the chords are presented in Figure 142. This shows that the force is evenly distributed in among the bolts and due to the large number of them no local plasticity is observed.
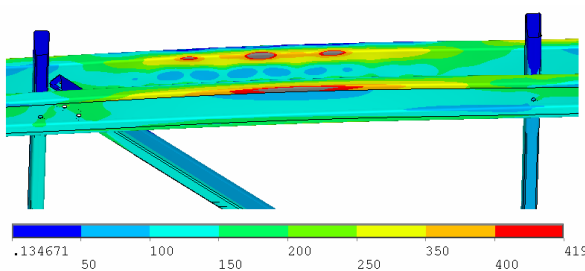
Figure 141.: Stress distribution in the joints of the chords at ULS load level.
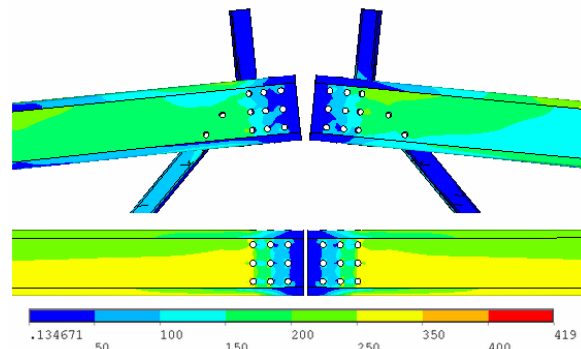
Figure 142.: Stress distribution in the joints of the chords at ULS load level.

86

The von Mises stress distribution in the truss at the ultimate failure is shown in Figure 143. Figure 144. and Figure 145. show the stress distribution on the deformed shape at failure, yielded parts are highlighted.
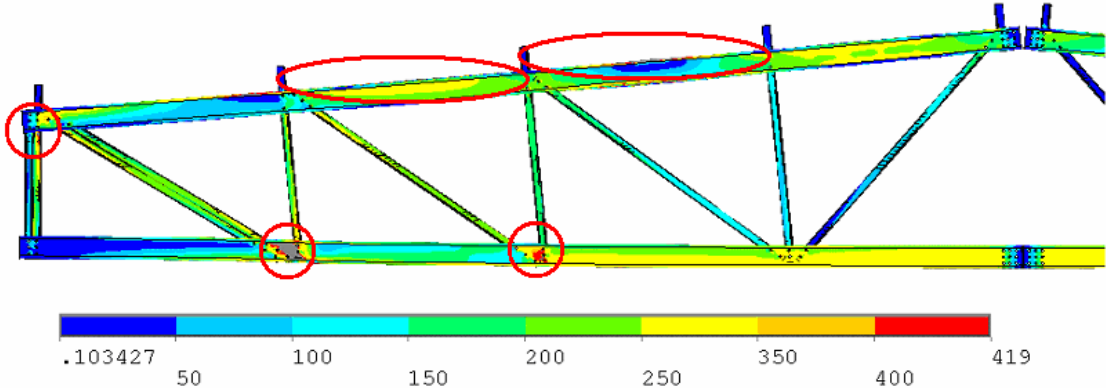
Figure 143.: Stress distribution in the truss at failure, with parts yielding highlighted.
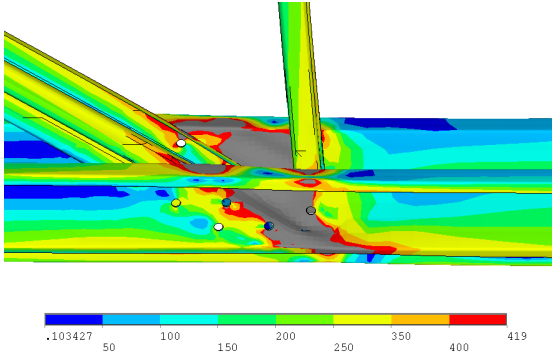
Figure 144.: Yielding zone in the lower chord at ultimate failure.
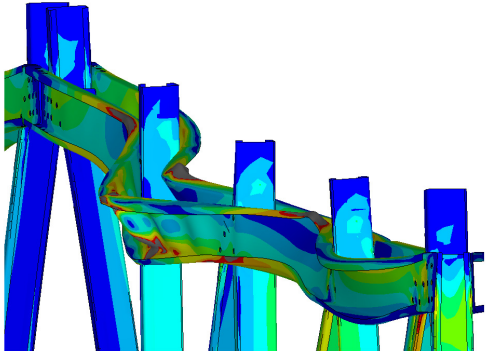
Figure 145.: Yielding zones in the upper chord at failure. 6x magnified deflections.

The figures show, that the webs of the sections in the lower chord joint are in fully plastic state at the failure of the upper chord. The stress distribution of the upper chord shows, that as plastic deformations develop, the stress in other parts of the chord reduces.

The yielding of the webs of the chord members lead to the reduction of the bending resistance in the joint; hence to the reduction of bending in the connecting members. Although the first two eigenmodes of the model were associated the lateral-torsional buckling of the lower chord, this, due to the reduced active moments cannot occur.

4.4. Summary

Numerical modelling is an efficient tool to complement laboratory test results, once a verified model of the studied structure capable of carrying out virtual experiments is available. A verified model can be used to study the behaviour of details not included in the measurement program or study the effect of changes in detailing. The results of the model can be incorporated in the design method on different levels, ultimately, the model can be used to directly determine the load-bearing capacity of the structure.

In this Chapter two shell finite element models were presented: that of a single C-section in compression and bending about the minor axis, and that of a truss made of C-sections. In both cases geometrically and materially nonlinear analyses were carried out on models with imperfect geometry; the thicknesses of the cross-sections and the material properties were those of the real structure. The models were verified using the laboratory test results presented in Chapters 2 and 3.

In the two models a unified approach regarding the geometry and the modelling of contact areas was utilized, however, the two major obstacles of such models: the question of modelling imperfections and connector elements was solved different ways.

In the case of the single C-section members a model of the self-drilling screws used to introduce the load in the member was developed. The model consists of beam elements only, hence it is compatible with shell elements, and can be calibrated by changing two of its stiffness parameters. Imperfections were added to the perfect geometry based on pure buckling shapes, derived using the constrained finite strip method. As using this method different shapes of imperfections can be applied to the model in a controlled way, this approach enables studying the imperfection sensitivity of the members. The calibration of the model was carried out taking into account both screws and imperfections to result a model capable of accurately reproducing rigidity, load-bearing capacity and failure mode of the specimens tested in the laboratory.

In the case of the truss girders the connector elements used were metric bolts. To model the structural behaviour of them a model consisting of linear and nonlinear line elements was developed, which, similarly to the model of the self-drilling screws is compatible with the shell elements. This model can be calibrated by one parameter representing the bearing stiffness of the bolted connection. The imperfections of the truss model were derived from its eigenshapes and used with amplitudes derived from recommended values of EC3. The model was used to reproduce the results of one of the tests carried out in the laboratory, and it was shown, how such models can be used to investigate parts of the structure not included in the measurement program of the test.

The presented models can further be used at two fields. Directly, they can be used on a different modelling level, i.e. in simulation-based design, to directly obtain design resistances. The general approach utilized in modelling geometry, contacts and connector elements, can be used in the case of other types of cold-formed structures as well: frames, purlin systems, etc.

5. Summary and conclusions

5.1. New scientific results

5.1.1. The theses of the PhD dissertation in English

The presented research and its scientific results can be summarized as follows:

Thesis 1

I worked out and completed an experimental test program on compression members made of cold-formed C-sections with cross-sectional configurations and supporting conditions, which were not analysed previously.

I determined and classified the stability behaviour of
  a) single C-section members with load introduction in the web or in the web and the flanges using self-drilling screws, and load introduction in the flanges using bolts,
  b) single C-section members with load introduction in the web using self-drilling screws, laterally supported by hat sections in discrete points at one flange,
  c) members made of two C-sections in a back-to-back arrangement connected to each-other at the webs by self-drilling screws, with load introduction in the web or in the flanges using bolts,
  d) members made by sticking two C-sections in each-other, connected at the flanges by self-drilling screws, with load introduction in the webs or in the web and the flanges using self-drilling screws,
  e) members made by sticking a C- and a U-section in each-other, connected at the flanges by self-drilling screws, with load introduction in web of the C-section and the flanges using self-drilling screws.

Publications connected to the thesis: A3, A7, A8, A9, A10, A11.

Thesis 2

I developed Eurocode-based design methods for the members studied in the laboratory tests based on the comparative analysis of the test-based design resistances and behaviour modes.
  a) I defined the eccentricity to be taken into account in the design of single C-section members without lateral support,
  b) I defined the interaction formula of single C-section members without lateral support in compression and bending about the weak axis,
  c) I developed a design method for single C-section members laterally supported at one flange,
  d) I derived the design resistances of members with complex cross-sectional arrangement on the basis of the design resistance of single members.

Publications connected to the thesis: A1, A4, A11.

Thesis 3

I completed an experimental test program on prototypes of a truss system made of cold-formed C-sections. The specialities of the structural arrangement are: i) the chord members consist of two C-sections in a back-to-back arrangement, with a distance equal to the web height of the brace members, ii) brace members are stuck between the chord members, iii) structural joints are made using fitted bolts, iv) brace members may be of single sections or doubled in a back-to-back arrangement.

I determined and characterized the behaviour of the truss based on the following observed failure modes:
   a) interacting out-of-plane global and local buckling of compression chord members,
   b) interacting out-of-plane global and local buckling of built-up compression chord members,
   c) cross-section failure of compression brace members at the element end,
   d) cross-section failure of brace-to-chord and chord-to-chord structural joints.

Based on the observed behaviour I defined constructional rules regarding the detailing of the joints ensuring favourable structural behaviour.

Publications connected to the thesis:A5, A6.

Thesis 4

I developed Eurocode-based design method for the structural members of the trusses studied in the laboratory tests based on the observed behaviour and failure modes and validated them based on the measured load-bearing capacities.
   a) I defined the modelling level to be applied in global analysis and verified the model based on the results of strain and deflection measurements,
   b) I defined the magnitude of eccentricity to be taken into account in the design of compression chord and brace members,
   c) I developed a design method to calculate the design resistance of structural joints, taking into account the interaction of structural members and joints.

Publications connected to the thesis: A5, A6.

Thesis 5

I developed shell finite element models of the single C-section members with load introduction in the web using self-drilling screws and of the truss girders, both capable of carrying out virtual experiments by materially and geometrically nonlinear analysis. The specialities of the models are the modelling of equivalent geometrical imperfections and modelling connector elements.

I generated the imperfections of the models as follows:
   a) in the case of the single C-section members using the constrained finite strip method enabling the control of the weight of pure – local, distortional, global – buckling modes in the generated imperfect shape,
   b) in the case of the truss girders based on selected eigenshapes of the model.

I developed models of connector elements used in the laboratory tests, compatible with shell elements and capable of following the structural behaviour as: tilting and pull-out in the case of self-drilling screws, shear and bearing in the case of bolts.

I used the laboratory test results to determine the stiffness parameters of the models of the connector elements and the shape and amplitude of imperfections to be applied on the model.

Publications connected to the thesis: A2.

5.1.2. The theses of the PhD dissertation in Hungarian

Az ismertetett kutatás és tudományos eredményei a következőképpen foglalhatóak össze:

1. Tézis

Megterveztem és végrehajtottam egy kísérleti programot korábban nem vizsgált keresztmetszeti elrendezésű és megtámasztási viszonyokkal rendelkező vékonyfalú, hidegen hajlított C-szelvényű nyomott szerkezeti elemek vizsgálatára.

Meghatároztam és stabilitási viselkedésük alapján osztályoztam a vizsgált szerkezeti elemek viselkedését. A vizsgált kialakítások:
   a) egy C-szelvényből álló, gerincén vagy gerincén és övein önfúrócsavaros kapcsolaton keresztül, vagy övein csavarozott kapcsolaton keresztül terhelt elemek,
   b) egy C-szelvényből álló, gerincén önfúrócsavaros kapcsolaton keresztül terhelt, egyik övén pontonként kalapszelvényekkel oldalirányban megtámasztott elemek,
   c) két egymásnak háttal fordított, gerincüknél önfúró csavarokkal összekapcsolt szelvényből készített, gerincén vagy övein csavarozott kapcsolaton keresztül terhelt elemek,
   d) két egymásba illesztett és öveiknél önfúró csavarokkal összekapcsolt C-szelvényből készített a gerinceken vagy egy gerincen és az öveken önfúrócsavaros kapcsolaton keresztül terhelt elemek,
   e) egy C- és egy U-szelvény egymásba illesztésével és öveik önfúró csavarokkal való összekapcsolásával készített, a C-szelvény gerincén és az öveken önfúrócsavaros kapcsolaton keresztül terhelt elemek.

A tézishez kapcsolódó publikációk: A3, A7, A8, A9, A10, A11.

2. Tézis

A laboratóriumi kísérletekben vizsgált szerkezeti elemek stabilitási viselkedése és a kísérletek alapján megállapított tervezési ellenállások összehasonlító elemzése alapján kifejlesztettem a vizsgált kialakítású elemek Eurocode 3 alapú méretezési eljárásait.
   a) Meghatároztam az egy C-szelvényből álló, oldalirányú megtámasztással nem rendelkező szerkezeti elemek méretezése során figyelembe veendő külpontosságot.
   b) Meghatároztam az egy C-szelvényből álló, oldalirányú megtámasztással nem rendelkező szerkezeti elemek normálerő-nyomatéki interakciós képletét.
   c) Méretezési eljárást fejlesztettem az egyik övükön kalapszelvénnyel oldalirányban megtámasztott C-szelvényű elemek teherbírásának meghatározására.
   d) Az egy C-szelvényből álló elemek méretezési eljárása alapján eljárást adtam a több szelvényből összetett szerkezeti elemek méretezésére.

A tézishez kapcsolódó publikációk: A1, A4, A11.

3. Tézis

Kísérletsorozatot hajtottam végre hidegen hajlított, C-szelvényű elemekből készített rácsos tartók prototípusain. A vizsgált szerkezet különlegessége, hogy i) az övrudak két, egymásnak háttal fordított C-szelvényből állnak, távolságuk egyenlő a rácsrudak gerincmagasságával, ii) a rácsrudak az övrúd elemek közé illeszkednek, iii) a szerkezeti csomópontok illesztőcsavaros kialakításúak, iv) a rácsrudak egy szelvényből, vagy két, háttal egymásnak fordított C-szelvényű elemből készülnek.

A kísérleti viselkedés alapján meghatároztam és osztályoztam a tartók tönkremeneteli módjait.

a) A nyomott övrudak tartósíkra merőleges globális stabilitásvesztése és lokális horpadása interakcióját.

b) Az összetett szelvényű nyomott övrudak tartósíkra merőleges globális stabilitásvesztését és lokális horpadása interakcióját.

c) A nyomott rácsrudak elemvégi szilárdsági tönkremenetelét.

d) A szerkezeti csomópontok szilárdsági tönkremenetelét rács-öv és öv-öv kapcsolatokra.

A tartók kísérletek során megfigyelt viselkedése alapján a szerkezeti kialakításra vonatkozó, kedvező szerkezeti viselkedést biztosító szerkesztési szabályokat dolgoztam ki.

A tézishez kapcsolódó publikációk:A5, A6.

4. Tézis

A laboratóriumi kísérletek során megfigyelt szerkezeti viselkedés és tönkremeneteli módok alapján Eurocode 3 alapú eljárást fejlesztettem a rácsos tartók szerkezeti elemeinek méretezésére, az eljárások alkalmazhatóságát a mérési eredményekkel igazoltam.

a) Meghatároztam a rácsos tartók erőjátékának vizsgálatához szükséges modellezési szintet, a modell alkalmazhatóságát nyúlás- és lehajlásmérési eredményekkel igazoltam.

b) Meghatároztam a nyomott övrudak, illetve nyomott- vagy húzott rácsrudak méretezési eljárásában alkalmazandó külpontosság nagyságát.

c) A rácsrúd elemeinek és csomópontjainak interakcióját figyelembe vevő méretezési eljárást dolgoztam ki a szerkezeti csomópontok teherbírásának meghatározására.

A tézishez kapcsolódó publikációk:A5, A6.

5. Tézis

Virtuális kísérletek végrehajtására alkalmas anyagilag és geometriailag nemlineáris felületszerkezeti végeselemes modellt fejlesztettem az egy C-szelvényből álló, gerincén önfúrócsavaros kapcsolaton keresztül terhelt elemek és a rácsos tartók vizsgálatához. A modellek különlegessége a helyettesítő geometriai imperfekciók és a kapcsolóelemek figyelembe vétele.

A helyettesítő geometriai imperfekciókat

a) a C-szelvényű elemek esetében a kényszermátrixokat alkalmazó végessávos módszerrel határoztam meg, lehetővé téve az alkalmazott imperfekt alakban a tiszta – lokális, torzulásos horpadási és globális – stabilitásvesztési alakok súlyának beállítását.

b) a rácsos tartó modellje esetében a modell sajátalakjaiból állítottam össze.

A felületszerkezeti modellel kompatibilis modelleket fejlesztettem a kísérletekben alkalmazott kapcsolóelemek releváns szerkezeti viselkedésének figyelembe vételére, melyek az önfúró csavarok esetében a ferdülés és kihúzódás, a csavarok esetében pedig nyírás és palástnyomás.

A laboratóriumi kísérletek eredményei alapján megállapítottam a kapcsolóelemek modelljeinek merevségi paramétereit és a globális modellben alkalmazandó imperfekciók alakját és nagyságát.

A tézishez kapcsolódó publikációk: A2.

5.2. Application of the results

The first part of the research presented in Chapter 2 can be considered as basic research: the characterized stability behaviour modes of the test members can be useful in studying members with similar supporting conditions or developing design methods based on standards different from Eurocode. The developed standard-based design methods are system-independent and can be used in any building system where members of the same type of sections, and supporting and loading conditions are used.

Part of the structural arrangements (e.g.: single C-section members) presented are extensively used in building systems in the industry (members of frames, trusses, wall panels, etc.). The members with complex cross-section are potential solutions for structural problems where enhanced load-bearing capacity is needed, e.g. members with a DoubleC arrangement can be used in situations where no lateral support can be provided to the member; CU sections may be an effective solution in refurbishment of existing structures.

The results on the complex arrangements provide insight, how detailing affects the structural behaviour – e.g. IC Brace and IC Column members, although of similar arrangement exhibit completely different structural behaviour – the findings regarding the performance of the studied members can be the basis for decisions in future system developments.

The truss system developed is a commercial product of the industrial partner; the presented results make up the core of the design method of such girders. To enable rapid design of the trusses a software utilizing the design method of the truss system has been developed; the program is used by the designers of the company in everyday practice. Note that during the software development the design method has been extended to handle structural arrangements not studied in the laboratory.

The results concerning the numerical modelling of cold-formed structures are not yet used either in research or on an industrial level, since these can be considered as a first step towards studying other types or more complex problems of cold-formed structures.

5.3. Further research needs

As the most authentic way to study the behaviour of structures is carrying out laboratory tests continuing and/or extending the work in this direction is an obvious possibility; the tests on the studied arrangements with different member lengths and/or different sections can be used to refine the design methods presented in Chapter 2. The C-section members failed in the tests can further be used to study the geometry of the plastic mechanisms arisen due to the failure, to enable analysing the post-failure behaviour of them.

Regarding the tests on the truss girders: further tests could be carried out, either by following the method presented in section 3.2.2, that is, in each subsequent test changing the failed member to a stronger one, or by designing the truss with the aim to obtain a given failure mode, e.g. the failure of the lower chord, a failure mode not observed in the tests. Either way, it is possible to study the failure modes relevant from the truss behaviour point-of-view. It would be very useful to study a different structural arrangement as well: one of the critical points of the structure is the upper chord and its sensitivity to out-of-plane global buckling. It seems logical to prevent this failure mode by using trapezoidal sheeting instead of purlins to provide a continuous lateral support for these members; however, this arrangement certainly results failure modes not covered by the design method presented in the dissertation.

The behaviour of the truss with this arrangement, however, can be studied using the numerical model developed to study the truss as well. Although laboratory tests will always be a cornerstone of studying structures, numerical models can, and should be used to speed up the development work and make more detailed analysis possible. The numerical models presented in Chapter 4 can be considered a first step towards numerical modelling different structures or structural details, as the aspects most important to accurately predict such structures are included in these. However, lacking standardized methods to incorporate imperfections in the models calls for studying this problem and working out a consistent system for these. The laboratory test results presented in Chapter 2 provide basis for such a research, as local, distortional and global failure modes were all obtained in the tests; these results, complemented with parametric studies using models capable of virtual experiments may be enough to lay the foundations of a such a system. Note that equivalent geometrical imperfections are not the only way to apply imperfections to the model; as the fabrication process of cold-formed members and sheeting is well-controlled and relatively simple from the mechanics point-of-view, it is possible, that in case of cold-formed structures it is more prosperous not to treat mechanical and geometrical imperfections together.

Connector elements are similarly important from the structural behaviour – and accordingly from the modelling – point-of-view. The models presented in Chapter 4 need more study primarily to prove their applicability in other structural details and to establish a method to calculate the stiffness parameters to be used depending on the properties of the connected plates.

5.4. Main publications on the subject of the thesis

International journal paper

[A1] Jakab, G., Dunai, L.: *Resistance of C-profile cold-formed compression members: Test and standard*, Journal of Constructional Steel Research, 64 (2008), 802-807. doi: 10.1016/j.jcsr.2008.01.037.

[A2] Jakab, G., Dunai, L.: *Laboratory and virtual experiments on cold-formed C-section compression members with semi-rigid connections*, Periodica Polytechnica, Civil Engineering (accepted for publication), 2009.

International conference papers

[A3] Dunai, L., Jakab, G., Joó, A. L.: *Experiments on C/Z-Profile Compression Members*, Proceedings of the 4th International Conference on Coupled Instabilities in Metal Structures (CIMS 2004), Rome, Italy, 27-29 September 2004, pp. 429-438.

[A4] Jakab, G., Dunai, L.: *Resistance of C-profile cold-formed compression members: Test and standard*, Proceedings of the Conference on Stability and Ductility of Steel Structures (SDSS 2006), Lisbon, Portugal, 6-8 September 2006, Eds.: D. Camotim, N. Silvestre, P.B. Dinis, Vol. 2, pp. 631-638. ISBN 972-8469-61-6.

[A5] Jakab, G., Dunai, L.: *Development of a new cold-formed steel truss system*, Proceedings of the fifth International Conference on Thin-Walled Structures, Gold Coast, Australia, 18-20 June 2008, Ed.: M. Mahendran, Vol. 1, pp. 485-492. ISBN 978-1-74107-239-6.

[A6] Jakab, G., Dunai, L.: *Interaction phenomena of cold-formed truss members and joints*, Proceedings of the fifth International Conference on Coupled Instabilities in Metal Structures (CIMS 2008), Sydney, Australia, 23-25 June 2008, Eds.: K. Rasmussen, T. Wilkinson, Vol. 1, pp. 515-522. ISBN 978-0-646-49439-5.

Paper in edited book

[A7] Jakab, G.: *Tragverhalten Kaltgeformter C-Profile unter axialer Druckbelastung*, A Hidak és Szerkezetek Tanszéke Tudományos Közleményei 2006. évi kiadása, Szerk.: Tassi, G., Hegedűs, I., Kovács, T., pp. 93-100. HU ISSN 1586-7196.

Conference papers (abstract and presentation only)

[A8] Jakab, G., Dunai, L.: *Vékonyfalú nyomott rudak stabilitási jelenségei*, XXVI. Országos Tudományos Diákköri Konferencia, Műszaki Tudományok Szekció kiadványa, Debrecen, 2003. április 15-17, pp. 223.

[A9] Jakab, G., Dunai, L.: *C- és Z-szelvényű nyomott rudak kísérleti vizsgálata*, XXVI. Országos Tudományos Diákköri Konferencia, Műszaki Tudományok Szekció kiadványa, Debrecen, 2003. április 15-17, pp. 225.

[A10] Jakab, G., Dunai, L.: *Stabilitási jelenségek kölcsönhatása C-szelvényű nyomott rúd viselkedésében*, IX. Magyar Mechanikai Konferencia kiadványa, Miskolc, 2003. augusztus 27-29, pp. 40.

[A11] Jakab, G.: *Untersuchung und Bemessung von Staeben mit kaltgeformten Querschnitte*, Diplomwork, BME – Universität Karlsruhe (TH), 2003.

References

[1] *EN 1993-1-1:2006 Eurocode 3: Design of steel structures. Part 1-1: General rules and rules for buildings.*

[2] Fóti, P., Dunai, L.: *Interaction phenomena in the cold-formed frame corner behaviour*, Proceedings of the Third International Conference on Coupled Instabilities in Metal Structures (CIMS 2000), Lisbon, Portugal, 2000., Eds. Camotim, D., Dubina, D., Rondal, J., pp. 459-466.

[3] Erdélyi, Sz.: *Light-gauge steel and concrete composite beams*, PhD. Dissertation, BME, 2008.

[4] Dunai, L.: *Innovative steel and composite structures*, Doctor of Hungarian Academy of Sciences Thesis, 2007.

[5] Joó, A. L.: *Analysis and design of thin-walled roof systems*, PhD Dissertation, BME, 2009.

[6] Kachichian, M., Dunai, L., Macdonald, R., Werner, F.: *Full scale testing of cold-formed Z-purlins*, Proceedings of the International Colloquium on Stability and Ductility of Steel Structures, Prof. O. Halász Memorial Session, Budapest, Hungary, 26-28 September 2002., Ed.: Iványi M., pp. 203-210, Akadémia Kiadó.

[7] Iványi M.: *Hídépítéstan – Acélszerkezetek*, Műegyetemi Kiadó, Budapest 1998, ISBN 963 420 578 X

[8] Moen, C. D., Igusa, T., Schafer, B.W.: *Prediction of residual stresses and strains in cold-formed steel members*, Thin-Walled Structures, Volume 46 (2008), pp. 1274-1289. doi:10.1016/j.tws.2008.02.002

[9] Gehring, A., Saal, H.: *Robust finite element analysis of light gauge cold-formed sections*, Proceedings of the Fifth International Conference on Thin-Walled Structures. Gold Coast, Australia, 18-20 June 2008, Ed.: M. Mahendran, Vol. 1, pp. 297-304. ISBN 978-1-74107-239-6.

[10] Schafer, B.W., Peköz, T.: *Computational modelling of cold-formed steel: characterizing geometric imperfections and residual stresses*, Journal of Constructional Steel Research, Volume 47 (1998), pp. 193–210. doi:10.1016/S0143-974X(98)00007-8

[11] *North American specification for the design of cold-formed steel structural members*, AISI, Washington, DC: American Iron and Steel Institute; 2007.

[12] *Cold-formed steel structures, Australian/New Zealand Standard*, AS/NZS 4600:1996, Standards Australia, Sydney, Australia; 1996.

[13] *EN 1993-1-3:2006 Eurocode 3: Design of steel structures. Part 1-3 General rules. Supplementary rules for cold-formed members and sheeting.*

[14] *ENV 1993-1-3:1996 Eurocode 3: Design of steel structures. Part 1-3 General rules. Supplementary rules for cold-formed members and sheeting.*

[15] Young, B.: *Research of cold-formed steel columns*, Thin Walled Structures, Volume 46 (2008), pp. 731-740. doi:10.1016/j.tws.2008.01.025

[16] Kwon, Y.B., Kim, B.S., Hancock, G.J.: *Compression tests of high strength cold-formed steel channels with buckling interaction*, Journal of Constructional Steel Research, Volume 65 (2009), Issue 2, pp. 278-289. doi:10.1016/j.jcsr.2008.07.005

[17] Young, B., Rasmussen, K.J.R.: *Design of lipped channel columns*, Journal of Constructional Steel Research, Volume 124 (1998), Issue 2, pp. 140-148. doi:10.1061/(ASCE)0733-9445(1998)124:2(140)

[18] Young, B., Rasmussen, K.J.R.: *Shift of effective centroid of channel columns,* Journal of Constructional Steel Research, Volume 125 (1999), Issue 5, pp. 524-531. http://dx.doi.org/10.1061/(ASCE)0733-9445(1999)125:5(524)

[19] Lam, S.S.E., Chung, K.F., Wang, X.P.: *Load-carrying capacities of cold-formed steel cut stub with lipped C-section*, Thin-Walled Structures, Volume 44 (2006), pp. 1007-1083. doi:10.1016/j.tws.2006.10.011.

[20] Dubina, D., Stratan, A., Ciutina, A., Fulop, L., Nagy, Zs.: *Monotonic and cyclic performance of joints of cold-formed steel portal frames*. Proceedings of the fourth International Conference On Thin-Walled Structures, ICTWS04, Loughborough, UK, 23-24 June 2004.

[21] Dubina, D.: *General report on cold-formed steel structures recent design and research advances*. Stability and Ductility of Steel Structures, SDSS 2002. Budapest, Hungary, 26-28 September 2002, Ed.: Iványi M, pp. 137-146. ISBN963 05 7950 2.

[22] Zaharia, R., Dubina, D.: *Stiffness of joints in bolted connected cold-formed steel trusses*, Journal of Constructional Steel Research, Volume 62 (2006), pp. 240-249. doi:10.1016/j.jcsr.2005.07.002

[23] Dubina, D.: *Structural analysis and design assisted by testing of cold-formed steel structures*, Thin-Walled Structures, Volume 46 (2008) pp. 741-764. doi:10.1016/j.tws.2008.01.030

[24] Kármán, T.: *Festigkeitsprobleme in Maschinenbau*, Enziklopädie der Mathematischen Wissenschaften, Band 4, Leipzig, 1910

[25] Winter, G.: *Strength of thin steel compression flanges*, Transactions of the ASCE, Vol. 112, 1947.

[26] Vlasov, V.Z., *Thin-Walled Elastic Beams*, 2nd edn, Gosudarstvenoe izdatelstvo fiziko-matematicheskoi literaturi, (in Russian), Moscow, 1959.

[27] Csellár Ö., Halász O., Réti V.: *Vékonyfalú acélszerkezetek*, Műszaki Könyvkiadó, Budapest, 1965.

[28] Silvestre, N., Camotim, D.: *Nonlinear generalized beam theory for cold-formed steel members*, International Journal of Structural Stability and Dynamics. Volume 3 (2003) pp. 461-490. doi:10.1142/S0219455403001002

[29] Schardt, R.: *Verallgemeinerte technische Biegetheorie*, Springer-Verlag, Berlin, 1989. ISBN 3-540-51339-6, www.vtb.info.

[30] Bebiano R., Pina P., Silvestre N. Camotim D.: *GBTUL – buckling and vibration analysis of thin-walled members*, DECivil/IST, Technical University of Lisbon (http://www.civil.ist.utl.pt/gbt).

[31] Papangelis, J. P., Hancock, G. J.: *Computer analysis of thin-walled structural members*, Computers and Structures, Volume 56 (1995), pp. 157-176. doi:10.1016/0045-7949(94)00545-E

[32] Current versions of CUFSM: http://www.ce.jhu.edu/bschafer/cufsm/

[33] Ádány, S., Schafer, B.W.: *Buckling mode decomposition of single-branched open cross-section members via finite strip method: derivation*, Thin-walled Structures Journal, Volume 44 (2006), pp. 563-584. doi:10.1016/j.jcsr.2007.04.004

[34] Ádány, S., Schafer, B.W.: *Buckling mode decomposition of single-branched open cross-section members via finite strip method: application and examples*, Thin-walled Structures Journal, Volume 44 (2006), pp. 585-600. doi:10.1016/j.tws.2006.03.014

[35] Vigh, L.G.: *Virtual and real test based analysis and design of non-conventional thin-walled metal structures*, PhD Dissertation, BME, 2006.

[36] Sivakumaran, K.S., Abdel-Rahman, N.: *A finite element analysis model for the behaviour of cold-formed steel members*, Thin-Walled Structures, Volume 31 (1998), pp. 305-324. doi:10.1016/S0263-8231(98)00017-2

[37] *EN 1993-1-5:2005 Eurocode 3: Design of steel structures. Part 1-5: Plated structural elements.*

[38] Telue, Y., Mahendran, M.: *Behaviour and design of cold-formed steel wall frames lined with plasterboard on both sides*, Engineering Structures, Volume 26 (2004), pp. 567-579. doi:10.1016/j.engstruct.2003.12.003

[39] Yu, C., Schafer, B.W.: *Simulation of cold-formed steel beams in local and distortional buckling with applications to the direct strength method*, Journal of Constructional Steel Research, Volume 63 (2007), pp. 581-590. doi:10.1016/j.jcsr.2006.07.008

[40] *EN 1993-1-8:2005 Eurocode 3: Design of steel structures. Part 1-8: Design of joints.*

[41] Ádány, S., Kósa, Z., Jakab, G.: *DimTruss v1.00*, Design software for the LindabTruss System (Commercially not available), 2009.

[42] *EN 1993-1-6:2005 Eurocode 3: Design of steel structures. Part 1-6: Strength and stability of shell structures.*

[43] Ansys 11.0. www.ansys.com

[44] MATLAB. www.mathworks.com

[45] Borges Dinis, P., Camotim, D., Silvestre, N.: *FEM-based analysis of the local-plate/distortional mode interaction in cold-formed steel lipped channel columns*, Computers & Structures, Volume 85 (2007), pp. 1461-1474. doi:10.1016/j.compstruc.2007.02.013

[46] Joó, A. L., Ádány, S.: *FEM-based approach for the stability design of thin-walled members by using cFSM base functions*, Periodica Polytechnica, Civil Engineering (accepted for publication), 2009.

Annex

The measured load-bearing capacities and the observed failure modes are listed for each test in Table A1 – Table A11 for the different specimen arrangements, failure modes are designated by small-case letters. The tests are commented if necessary to highlight important aspects of the given arrangement or result.

Table A1: Results of SimpleC specimens.

Length [mm]	Section	Test	Ultimate load [kN]	Failure mode	Comment
800	C150/1.0	C03	18.05	a	
	C200/1.0	C04	21.86	c	
	C200/2.0	C01	85.92	a	
1500	C200/1.5	C65	52.26	a	C69 with short, wide screw layout
		C68	38.53	b	
	C200/2.0	C66	78.97	a	different number of screws at load drive-in. C66: 16; C81: 9; C82:49
		C81	79.23	a	
		C82	78.86	a	
	C200/2.5	C67	111.10	a	different number of screws at load drive-in. C67: 25; C80: 16
		C80	114.24	a	
2000	C150/1.0	C14	12.50	a	
	C200/1.0	C15	24.16	a	
	C200/2.0	C12	71.11	a	
2500	C200/1.5	C40	41.02	a	
	C200/2.0	C41	63.99	a	
	C200/2.5	C42	94.34	a	
3600	C150/1.0	C25	9.47	a	
	C200/1.0	C26	17.24	d	
	C200/2.0	C23	46.77	a	no differences
		C34	46.67	a	

a - interaction of flexural buckling and bending; plastic mechanism at the middle of the column
b - interaction of joint failure and crushing of the web at load introduction
c - distortional buckling; interaction of joint failure and crushing of the web at load introduction
d - torsional-flexural buckling; plastic mechanism at the middle of the column

Table A2: Results of C specimens.

Length [mm]	Section	Test	Ultimate load [kN]	Failure mode	Comment
1500	C200/1.5	C70	58.91	a	
	C200/2.0	C77	87.76	a	
	C200/2.5	C72	123.90	a	
2500	C200/1.5	C45	53.76	a	different screw positions in the flanges
		C55	55.38	a	
		C56	56.16	a	
	C200/2.0	C48	89.61	a	
	C200/2.5	C51	113.05	a	

a - interaction of flexural buckling and bending; plastic mechanism at the middle of the column

Table A3: Results of CU specimens with different thickness.

Length [mm]	Section		Test	Ultimate load [kN]	Failure mode	Comment
	C	U				
2500	C200/2.5	U200/2.0	C99	123.20	f	reference: C52
	C200/1.5	U200/2.5	C100	71.55	f	reference: C54

f - interaction of distortional and flexural buckling; plastic mechanism at the middle of the column

Table A4: Results of CompressionC specimens.

Length [mm]	Section	Test	Ultimate load [kN]	Failure mode	Comment
800	C200/1.0	C05	35.91	e	
	C200/2.0	C02	133.57	e	
2000	C200/1.0	C16	25.62	e	specimen with initial defects
	C200/2.0	C13	104.34	f	
3600	C200/1.0	C27	24.65	d	local buckling in the flanges and lips
	C200/2.0	C24	53.16	a	local buckling in the flanges as well

a - interaction of flexural buckling and bending; plastic mechanism at the middle of the column
d - torsional-flexural buckling; plastic mechanism at the middle of the column
e - crushing of the web and flanges at load-drive in
f - interaction of distortional and flexural buckling; plastic mechanism at the middle of the column

Table A5: Results of CC specimens.

Length [mm]	Section	Test	Ultimate load [kN]	Failure mode	Comment
1500	C200/1.5	C75	91.43	f	
		C78	92.45	f	
	C200/2.0	C74	156.60	f	
	C200/2.5	C71	214.10	f	
2500	C200/1.5	C43	62.76	b	no screws in the flanges
		C47	97.23	f	
	C200/2.0	C50	146.41	f	
	C200/2.5	C53	182.27	f	

b - interaction of joint failure and crushing of the web at load introduction
f - interaction of distortional and flexural buckling; plastic mechanism at the middle

Table A6: Results of CU specimens.

Length [mm]	Section	Test	Ultimate load [kN]	Failure mode	Comment
1500	C200/1.5	C76	74.63	f	
	C200/2.0	C73	109.80	f	
	C200/2.5	C69	179.20	f	load introduction in the C-section
		C79	213.00	f	load introduction in the U-section
2500	C200/1.5	C46	98.87	f	load introduction in the U-section
		C54	68.37	f	load introduction in the C-section
	C200/2.0	C49	111.45	f	
	C200/2.5	C52	146.21	f	

f - interaction of distortional and flexural buckling; plastic mechanism at the middle of the column

Table A7: Results of DoubleC specimens.

Length [mm]	Section	Test	Ultimate load [kN]	Failure mode	Comment
800	C150/1.0	C10	55.27	b	
	C200/1.0	C11	47.28	b	
	C200/2.0	C09	200.78	b	
2000	C150/1.0	C21	45.78	f	
	C200/1.0	C22	58.66	b	
	C200/2.0	C20	219.02	b	distortional behaviour at load-introduction
2500	C200/1.5	C44	131.80	b	
3600	C150/1.0	C32	26.04	f	
	C200/1.0	C33	58.00	f	plastic mechanism at the upper end as well
		C35	56.17	f	no connecting screws in the flanges
	C200/2.0	C31	150.87	f	screw distance in the flanges: 500 mm
		C36	140.44	f	no connecting screws in the flanges
		C37	180.67	f	screw distance in the flanges: 1000 mm

b - interaction of joint failure and crushing of the web at load introduction
f - interaction of distortional and flexural buckling; plastic mechanism at the middle of the column

Table A8: Brace specimens.

Length [mm]	Section	Test	Ultimate load [kN]	Failure mode	Comment
1500	C200/1.5	C63	81.61	g	
	C200/2.0	C62	116.85	g	
		C64	129.12	g	bolt position: 10 mm towards the web
	C200/2.5	C61	181.20	g	
2500	C200/1.5	C59	58.17	g	
	C200/2.0	C58	108.97	g	
	C200/2.5	C57	166.90	g	
		C60	166.26	g	with strain measurement

g - interaction of distortional buckling and flexural buckling; plastic mechanism in the flanges

Table A9: IC Brace specimens.

Length [mm]	Section	Test	Ultimate load [kN]	Failure mode	Comment
1500	C200/1.5	C91	174.40	h	
	C200/2.0	C90	291.70	h	
	C200/2.5	C89	-	-	capacity of the hydraulic jack exhausted
2500	C200/1.5	C95	146.70	h	
	C200/2.0	C97	239.20	h	no differences; C97 highly imperfect
		C98	323.40	h	
	C200/2.5	C96	-	-	capacity of the hydraulic jack exhausted

h - distortional buckling; plastic mechanism

Table A10: IC Column specimens.

Length [mm]	Section	Test	Ultimate load [kN]	Failure mode	Comment
1500	C200/1.5	C85	132.80	i	
	C200/2.0	C83	205.00		failure of the gusset plate
		C84	213.40	i	
		C86	190.00	i	
		C87	236.60	i	
	C200/2.5	C88	214.20		bolt shear failure at load introduction
2500	C200/1.5	C94	138.80	i	
	C200/2.0	C93	207.10	i	
	C200/2.5	C92	281.11		bolt shear failure at load introduction

i - interaction of local buckling, and flexural buckling of chord member

Table A11: HatC specimens.

Length [mm]	Section	Test	Ultimate load [kN]	Failure mode	Comment
800	C150/1.0	C07	21.90	j	
	C200/1.0	C08	19.36	j	
	C200/2.0	C06	94.19	j	
2000	C150/1.0	C18	20.49	j	
	C200/1.0	C19	22.14	j	
	C200/2.0	C17	93.81	j	
3600	C150/1.0	C29	21.81	j	
	C200/1.0	C30	23.55	j	
	C200/2.0	C28	104.25	j	

j - distortional buckling of the free flange; crippling of the web

Results of material coupon tests

Tensile material tests were carried out on coupons cut out of the tested specimens, from areas exhibiting only elastic deformations, test results are presented in Table A12. In case of the first set the tests were carried out in the Structural Laboratory of BME; the results presented are averaged values from 6 tests (C150 section) or 10 tests (C200 sections) coupons. The results for the second test set are based on a single test for each thickness, test were carried out by AGMI Zrt, Budapest.

Table A12: Results of material tests.

| Set | Specimen | Coupon | | Yield stress [MPa] | Ultimate strength [MPa] |
		Thickness (without zinc coating) [mm]	Width [mm]	$R_{p0.2}$	R_m
First set	C15-1	1.01 (0.98)	19.95	344	409
	C20-1	1.01 (0.98)	19.95	352	416
	C20-2	2.02 (1.99)	19.96	420	488
Second set	C15-1	1.42 (1.40)	19.81	438	532
	C20-1	1.91 (1.87)	19.82	460	501
	C25-1	2.44 (2.39)	19.81	460	543

Cross-sectional properties of the C-sections used in the tests are summarized in Table A13 – Table A14.

Table A13: Cross-sectional properties.

EC3-1-3: 1996	A_g [cm^2]	I_y [cm^4]	I_z [cm^4]	y_g [mm]	A_{eff} [cm^2]	eN_y [mm]
C150/1.0	2.60	88.51	7.46	12.43	1.04	1.72
C200/1.0	3.64	218.31	23.69	20.18	0.96	-4.45
C200/1.5	5.58	351.44	40.09	20.58	2.33	0.77
C200/2.0	7.44	468.34	54.50	20.99	4.17	3.55
C200/2.5	9.41	591.77	70.19	21.39	6.27	4.16

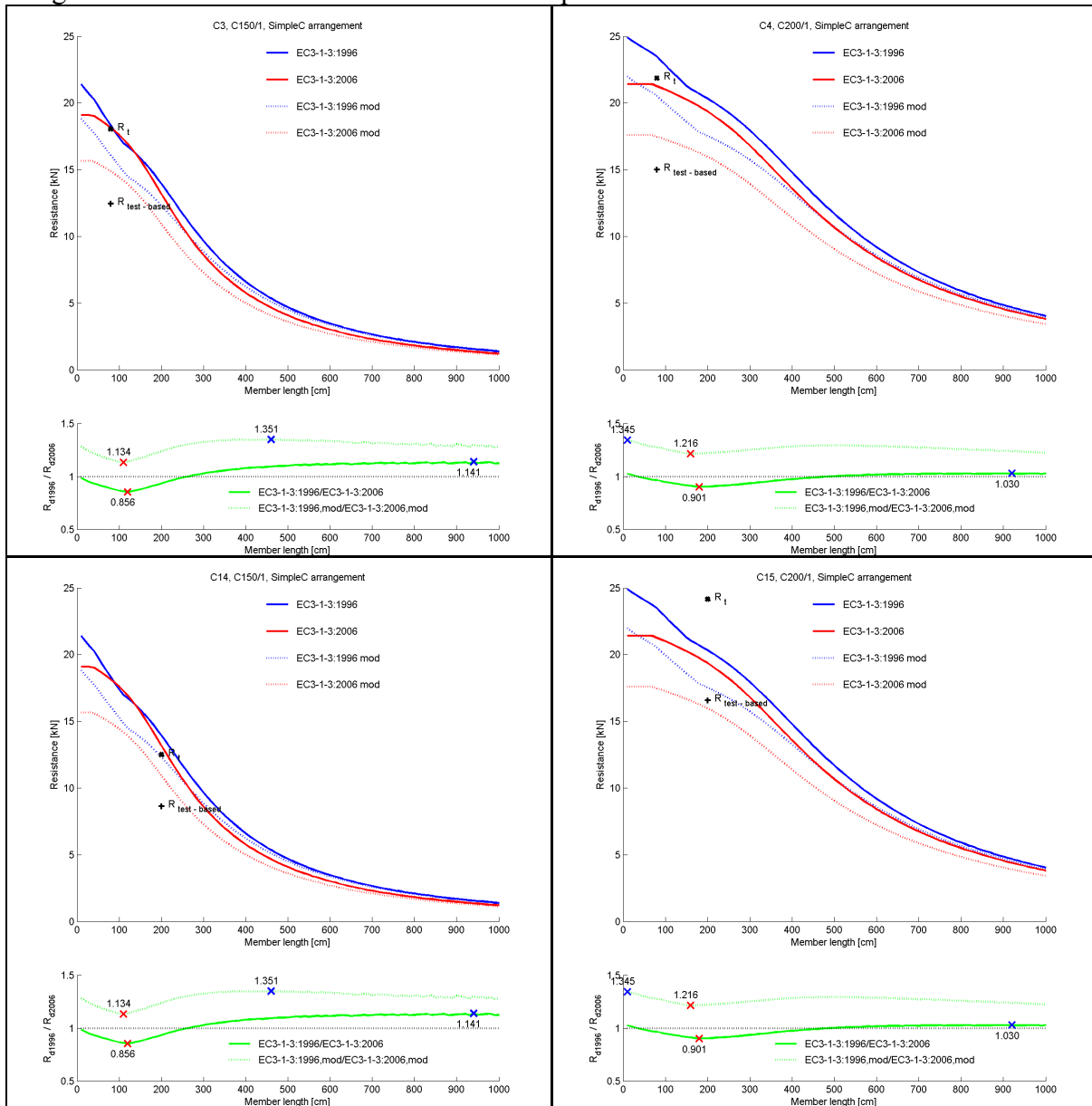| EC3-1-3: 2006	A_g [cm^2]	I_y [cm^4]	I_z [cm^4]	y_g [mm]	A_{eff} [cm^2]	eN_y [mm]
C150/1.0	2.50	82.48	6.64	11.79	1.19	5.04
C200/1.0	3.55	218.31	23.69	19.50	1.18	4.26
C200/1.5	5.40	330.31	36.18	19.66	2.64	5.23
C200/2.0	7.27	441.29	48.82	19.84	4.45	5.51
C200/2.5	9.14	551.02	61.54	20.01	6.36	5.08

Table A14: Cross-sectional properties.

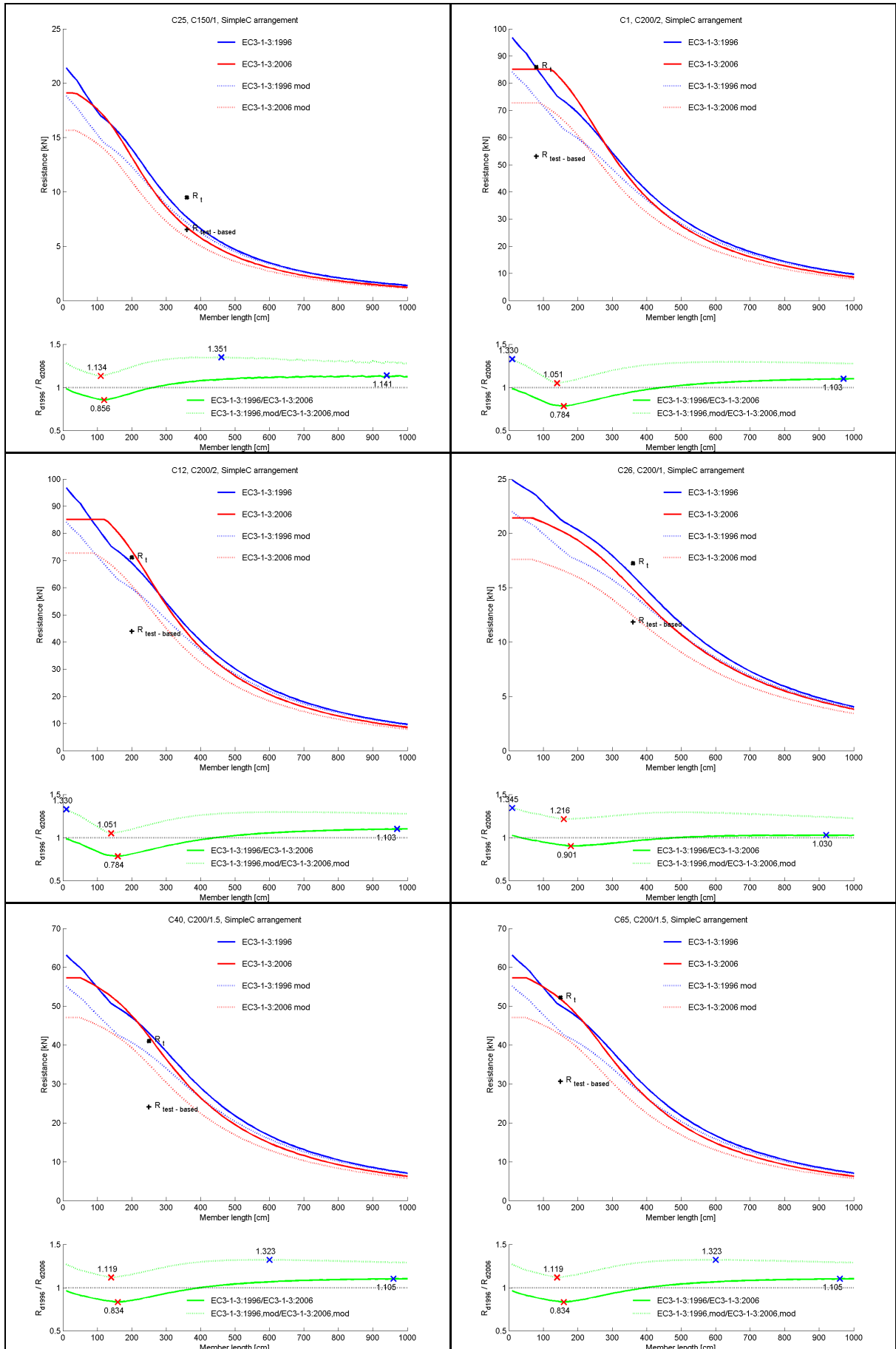| EC3-1-3: 1996	$W_{y,com}$ [cm^3]	$W_{y,ten}$ [cm^3]	$W_{z,pos,com}$ [cm^3]	$W_{z,pos,ten}$ [cm^3]	$W_{z,neg,com}$ [cm^3]	$W_{z,neg,ten}$ [cm^3]
C150/1.0	7.15	11.14	1.54	5.52	2.31	2.06
C200/1.0	20.43	9.02	1.67	10.35	4.38	4.26
C200/1.5	21.44	33.03	5.30	17.81	8.38	7.90
C200/2.0	37.22	45.44	9.22	25.07	13.13	10.05
C200/2.5	53.94	58.30	12.97	32.20	19.02	13.39

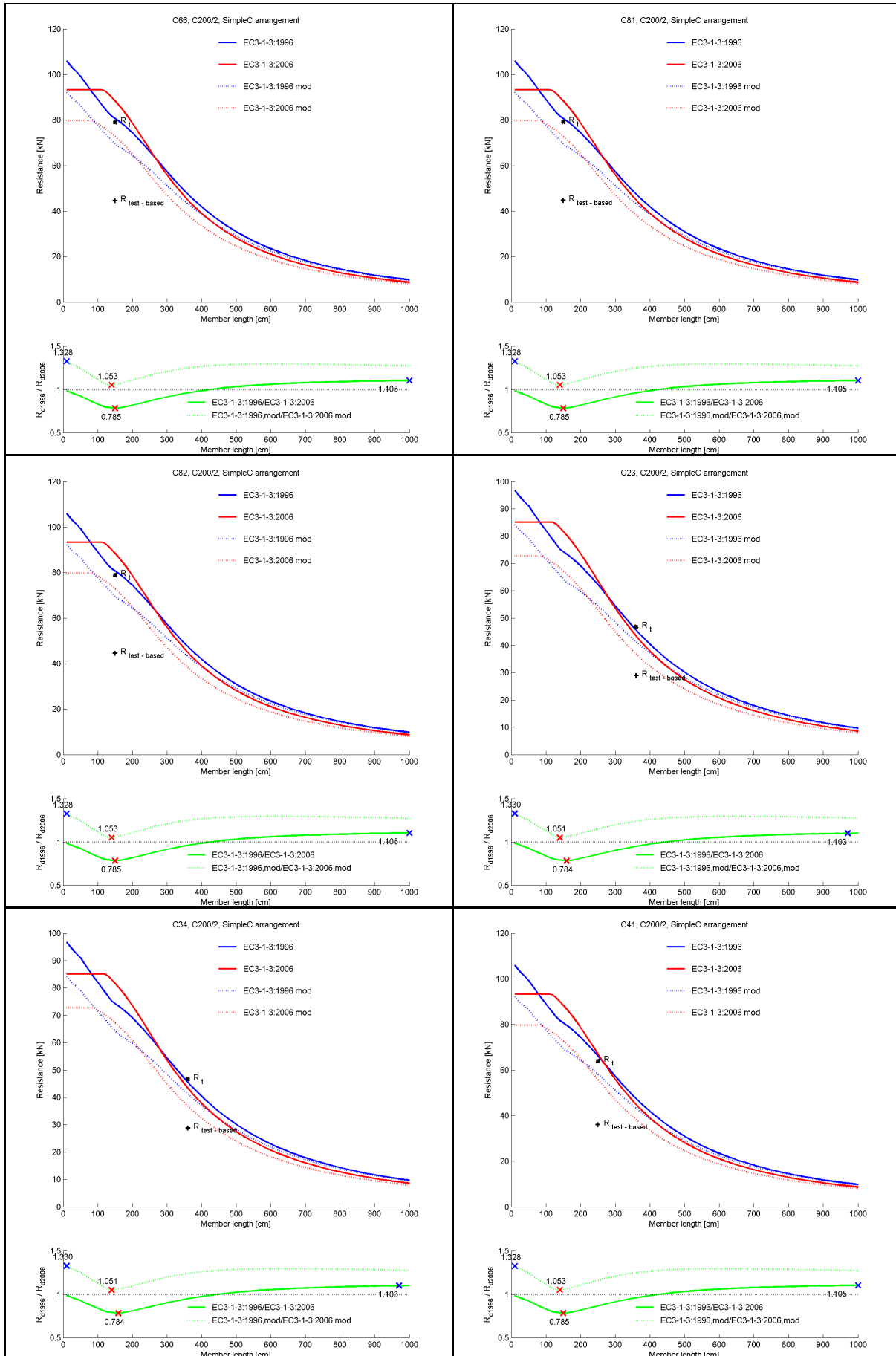| EC3-1-3: 2006	$W_{y,com}$ [cm^3]	$W_{y,ten}$ [cm^3]	$W_{z,pos,com}$ [cm^3]	$W_{z,pos,ten}$ [cm^3]	$W_{z,neg,com}$ [cm^3]	$W_{z,neg,ten}$ [cm^3]
C150/1.0	8.26	10.65	2.00	5.54	2.49	1.87
C200/1.0	11.13	20.17	3.30	11.40	4.37	3.95
C200/1.5	24.67	31.87	6.77	18.04	9.35	6.60
C200/2.0	41.22	43.53	10.00	24.44	15.92	9.44
C200/2.5	54.35	55.01	12.78	30.54	24.17	12.42

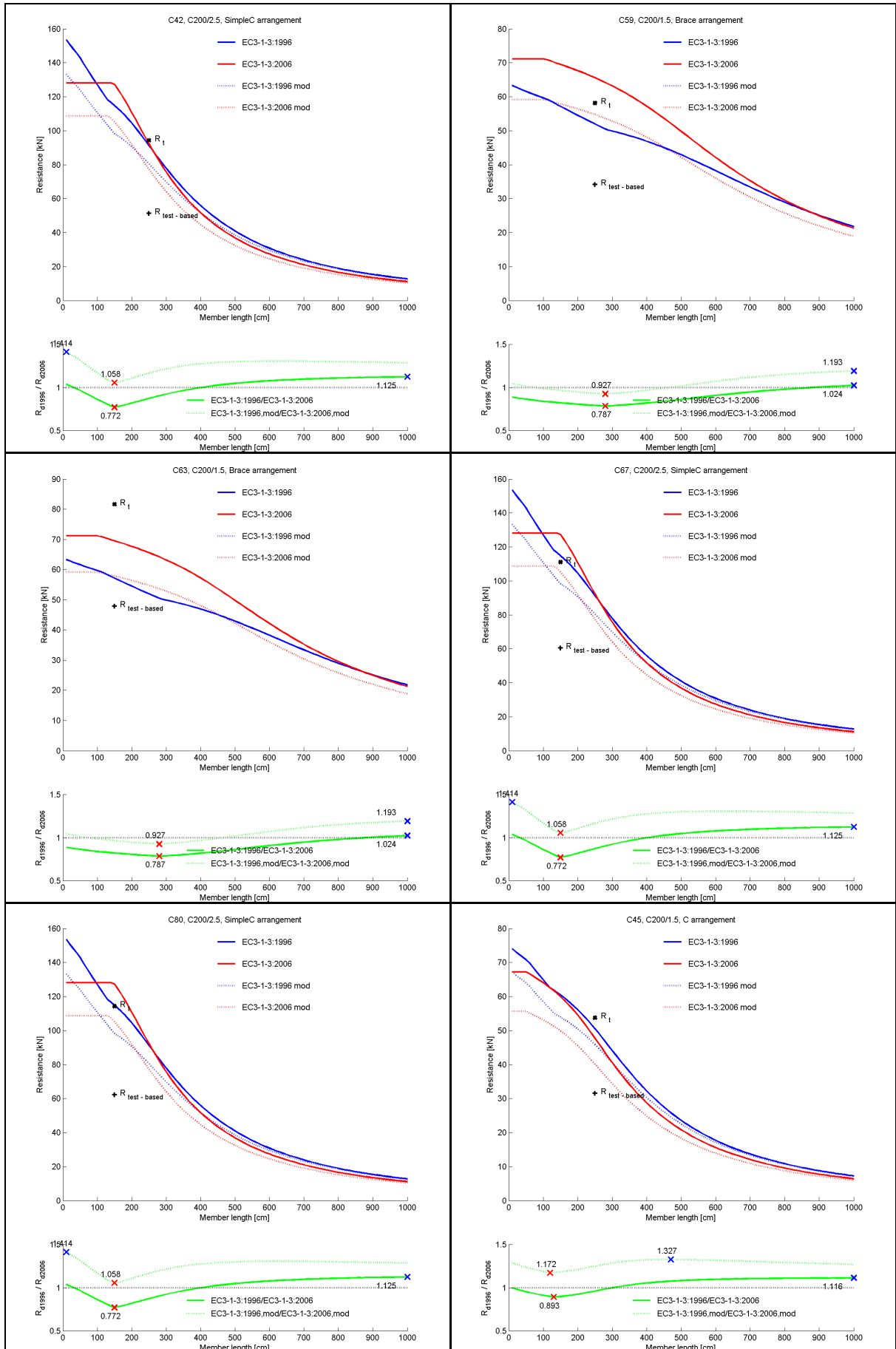|	
A_g	area of the gross cross-section,
A_{eff}	area os the effective cross-section for pure compression
I_y, I_z	second moment of intertia about the strong and weak axis, respectively,
y_g	distance of the centroid of the gross cross-section from the web,
eN_y	shift of the centroid (distance of the centroid of the gross cross-section and that of the effective cross-section for pure compression); if negative, the centroid moves towards the web,
$W_{y,com}$, $W_{y,ten}$	section moduli of the effective cross section for bending about the strong axis,
$W_{z,pos,com}$, $W_{z,pos,ten}$	section moduli of the effective cross-section for bending about the weak axis; due to the moment the web is in tension, the lips in compression,
$W_{z,neg,com}$, $W_{z,neg,ten}$	section moduli of the effective cross-section for bending about the weak axis; due to the moment the web is in compression, the lips in tension.

Load-bearing capacities calculated according to the application rules of both versions of EC3 (continuous blue and red lines) and the modified formulae presented in Chapter 2.4.5 (dotted blue and red lines). Continuous and dotted green lines show the ratio of the design resistances in function of the member length, for the original formulae and for the modified ones, respectively.
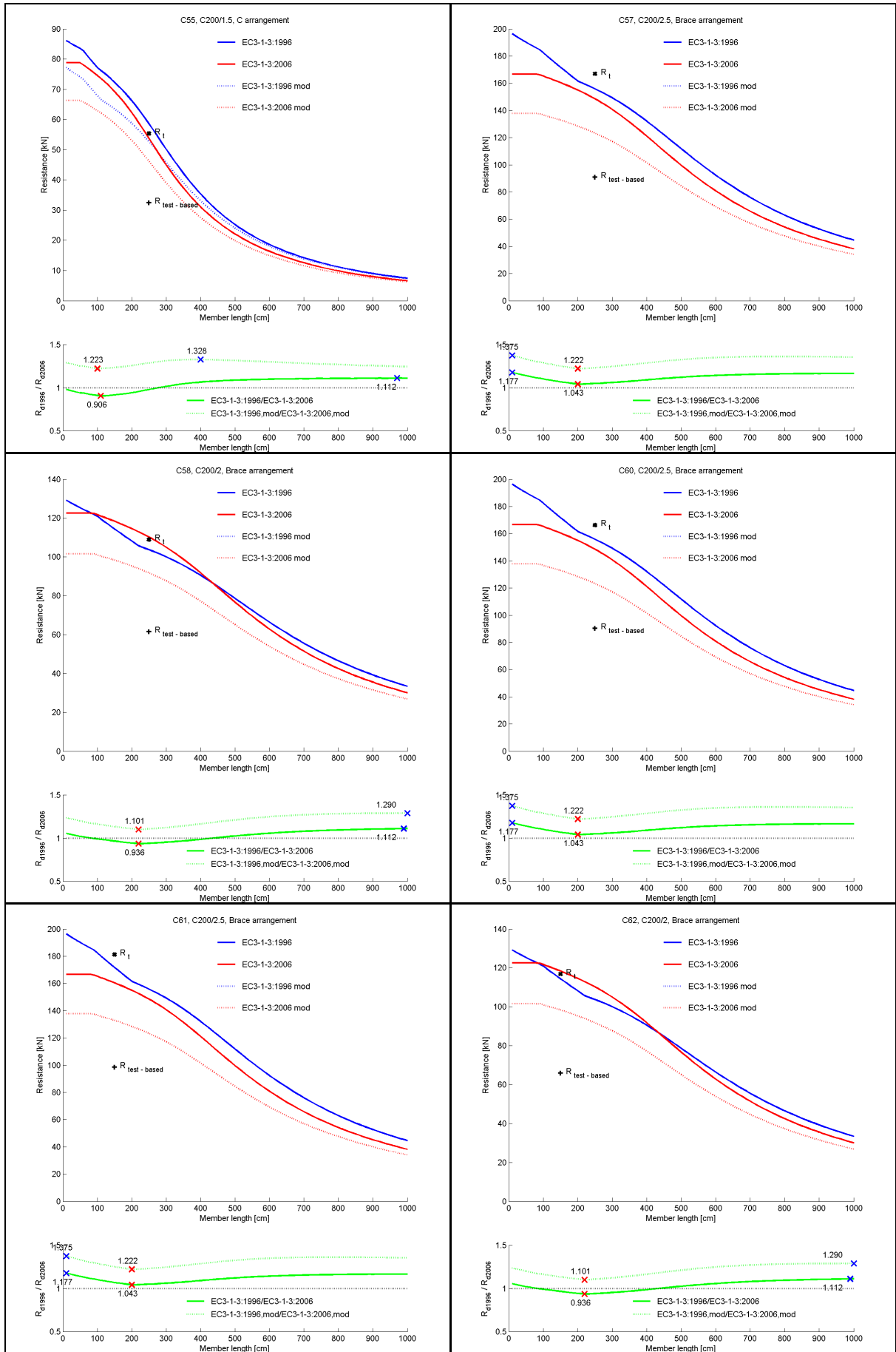
R_t refers to the load-bearing capacity measured in the laboratory test; $R_{test-based}$ denotes the design resistance calculated as described in Chapter 2.3.1.

C55, C200/1.5, C arrangement

C57, C200/2.5, Brace arrangement

C58, C200/2, Brace arrangement

C60, C200/2.5, Brace arrangement

C61, C200/2.5, Brace arrangement
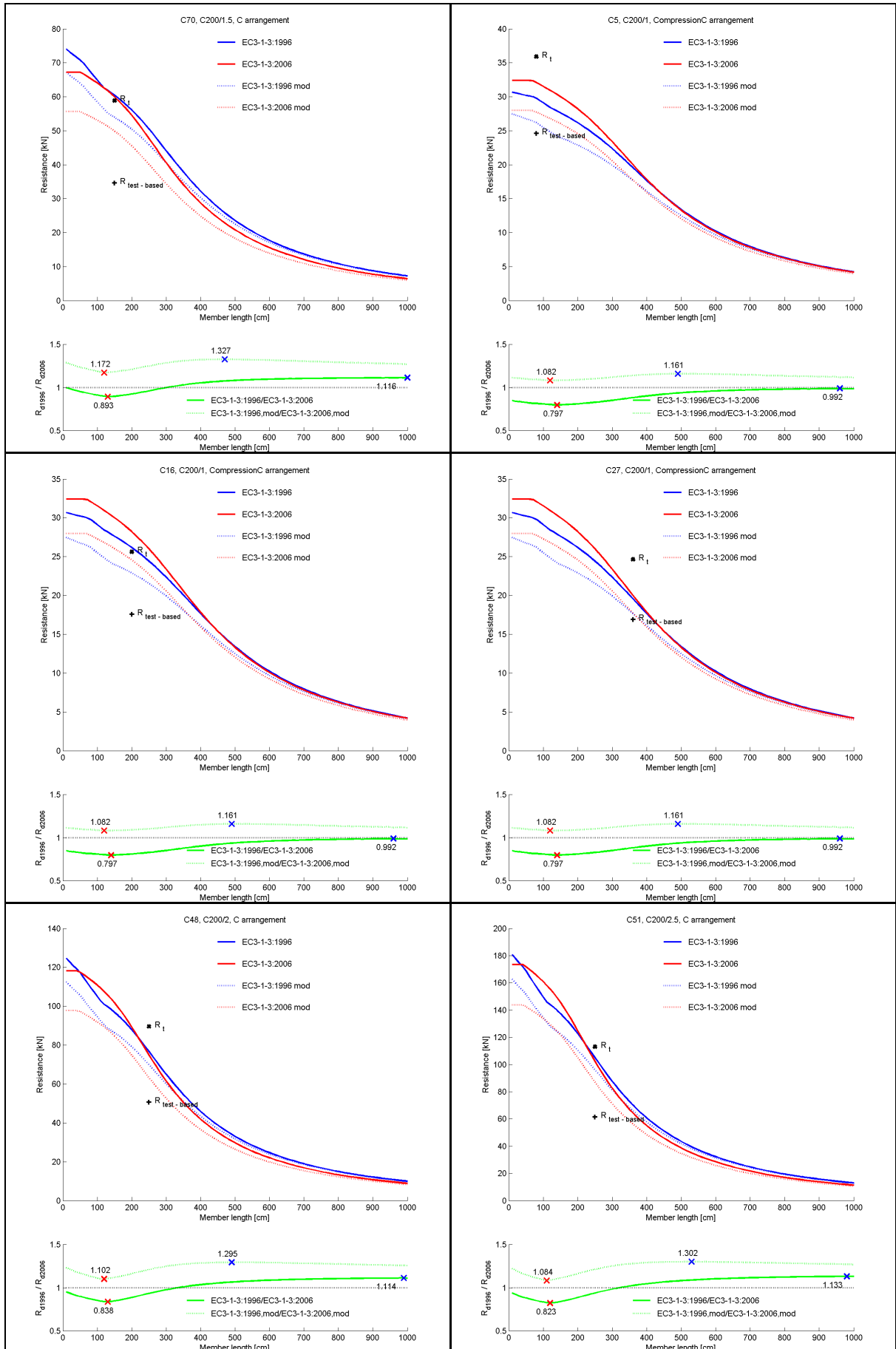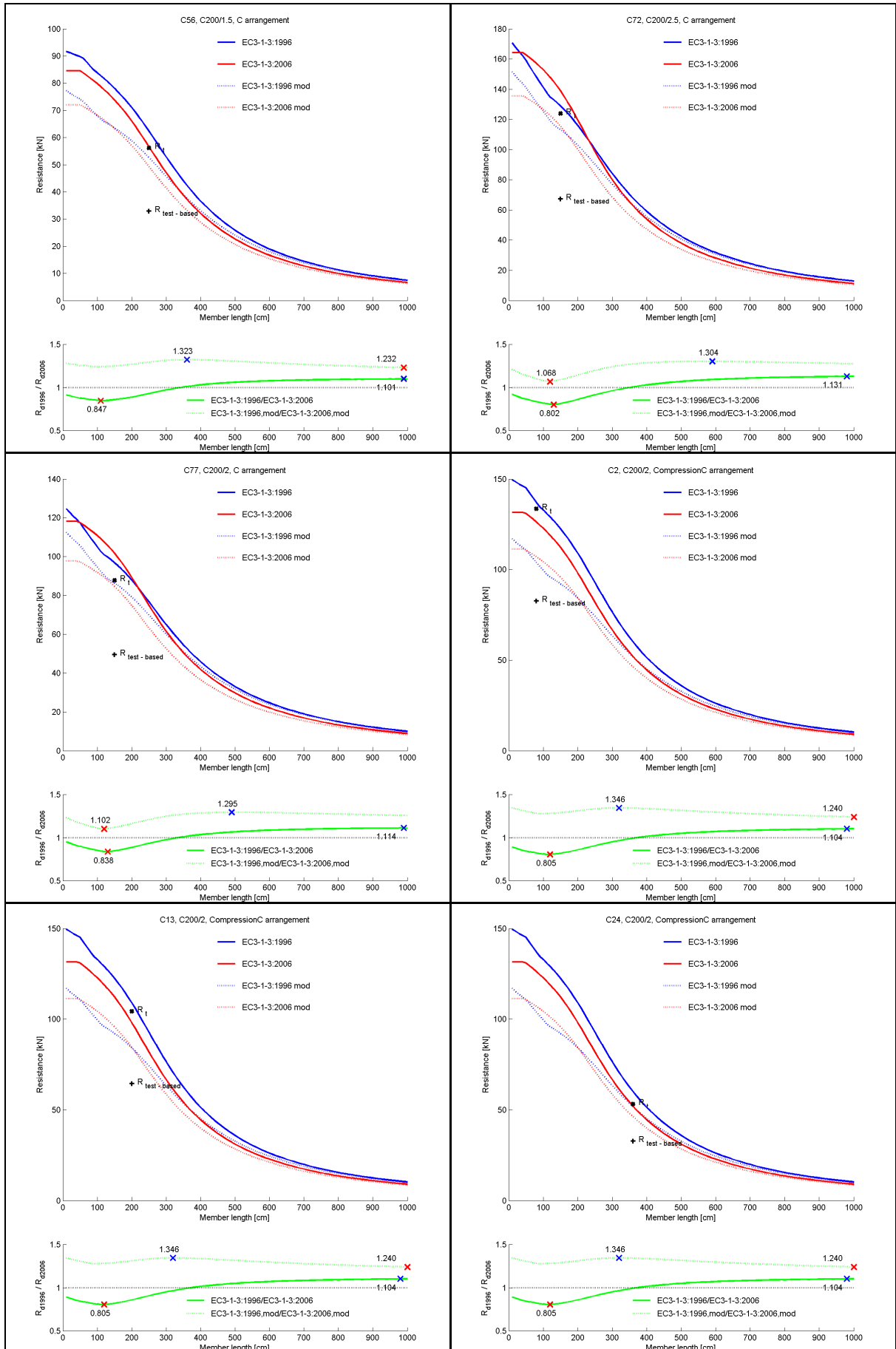
C62, C200/2, Brace arrangement

Table A15: Test and design resistances of SimpleC specimens.

Test	Section	Length [mm]	R_t [kN]	$R_{d(1996)}$ [kN]	$R_{d(2006)}$ [kN]	ratio $(R_d/R_{t(1996)})$	ratio $(R_d/R_{t(2006)})$
C03	C150/1.0	800	18.05	18.31	18.14	1.014	1.005
C14		2000	12.50	13.94	13.18	1.115	1.054
C25		3600	9.47	7.67	6.73	0.809	0.711
C04	C200/1.0	800	21.86	23.48	21.26	1.074	0.973
C15		2000	24.16	20.33	19.36	0.841	0.801
C26		3600	17.24	16.10	14.87	0.934	0.863
C65	C200/1.5	1500	52.26	50.12	51.82	0.959	0.992
C40		2500	41.02	43.08	42.17	1.050	1.028
C01	C200/2.0	800	85.92	85.50	85.13	0.995	0.991
C66		1500	78.97	80.69	88.43	1.022	1.120
C81		1500	79.23	80.69	88.43	1.018	1.116
C82		1500	78.86	80.69	88.43	1.023	1.121
C12		2000	71.11	69.06	73.50	0.971	1.034
C23		2000	46.77	45.60	43.42	0.975	0.928
C41		2500	63.99	66.16	66.98	1.034	1.047
C34		3600	46.67	45.60	43.42	0.977	0.930
C67	C200/2.5	1500	111.10	114.87	127.30	1.034	1.146
C80		1500	114.24	114.87	127.30	1.005	1.114
C42		2500	94.34	91.29	92.27	0.968	0.978

Table A16: Test and design resistances of CompressionC specimens.

Test	Section	Length [mm]	R_t [kN]	$R_{d(1996)}$ [kN]	$R_{d(2006)}$ [kN]	ratio $(R_d/R_{t(1996)})$	ratio $(R_d/R_{t(2006)})$
C05	C200/1.0	800	35.91	29.81	32.08	0.830	0.893
C16		2000	25.62	26.16	28.21	1.021	1.101
C27		3600	24.65	19.57	20.00	0.794	0.812
C02	C200/2.0	800	133.57	136.97	126.21	1.025	0.945
C13		2000	104.34	108.97	98.06	1.044	0.940
C24		3600	53.16	60.13	52.06	1.131	0.979

Table A17: Test and design resistances of C specimens.

Test	Section	Length [mm]	R_t [kN]	$R_{d(1996)}$ [kN]	$R_{d(2006)}$ [kN]	ratio $(R_d/R_{t(1996)})$	ratio $(R_d/R_{t(2006)})$
C70	C200/1.5	1500	58.91	60.44	59.98	1.026	1.018
C45		2500	53.76	50.50	47.68	0.939	0.887
C55		2500	55.38	58.55	53.69	1.057	0.969
C56		2500	56.16	62.27	56.53	1.109	1.007
C77	C200/2.0	1500	87.76	96.88	101.73	1.104	1.159
C48		2500	89.61	76.67	74.82	0.856	0.835
C72	C200/2.5	1500	123.90	128.98	138.82	1.041	1.120
C51		2500	113.05	104.99	102.20	0.929	0.904

Table A18: Test and design resistances of Brace specimens.

Test	Section	Length [mm]	R_t [kN]	$R_{d(1996)}$ [kN]	$R_{d(2006)}$ [kN]	ratio $(R_d/R_{t(1996)})$	ratio $(R_d/R_{t(2006)})$
C63	C200/1.5	1500	81.61	57.16	69.51	0.700	0.852
C59		2500	58.17	51.99	65.59	0.894	1.128
C62	C200/2.0	1500	116.85	114.37	118.36	0.979	1.013
C58		2500	108.97	103.73	110.19	0.952	1.011
C61	C200/2.5	1500	181.20	171.72	160.45	0.948	0.885
C57		2500	166.90	155.87	148.51	0.934	0.890
C60		2500	166.26	155.87	148.51	0.938	0.893

Table A19: Test and design resistances of all studied specimens.

Arrangement	SimpleC		CompressionC		C		Brace		all	
EC3-1-3:	1996	2006	1996	2006	1996	2006	1996	2006	1996	2006
Minimum	0.809	0.711	0.794	0.812	0.856	0.835	0.700	0.852	0.700	0.711
Maximum	1.115	1.146	1.131	1.101	1.109	1.159	0.979	1.128	1.131	1.159
Average	0.991	0.997	0.974	0.945	1.002	0.989	0.891	0.961	0.977	0.980
Median	1.005	1.005	1.023	0.942	1.033	0.988	0.938	0.893	0.987	0.985
Std. Dev.	0.072	0.115	0.132	0.096	0.091	0.113	0.094	0.100	0.093	0.108
Slope[*]	1.004	1.064	1.093	1.228	0.996	1.003	0.985	1.127	0.975	0.978
Fitness[*]	0.996	0.983	0.995	0.953	0.925	0.889	0.803	0.852	0.980	0.960

[*] Slope and fitness of the regression line

Table A20: Comparison of two modified versions of EC3-1-3:2006.

Arrangement	SimpleC		CompressionC		C		Brace		all	
Approach	1st	2nd	1st	2nd	1st	2nd	1st	2nd	1st	2nd
Minimum	0.725	0.610	0.716	0.719	0.780	0.706	0.700	0.709	0.700	0.610
Maximum	0.986	0.946	0.974	0.958	0.984	0.965	0.979	0.941	0.986	0.965
Average	0.868	0.829	0.816	0.822	0.895	0.835	0.891	0.800	0.873	0.823
Median	0.879	0.847	0.793	0.805	0.914	0.840	0.938	0.742	0.884	0.829
Std. Dev.	0.059	0.090	0.100	0.083	0.066	0.090	0.094	0.085	0.076	0.086
Slope[*]	0.909	0.884	0.801	0.810	0.852	0.844	0.783	0.763	0.833	0.817
Fitness[*]	0.982	0.986	0.996	0.995	0.885	0.900	0.948	0.943	0.958	0.961

[*] Slope and fitness of the regression line

Table A21: Comparison of two modified versions of EC3-1-3:2006.

Test	Section	Length [mm]	R_t [kN]	$R_{d, HatC}$ [kN]	$R_d/R_{t, HatC}$
C07	C150/1.0	800	21.90	17.87	0.816
C18		2000	20.49	17.87	0.872
C29		3600	21.81	17.87	0.819
C08	C200/1.0	800	19.36	16.90	0.873
C19		2000	22.14	16.90	0.763
C30		3600	23.55	16.90	0.717
C06	C200/2.0	800	94.19	87.54	0.929
C17		2000	93.81	87.54	0.933
C28		3600	104.25	87.54	0.840

Table A22: Results of the design method of IC Column specimens.

Test	Section	Length [mm]	R_t [kN]	$R_{d, SimpleC}$ [kN]	R_{d, IC_Column} [kN]	$R_{d, IC\_Column}/R_{d, SimpleC}$	$R_t/R_{d, C\_Column}$
C85	C200/1.5	1500	132.80	50.12	110.26	2.200	0.830
C94		2500	138.80	43.08	129.24	3.000	0.931
C83	C200/2.0	1500	205.00	80.69	177.52	2.200	0.866
C84		1500	213.40	80.69	177.52	2.200	0.832
C86		1500	190.00	80.69	177.52	2.200	0.934
C87		1500	236.60	80.69	177.52	2.200	0.750
C93		2500	207.10	66.16	198.47	3.000	0.958

Table A23: Results of the design method of CC specimens.

Test	Section	Length [mm]	R_t [kN]	$R_{d, SimpleC}$ [kN]	$R_{d, CC}$ [kN]	$R_{d, CC}/R_{d, SimpleC}$	$R_t/R_{d, CC}$
C75	C200/1.5	1500	91.43	50.12	90.21	1.800	0.987
C78		1500	92.45	50.12	90.21	1.800	0.976
C47		2500	97.23	43.08	77.55	1.800	0.798
C74	C200/2.0	1500	156.60	80.69	145.24	1.800	0.927
C50		2500	146.41	66.16	119.08	1.800	0.813
C71	C200/2.5	1500	214.10	114.87	206.76	1.800	0.966
C53		2500	182.27	91.29	164.33	1.800	0.902

Table A24: Results of the design method of CU specimens.

Test	Section	Length [mm]	R_t [kN]	$R_{d, SimpleC}$ [kN]	$R_{d, CU}$ [kN]	$R_{d, CU}/R_{d, SimpleC}$	$R_t/R_{d, CU}$
C76	C200/1.5	1500	74.63	50.12	65.15	1.30	0.873
C46		2500	98.87	43.08	77.55	1.80	0.784
C54		2500	68.37	43.08	56.01	1.30	0.819
C73	C200/2.0	1500	109.80	80.69	104.90	1.30	0.955
C49		2500	111.45	66.16	86.01	1.30	0.772
C69	C200/2.5	1500	179.20	114.87	149.33	1.30	0.833
C79		1500	213.00	114.87	206.76	1.80	0.971
C52		2500	146.21	91.29	118.68	1.30	0.812

Table A25: Results of the design method of IC Brace specimens.

Test	Section	Length [mm]	R_t [kN]	$R_{d, Brace}$ [kN]	$R_{d, IC Brace}$ [kN]	$R_{d, IC Brace}/R_{d, Brace}$	$R_t / R_{d, IC Brace}$
C91	C200/1.5	1500	174.40	57.16	142.89	2.50	0.819
C95		2500	146.70	51.99	129.97	2.50	0.886
C90	C200/2.0	1500	291.70	114.37	285.93	2.50	0.980
C98		2500	323.40	103.73	259.32	2.50	0.802

Table A26: Results of the design method of DoubleC specimens.

Test	Section	Length [mm]	R_t [kN]	$R_{d, DoubleC}$ [kN]	$R_{d,DoubleC}/R_{t,DoubleC}$
C10	C150/1.0	800	55.27	35.79	0.647
C21		2000	45.78	35.79	0.782
C32		3600	26.04	20.26	0.778
C11	C200/1.0	800	47.28	41.58	0.879
C22		2000	58.66	41.58	0.709
C33		3600	58.00	41.58	0.717
C35		3600	56.17	41.58	0.740
C09	C200/2.0	800	200.78	157.46	0.784
C20		2000	219.02	157.46	0.719
C31		3600	150.87	132.29	0.877
C36		3600	140.44	132.29	0.942
C37		3600	180.67	132.29	0.732